Biomaterial surfaces differentially adhesive to microbes and mammalian cells

Wang, Yi

Biomaterial surfaces differentially adhesive to microbes and mammalian cells

Yi Wang

Biomaterial surfaces differentially adhesive to microbes and mammalian cells

University Medical Center Groningen, University of Groningen

Groningen, The Netherlands

Printed by Drukkerij van Denderen B.V., Groningen, The Netherlands

ISBN (printed version): 978-90-367-5458-3

ISBN (electronic version): 978-90-367-5461-3

rijksuniversiteit groningen

Biomaterial surfaces differentially adhesive to microbes and mammalian cells

Proefschrift

ter verkrijging van het doctoraat in de
Medische Wetenschappen
aan de Rijksuniversiteit Groningen
op gezag van de
Rector Magnificus, dr. E. Sterken,
in het openbaar te verdedigen op
woensdag 18 april 2012
om 14.30 uur

door

Yi Wang

geboren op 27 februari 1982
te Sichuan, China

Promotores:	Prof. dr. ir. H.J. Busscher
	Prof. dr. M. Libera
	Prof. dr. H.C. van der Mei
Copromotor:	Dr. G. Subbiahdoss

Beoordelingscommissie :	Prof. dr. S.K. Bulstra
	Prof. dr. R.A. Bank
	Prof. dr. K.U. Loos

Paranimfen:

Jan Swartjes

Yan He

Contents

Chapter 1

1.1. General Introduction

Mono-Functional to Multi-Functional Coatings:
the Changing Paradigm to Control Biofilm Formation on
Biomedical Implants

Book Chapter accepted in: 'Biofilms in Bioengineering'
Yi Wang, Matthew Libera, Henk J. Busscher, Henny C. van der Mei

ABSTRACT

Infection is the number one cause of failure of biomaterials implants and devices, despite decades of research into the development of anti-adhesive coatings. In this chapter we postulate that whereas anti-adhesive coatings may be of value for particular applications, such as urinary or intravenous catheters, contact lens cases, and voice prostheses, the paradigm underlying the ideal biomaterial for biofilm control on totally internal, permanent implants needs to change if we want to effectively reduce the occurrence of biomaterials-associated infections. Rather than focusing on the design of mono-functional coatings, multi-functional coatings need to be developed. These must include both anti-adhesive and anti-microbial functionalities, promote a proper immune response, and stimulate tissue integration while simultaneously reducing the threat of bacterial colonization of an implant surface.

INTRODUCTION

Biomaterials-associated infection (BAI) of medical implants and devices is a serious complication that often occurs after an otherwise technically successful surgical procedure or after the prolonged use of contact lenses, catheters, or other percutaneous devices. BAI of totally internal implants nearly always results in the surgical removal and replacement of the implant, because antibiotics are not able to effectively kill bacteria in their biofilm mode of growth such as that typical on an implant surface. Similarly, the removal of an infected, temporary percutaneous device, such as a central intravenous catheter, poses a clinical dilemma. Removal often is synonymous with interruption of a desired therapy, and this can often have disastrous consequences in cases such as chemotherapies. On the other hand, not controlling the infection can also evolve into a life-threatening situation.

Over the past decades our knowledge of how bacteria adhere to surfaces and develop into biofilms has grown rapidly. Substratum surface properties like charge [1-3], hydrophobicity [4-6], and roughness [7-9] are now known to be major determinants of bacterial adhesion. Positively charged surfaces usually stimulate bacterial adhesion, because most bacterial strains carry a net negative cell surface charge [10]. However, at the same time, substrata carrying a positive surface charge through immobilization of, for example, quaternary ammonium compounds are known to become bactericidal upon contact [11, 12]. Acid-base interactions form the basis for the hydrophobicity of bacterial cell and substratum surfaces [13]. They also play a role in bacterial adhesion and, depending on the environmental conditions, can increase or decrease bacterial adhesion. Often hydrophobic surfaces attract equal numbers of adhering bacteria as do hydrophilic surfaces, but they appear free of biofilm after several hours or days under fluctuating environmental shear conditions [14]. Similarly, surface roughness has an effect on bacterial adhesion, but this depends on the scale of the roughness. Some studies have demonstrated that roughness on a scale much smaller than bacterial dimensions does not influence adhesion [15, 16], but other studies have shown that even nanometer-scale roughness may impact bacterial adhesion [16-18]. Interestingly, bacteria do not adhere

preferentially on surface features such as scratches, but they appear to have better opportunities to grow into a biofilm once they adhere to surface irregularities of bacterial or larger dimensions due to the fact that they are protected against environmental shear forces [9].

The body of literature on bacterial adhesion mechanisms has stimulated the development of anti-adhesive coatings for biomaterials. Whereas anti-adhesiveness may be a sufficient single functionality for a coating when applied on such devices as urinary or intravenous catheters, contact lens cases, and voice prostheses, an anti-adhesive functionality is not sufficient for totally internal, permanent implant coatings like vascular grafts, surgical meshes, and hip or knee prostheses. Tissue integration has been described to offer the best protection of such implants [19, 20]. However, many microbial strains known to cause BAI, adhere to the same serum- or plasma-coated surface receptor sites as do mammalian cells [21], and they can thus colonize unmodified implant surfaces. When a coating is applied to such a surface, however, the anti-adhesive functionality is typically not limited to microorganisms but also to mammalian cells. Hence, many anti-adhesive coatings, while successfully repelling bacteria also repel the desirable tissue cells.

Since anti-adhesiveness is never absolute and may involve at best a 2 or 3-log units reduction in the number of adherent bacteria, implant surfaces can still become contaminated during surgery and hospitalization or become colonized by blood-born organisms from infections elsewhere in the body when not fully tissue integrated. Furthermore, the natural defenses offered by macrophages are often frustrated in the presence of a biomaterial, and macrophages are thus less able to eradicate the infecting organisms. Consequently, in addition to anti-adhesive functionalities, antimicrobial functionalities are desirable attributes for an implant coating, as well [22]. Antimicrobial functionalities can be introduced either by immobilizing antimicrobials on the surface yielding contact killing or by the application of antibiotic-release coatings.

Significantly, depending on the application, approximately 95% or more of all patients who receive biomaterial implants do not suffer adverse, long-term effects due to microbial interactions with the implant. However, the consequences when BAI does occur are severe. There can be substantial patient discomfort, complications that can lead to significant morbidity or mortality, significant stress on physicians and medical facilities, and a huge financial burden on the health care system. Clinically speaking, the major difference between revision patients receiving a secondary implant after BAI and primary implant patients receiving their first implant is that in revision surgery the tissue is compromised by infecting organisms [23]. Clearing the infection from surrounding tissue requires high local antibiotic concentrations, which can often be achieved by antibiotic-releasing beads, spacers, and sponges [24]. Thus, while antibiotic-release implant coatings can benefit primary orthopedic implants [25], such coatings are particular important for implants used in revision surgeries, and revision patients after BAI may require coatings with different functionalities than those used in a primary implant.

In this chapter we first briefly review past developments of biomaterials coatings and discuss their advantages and disadvantages. We argue that mono-functional coatings are applicable only for certain applications and the community must look beyond these for greater success in applications where an implant cannot be easily removed and where mammalian cells and microbial cells compete for surface colonization. Effective, infection-resisting permanent implants will require multi-functional surfaces that: (i) are not only anti-adhesive and antimicrobial but also stimulate tissue integration; (ii) do not hamper proper immune responses to microbial presence, and (iii) in revision surgery after BAI, clear infecting organisms from the tissue surrounding the implant.

MONO-FUNCTIONAL COATINGS

Table 1 summarizes some of the many different mono-functional coatings and surfaces that have been designed over the past decades. There are clearly no coatings that can be expected to perform well in each and every application. The general concern with many

of these coatings, especially those showing anti-adhesive functionality, is tissue integration.

Table 1 Different mono-functional coatings that influence bacterial adhesion and biofilm formation together with some of their advantages and disadvantages.

Types of coatings	Basis	Advantages (+) and disadvantages (-)	Ref
Anti-adhesive	Hydrophobic coatings	(+) reduced biofilm formation under fluctuating shear, depending on the strain involved (-) no tissue integration	[26-28]
	Hydrophilic coatings	(+) reduced adhesion, depending on the strain involved (+) good mammalian cell interaction	[29-31]
	Polymer brush coatings	(+) very low bacterial adhesion (-) biofilms do develop ultimately, though weakly adhering (-) no tissue integration	[32-37]
	Nano-patterned surfaces	(+) reduced biofilm formation (+) easy to clean	[38-40]
Tissue integrating	Fibronectin-based coatings	(+) good adhesion and spreading of tissue cells (-) many bacterial strains use the same receptor-sites for their adhesion as tissue cells	[41-43]
Immune-friendly	Polymer brush coatings	(+) allow macrophage mobility on a surface (-) no tissue integration	[44-47]
Antimicrobial	Positively-charged surfaces	(+) kill adhering organisms upon contact (-) layer of dead bacteria is left for subsequent adhesion	[48, 49]
	TiO_2 photocatalytic surfaces	(+) kill adhering bacteria after activation (+) can be re-activated depending on the application	[50-53]
Antibiotic-releasing	Antibiotic-loaded cements	(+) high burst release of antibiotics in surrounding tissue (-) long-term, low concentration tail-release may induce antibiotic resistance	[54]
	Antibiotic-loaded cements for beads, spacers and sponges	(+) high burst release of antibiotics in surrounding tissue (+) low tail release and short stay in the human body	[55]
	Antibiotic-releasing coatings	(+) high burst release of antibiotics in surrounding tissue (-) no tail-release due to limited reservoir volume	[49, 56, 57]

MULTI-FUNCTIONAL COATINGS: A SHIFT IN PARADIGM

Baier in 1982 [58] suggested that scientists and engineers should take lessons from nature when designing infection-resisting biomaterials coatings. Unfortunately, his approach was not widely adopted at that time, possibly because Baier defined the ideal biomaterials surface predominantly in terms of the so-called critical surface tension. This concept has since been recognized as too simple to cover all functionalities of the natural endothelium, designed by nature to withstand colonization by infecting organisms. Following Baier and taking lessons from nature, we postulate that the ideal biomaterials coating should possess multiple functionalities. The design of such multifunctional surfaces clearly requires a change in paradigm, abandoning the common concept of mono-functionality.

In the next section of this chapter, we briefly describe several examples of bi-functional coatings. Then, once the concept of multifunctional coatings is adopted, the number of possibilities of how to differentially control to surface interactions with mammalian cells and with infecting pathogens becomes huge.

SELECTED EXAMPLES

The anti-adhesiveness of PEG-based coatings

Poly(ethylene glycol) (PEG)-based coatings are highly hydrated gel-like structures that constitute the most anti-adhesive surfaces hitherto known [59]. Often alternatively described as PEO for poly(ethylene oxide), PEG chains attached to a flat surface can exist in two different conformations, the so called “mushroom structure” at low chain grafting densities and the “brush structure” at higher chain grafting densities, where the chains are forced to stretch in the medium (see Figure 1). Both structures are expected to create a barrier between the microorganism and the surface thereby preventing adhesion.

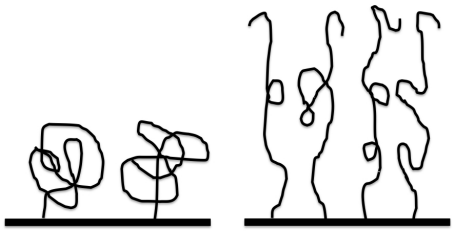

Figure 1 Schematic presentation of a monolayer PEG coating: mushroom conformation (left) and brush conformation (right).

Since PEG-based coatings have superior anti-adhesive properties and, importantly, also allow for enhanced macrophage mobility, they are increasingly being used as a starting point for adding other functionalities. Among these are antimicrobial character and/or tissue-integrating factors. In the design of a multifunctional PEG-based coating, the difference in dimensions between mammalian cells (average range from about 10 to 50 µm depending upon their degree of spreading) and bacteria (on average having a diameter of around 1 µm) needs to be taken into account. Antimicrobial or tissue-integrating functionalities must be applied in surface densities that do not negate the anti-adhesiveness of a multifunctional coating against the smaller bacteria.

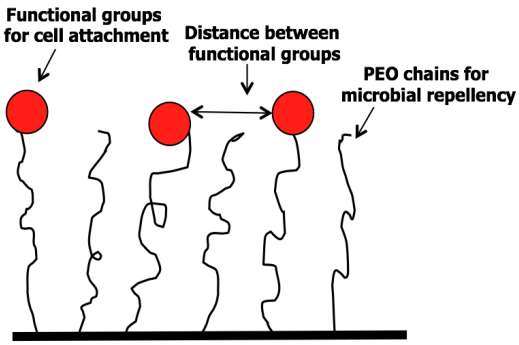

Figure 2 Schematic presentation of modified PEO polymer chains combining microbial repellency with cell-adhesive functional groups. The distance between the functional groups for cell attachment critically determines whether microbial repellency will be maintained or not.

PEG-based anti-adhesive coating with an antimicrobial functionality

PEG-based coatings on silicone rubber strongly reduce bacterial adhesion, but, despite 2-log units reduction in initial adhesion, significant numbers of biofilms can nevertheless form [60]. Conjugation of lysozyme to PEG-molecules and coating of silicone rubber surfaces with 68/32% PEG/lysozyme has yielded a bi-functional polymer brush, possessing both anti-adhesive activity due to the polymer brush combined with the antibacterial activity of lysozyme [61].

PEG-based anti-adhesive coating with RGD-containing peptides

The anti-adhesiveness of PEG-based coatings extends to mammalian cells. In order to prepare bi-functional coatings which prevent microbial adhesion while supporting tissue cell growth, a biologically inert poly(L-lysine)-graft-poly(ethylene glycol) (PLL-g-PEG) copolymer has been equipped with the arginine-glycine-aspartic acid (RGD) peptide sequence [62]. This RGD peptide is known as one of the major recognition sites of integrin receptors through which cells connect to their extracellular matrix [63]. Reduced bacterial adhesion on bi-functional PLL-g-PEG/PEG-RGD-modified surfaces has been demonstrated separately from their ability to support tissue cell growth [64, 65]. Significantly, when the "race for the surface" between staphylococci and osteoblasts was studied on such bi-functional coatings in a co-culture experiment [66], mammalian cells appeared to be much more at an advantage than on common biomaterials surfaces.

Differentially adhesive surfaces

PEG-based submicron-sized, non-adhesive microgels patterned on an otherwise cell-adhesive surface have recently been described as another example of a bi-functional, anti-adhesive and tissue-integrating coating. Such a structure creates a surfaces which is largely cell-adhesive but contains non-adhesive features, which, when spaced at distances comparable to bacterial dimensions, yield dramatically reduced staphylococcal deposition rates [67]. This has been attributed to the fact that staphylococci have relatively rigid cell walls that cannot easily conform to the substrate under conditions of modulated

adhesiveness. In contrast, mammalian cells have flexible cell membranes and adhere to extracellular structures via transmembrane integrins. Mammalian cells can consequently adhere to surfaces with modulated cell adhesiveness by adhering to adhesive patches in between non-adhesive structures (Figure 3).

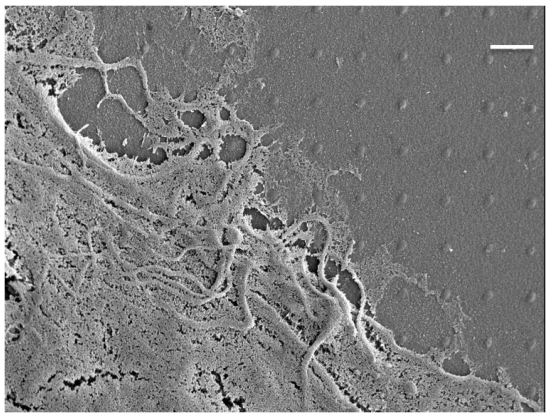

Figure 3 Scanning electron microscope image of a mammalian cell spreading on a PEG-microgel patterned surface with an inter-gel spacing of 1.5 µm. Dotted structures are PEG-microgels, while extensions from the cell circumference can be seen to grow over the microgels in search of the adhesive surface sites. The bar represents 1.5 µm.

CONCLUSION

A great variety of coatings have been described in the literature and claim to be promising for the prevention of biomaterials-associated infection. Most are based on reducing bacterial adhesion and the subsequent formation of surface-attached biofilms. While such coatings are useful in certain applications, there has been a general lack of clinically favorable outcomes when using these coatings on internal biomedical devices such as implanted prostheses. Applications such as these, which are meant to be both totally internal and permanent, require more cleverly designed coatings possessing multiple functionalities. Importantly, this approach represents a significant paradigm change from one where coatings are designed to reduce infection by minimizing all biological interaction to one where interactions with desirable tissue cells are amplified while

bacteria are simultaneously killed or blocked from the surface. Such an approach will require a far better understanding of how multiple cell types interact with synthetic surfaces together with a far greater level of creativity about how to design surfaces with differential cell-interactive properties.

1.2. Aim of this thesis

The competitive growth between microbial and mammalian cells begins immediately after insertion of a biomaterials implant or device in the human body. No biomaterials or functional coating hitherto exists that can resist microbial biofilm formation and support mammalian cell adhesion at the same time.

The aim of this thesis is to investigate up to what extent spatially modified biomaterial surfaces, consisting of non-adhesive hydrogel patterns, can favorably influence microbial adhesion, mammalian cell adhesion and spreading and ultimately the race for the surface to reduce the chance of occurrence of biomaterials-associated-infection.

REFERENCES

1. Jones CR, Adams MR, Zhdan PA, Chamberlain AH. The role of surface physicochemical properties in determining the distribution of the autochthonous microflora in mineral water bottles. J Appl Microbiol 1999:86;917-27.
2. Legeay G, Poncin-Epaillard F, Arciola CR. New surfaces with hydrophilic/hydrophobic characteristics in relation to (no)bioadhesion. Int J Artif Organs 2006;29:453-61.
3. Gottenbos B, Van der Mei HC, Klatter F, Grijpma DW, Feijen J, Nieuwenhuis P, Busscher HJ. Positively charged biomaterials exert antimicrobial effects on Gram-negative bacilli in rats. Biomaterials 2003;24:2707-10.
4. Andersen TE, Kingshott P, Palarasah Y, Benter M, Alei M, Kolmos HJ. A flow chamber assay for quantitative evaluation of bacterial surface colonization used to investigate the influence of temperature and surface hydrophilicity on the biofilm forming capacity of uropathogenic *Escherichia coli*. J Microbiol Methods 2010;81:135-40.
5. Schwarz F, Sculean A, Wieland M, Horn N, Nuesry E, Bube C, Becker, J. Effects of hydrophilicity and microtopography of titanium implant surfaces on initial supragingival plaque biofilm formation. A pilot study. Mund Kiefer Gesichtschir 2007;11:333-8.
6. Almaguer-Flores A, Olivares-Navarrete R, Wieland M, Ximenez-Fyvie LA, Schwartz Z, Boyan BD. Influence of topography and hydrophilicity on initial oral biofilm formation on microstructured titanium surfaces *in vitro*. Clin Oral Implants Res 2011;doi:101111/j.1600-0501.2011.02184.x.
7. Wu Y, Zitelli JP, TenHuisen KS, Yu X, Libera MR. Differential response of Staphylococci and osteoblasts to varying titanium surface roughness. Biomaterials 2011;32:951-60.
8. Tang L, Pillai S, Revsbech NP, Schramm A, Bischoff C, Meyer RL. Biofilm retention on surfaces with variable roughness and hydrophobicity. Biofouling 2011;27:111-21.
9. Charman KM, Fernandez P, Loewy Z, Middleton AM. Attachment of *Streptococcus oralis* on acrylic substrates of varying roughness. Lett Appl Microbiol 2009;48:472-7.

10. Jucker BA, Harms H, Zehnder AJ. Adhesion of the positively charged bacterium *Stenotrophomonas (Xanthomonas) maltophilia* 70401 to glass and Teflon. J Bacteriol 1996;178:5472-9.
11. Tiller JC, Liao CJ, Lewis K, Klibanov AM. Designing surfaces that kill bacteria on contact. Proc Nat Acad Sci U S A; 2001;98:5981-5.
12. Majumdar P, Lee E, Patel N, Ward K, Stafslien SJ, Daniels J, Chisholm BJ, Boudjouk P, Callow ME, Callow JA, Thompson SE. Combinatorial materials research applied to the development of new surface coatings IX: an investigation of novel antifouling/fouling-release coatings containing quaternary ammonium salt groups. Biofouling 2008;24(3):185-200.
13. Van Oss CJ. Hydrophobicity of biosurfaces -- Origin, quantitative determination and interaction energies. Colloids Surf B: Biointerf 1995;5:91-110.
14. Hermannson M. The DLVO theory in microbial adhesion. Colloids Surf B:Biointerf 1999;14:105-19.
15. Li B, Logan BE. Bacterial adhesion to glass and metal-oxide surfaces. Colloids Surf B: Biointerf 2004;36:81-90.
16. Mitik-Dineva N, Wang J, Mocanasu RC, Stoddart PR, Crawford RJ, Ivanova EP. Impact of nano-topography on bacterial attachment. Biotechnol J 2008;3:536-44.
17. Mitik-Dineva N, Wang J, Truong VK, Stoddart PR, Malherbe F, Crawford RJ, Ivanova EP. Differences in colonisation of five marine bacteria on two types of glass surfaces. Biofouling 2009;25:621-31.
18. Emmerson IV RJ, Bergstrom TS, Liu Y, Soto ER, Brown CA, McGimpsey WG, Camesano TA. Microscale correlation between surface chemistry, texture, and the adhesive strength of *Staphylococcus epidermidis*. Langmuir 2006;22:11311-21.
19. Gristina AG. Biomaterial-centered infection: microbial adhesion versus tissue integration. Science 1987;237:1588-95.
20. Deacon JM, Pagliaro AJ, Zelicof SB, Horowitz HW. Prophylactic use of antibiotics for procedures after total joint replacement. J Bone Joint Surg Am 1996;78:1755-70.

21. Patti JM, Allen BL, McGavin MJ, Hook M. MSCRAMM-mediated adherence of microorganisms to host tissues. Annu Rev Microbiol 1994;48:585-617.
22. Boelens JJ, Dankert J, Murk JL, Weening JJ, Van der Poll T, Dingemans KP, Koole L, Laman JD, Zaat SA. Biomaterial-associated persistence of *Staphylococcus epidermidis* in pericatheter macrophages. J Infect Dis 2000;181:1337-49.
23. Broekhuizen CAN, Schultz MJ, Van der Wal AC, Boszhard L, De Boer L, Vandenbroucke-Grauls CMJE, Zaat SAJ. Tissue around catheters is a niche for bacteria associated with medical device infection. Crit Care Med 2008;36:2395-402 .
24. Neut D, Van de Belt H, Van Horn JR, Van der Mei HC, Busscher HJ. Residual gentamicin-release from antibiotic-loaded polymethylmethacrylate beads after 5 years of implantation. Biomaterials 2003;24:1829-31.
25. Engesaeter LB, Lie SA, Espehaug B, Furnes O, Vollset SE, Havelin LI. Antibiotic prophylaxis in total hip arthroplasty: effects of antibiotic prophylaxis systemically and in bone cement on the revision rate of 22,170 primary hip replacements followed 0-14 years in the Norwegian Arthroplasty Register. Acta Orthop Scand 2003;74:644-51.
26. Legeay G, Poncin-Epaillard F, Arciola CR. New surfaces with hydrophilic/hydrophobic characteristics in relation to (no)bioadhesion. Internat J Artif Organs 2006;29:453-61.
27. Harris LG, Mead L, Muller-Oberlander E, Richards RG. Bacteria and cell cytocompatibility studies on coated medical grade titanium surfaces. J Biomed Mater Res Part A 2006;78:50-8.
28. Karakecili AG, Gumusderelioglu M. Comparison of bacterial and tissue cell initial adhesion on hydrophilic/hydrophobic biomaterials. J Biomater Sci Polym Ed 2002;13:185-96.
29. Tenke P, Riedl CR, Jones GL, Williams GJ, Stickler D, Nagy E. Bacterial biofilm formation on urologic devices and heparin coating as preventive strategy. Int J Antimicrob Agents 2004;23:67-74.
30. An YH, Bradley J, Powers DL, Friedman RJ. The prevention of prosthetic infection using a cross-linked albumin coating in a rabbit model. J Bone Joint Surg Br 1997;79:816-9.

31. Wilson M, Harvey W. Prevention of bacterial adhesion to denture acrylic. J Dent 1989;17:166-70.
32. Pechey A, Elwood CN, Wignall GR, Dalsin JL, Lee BP, Vanjecek M, Welch I, Ko R, Razvi H, Cadieux PA.. Anti-adhesive coating and clearance of device associated uropathogenic *Escherichia coli* cystitis. J Urol 2009;182:1628-36.
33. Zoulalian V, Zurcher S, Tosatti S, Textor M, Monge S, Robin JJ. Self-assembly of poly(ethylene glycol)-poly(alkyl phosphonate) terpolymers on titanium oxide surfaces: synthesis, interface characterization, investigation of nonfouling properties, and long-term stability. Langmuir 2010;26:74-82.
34. Paulsson M, Kober M, Freij-Larsson C, Stollenwerk M, Wesslen B, Ljungh A. Adhesion of staphylococci to chemically modified and native polymers, and the influence of preadsorbed fibronectin, vitronectin and fibrinogen. Biomaterials 1993;14:845-53.
35. Sankar S, Rajalakshmi T. Application of poly ethylene glycol hydrogel to overcome latex urinary catheter related problems. Biofactors 2007;30:217-25.
36. Muller R, Ruhl S, Hiller KA, Schmalz G, Schweikl H. Adhesion of eukaryotic cells and *Staphylococcus aureus* to silicon model surfaces. J Biomed Mat Res Part A 2008;84:817-27.
37. Saldarriaga Fernandez IC, Van der Mei HC, Metzger S, Grainger DW, Engelsman AF, Nejadnik MR, Busscher HJ. *In vitro* and *in vivo* comparisons of staphylococcal biofilm formation on a cross-linked poly(ethylene glycol)-based polymer coating. Acta Biomater 2010;6:1119-24.
38. Hannig M, Kriener L, Hoth-Hannig W, Becker-Willinger C, Schmidt H. Influence of nanocomposite surface coating on biofilm formation *in situ*. J Nanosci Nanotechnol 2007;7:4642-8.
39. Diaz C, Schilardi PL, Salvarezza RC, De Mele MF. Nano/microscale order affects the early stages of biofilm formation on metal surfaces. Langmuir 2007;23:11206-10.
40. Battin TJ, Kammer FV, Weilhartner A, Ottofuelling S, Hofmann T. Nanostructured TiO2: transport behavior and effects on aquatic microbial communities under environmental conditions. Environ Sci Technol 2009;43:8098-104.

41. Tweden KS, Harasaki H, Jones M, Blevitt JM, Craig WS, Pierschbacher M, Helmus MN. Accelerated healing of cardiovascular textiles promoted by an RGD peptide. J Heart Valve Dis 1995;4:90-7.
42. Clubb FJ, Clapper DL, Deferrari DA, Hu SP, Seare WJ, Jr., Capek PP, Armstrong J, McGee MG, Billings LA, Fuqua JM, Parins SM. Surface texturing and coating of biomaterial implants: effects on tissue integration and fibrosis. ASAIO J 1999;45:281-7.
43. Petrie TA, Raynor JE, Reyes CD, Burns KL, Collard DM, Garcia AJ. The effect of integrin-specific bioactive coatings on tissue healing and implant osseointegration. Biomaterials 2008;29:2849-57.
44. Hemmerlein JB, Trerotola SO, Kraus MA, Mendonca MS, Desmond LA. *In vitro* cytotoxicity of silver-impregnated collagen cuffs designed to decrease infection in tunneled catheters. Radiology 1997;204:363-7.
45. Atiyeh BS, Costagliola M, Hayek SN, Dibo SA. Effect of silver on burn wound infection control and healing: review of the literature. Burns 2007;33:139-48.
46. Widgerow AD. Nanocrystalline silver, gelatinases and the clinical implications. Burns 2010;36:965-74.
47. Bright KR, Gerba CP, Rusin PA. Rapid reduction of *Staphylococcus aureus* populations on stainless steel surfaces by zeolite ceramic coatings containing silver and zinc ions. J Hosp Infect 2002;52:307-9.
48. Cokeliler D, Goktas H, Tosun PD, Mutlu S. Infection free titanium alloys by stabile thiol based nanocoating. J Nanosci Nanotechnol 2010;10:2583-9.
49. Norowski PA, Bumgardner JD. Biomaterial and antibiotic strategies for peri-implantitis: a review. J Biomed Mater Res B Appl Biomater 2009;88:530-43.
50. Hochbaum AI, Aizenberg J. Bacteria pattern spontaneously on periodic nanostructure arrays. Nano Lett 2010;10:3717-21.
51. Kappell GM, Grover JP, Chrzanowski TH. Micro-scale surface-patterning influences biofilm formation. Electron J Biotechnol 2009;12:10-1.

52. Krsko P, McCann TE, Thach TT, Laabs TL, Geller HM, Libera MR. Length-scale mediated adhesion and directed growth of neural cells by surface-patterned poly(ethylene glycol) hydrogels. Biomaterials 2009;30:721-9.
53. Chung KK, Schumacher JF, Sampson EM, Burne RA, Antonelli PJ, Brennan AB. Impact of engineered surface microtopography on biofilm formation of *Staphylococcus aureus*. Biointerphases 2007;2:89-94.
54. Neut D, Dijkstra RJ, Thompson JI, Van der Mei HC, Busscher HJ. Antibacterial efficacy of a new gentamicin-coating for cementless prostheses compared to gentamicin-loaded bone cement. J Orthop Res 2011: 29:1654-61
55. Diefenbeck M, Muckley T, Hofmann GO. Prophylaxis and treatment of implant-related infections by local application of antibiotics. Injury 2006;37(Suppl 2):S95-104.
56. Kwok CS, Horbett TA, Ratner BD. Design of infection-resistant antibiotic-releasing polymers. II. Controlled release of antibiotics through a plasma-deposited thin film barrier. J Control Rel 1999;62:301-11.
57. Davidoff SN, Call BP, Hogrebe PC, Grainger DW, Brooks AE. A robust method to coat allograft bone with a drug-releasing polymer shell - biomed 2010. Biomed Sci Instrum 2010;46:184-9.
58. Baier RE. Conditioning surfaces to suit the biomedical environment: recent progress. J Biomech Eng 1982;104:257-71.
59. Schulte VA, Diez M, Hu Y, Moller M, Lensen MC. Combined influence of substrate stiffness and surface topography on the antiadhesive properties of Acr-sP(EO-stat-PO) hydrogels. Biomacromol 2010;11:3375-83.
60. Nejadnik MR, Van der Mei HC, Norde W, Busscher HJ. Bacterial adhesion and growth on a polymer brush-coating. Biomaterials 2008;29:4117-21.
61. Muszanska AK, Busscher HJ, Herrmann A, Van der Mei HC, Norde W. Pluronic-lysozyme conjugates as anti-adhesive and antibacterial bifunctional polymers for surface coating. Biomaterials 2011;32:6333-41.

62. VandeVondele S, Voros J, Hubbell JA. RGD-grafted poly-L-lysine-graft-(polyethylene glycol) copolymers block non-specific protein adsorption while promoting cell adhesion. Biotechnol Bioeng 2003;82:784-90.
63. LeBaron RG, Athanasiou KA. Extracellular matrix cell adhesion peptides: functional applications in orthopedic materials. Tissue Eng 2000;6:85-103.
64. Maddikeri RR, Tosatti S, Schuler M, Chessari S, Textor M, Richards RG, Harris LG. Reduced medical infection related bacterial strains adhesion on bioactive RGD modified titanium surfaces: a first step toward cell selective surfaces. J Biomed Mat Res Part A 2008;84:425-35.
65. Shi Z, Neoh KG, Kang ET, Poh C, Wang W. Bacterial adhesion and osteoblast function on titanium with surface-grafted chitosan and immobilized RGD peptide. J Biomed Mater Res Part A 2008;86:865-72.
66. Subbiahdoss G, Kuijer R, Grijpma DW, Van der Mei HC, Busscher HJ. Microbial biofilm growth vs. tissue integration: "the race for the surface" experimentally studied. Acta Biomater 2009;5:1399-404.
67. Wang Y, Subbiahdoss G, Swartjes J, Van der Mei HC, Busscher HJ, Libera M. Length-scale mediated differential adhesion of mammalian cells and microbes. Adv Funct Mater 2011: 21:3916-23

Chapter 2

Poly(ethylene glycol) as a Biointeractive Electron-Beam Resist

Will be submitted to Applied Physics Letters

Yi Wang, Emre Firlar, Xiaoguang Dai, Matthew Libera

ABSTRACT

Precisely patterned micro- and nano-sized hydrogels created by electron beam patterning have been increasingly used to control interactions between surfaces and biological structures such as proteins and cells. However, little work has been done to optimize electron-beam exposure conditions for patterned gel formation. We used a combination of experimental investigations and Monte Carlo simulations to explore the properties of poly(ethylene glycol) (PEG) as negative electron beam resist to control protein adsorption. PEG gels were patterned onto Si surfaces using focused electron beams with electron energies ranging from 2 to 30 keV over a dose range of 0.005-500 fC/point. Both the incident beam energy and the exposure dose affect electron scattering in the resist and the substrate. Immunofluorescence imaging proved that electron-beam scattering could generate a thin layer of lightly crosslinked PEG which largely extend the interactive volume excluded from normal measurement for surface architecture. High incident beam energy as 30 keV significantly minimized forward scattering on our thin PEG film (120 nm), consequently provide PEG gel with small interactive volume at lower electron doses. Although low electron energy (< 5 keV) is not a good option for industrialized lithography to provide high resolutions, it can decrease the proximity effect dramatically and maximally preserve non-fouling property of PEG.

INTRODUCTION

The recognition that patterning at nano/micro length scales can have a profound effect on how synthetic surfaces interact with physiological systems [1-3] has motivated tremendous interest in various surface-patterning technologies in the context of biological applications [4-7]. Among these patterning technologies, electron beam lithography (EBL) is often used in much the same ways in the semiconductor-device industry. Namely, a polymer resist film is used as a medium to record a pattern created by electron beam exposure and transfer that pattern to an underlying substrate. Increasingly, EBL technologies are being used to directly write structures that are either themselves biointeractive or can be chemically modified to confer some form of biospecific character to them.

In general, EBL is an attractive surface-patterning technology because of its ability to achieve patterns directly from a user-specified image without the need to create a mask [8, 9]. In its simplest embodiment, energy imparted by incident electrons onto a polymer film causes either e-beam-induced polymer chain scission and increased solubility (positive resist) or cross-linking and reduced solubility (negative resist). A continuous string of developments since the conception of e-beam lithography in the 1960's involving the electron-optical systems, the optimization of exposure, and the development of high-sensitivity photoresists has made this technique routine in many laboratory environments. In bio-relevant applications, the established exposure principles and practical experience can often be immediately translated from those experimental systems. Much less is known, however, about how electrons interact with the water soluble polymer precursors often used in bio-relevant patterning applications such as poly(ethylene glycol) (PEG) [10-12] poly(vinly pyrrolidone) (PVP) [13, 14], or poly (acrylic acid) (PAA) [15]. We and others, for example, have previously demonstrated that PEG films can be e-beam processed to create surface-patterned hydrogels that resist nonspecific protein adsorption and cell adhesion [16, 17]. Furthermore, by using PEG precursors with chemically active groups, post-irradiation chemical functionalization can confer precise biospecific character to such

gels [18-20]. Since, however, biointeractive properties are determined by molecular-level processes, subtle changes in electron-beam processing parameters can have a substantial effect on how the resulting surfaces will ultimately interact with cells and proteins. Relatively little systematic work has been done to characterize these effects and thus be used as a basis to choose processing parameters optimized to create patterns appropriate for some particular experiment.

We use a combination of experiments and Monte Carlo simulation to explore the effects of incident electron and dose on thin film of PEG polymer precursor film solvent cast onto silicon substrates. Electron energies of 2 keV, 10 keV and 30 keV were studied. We are particularly interested in the low-keV experiments because of the opportunities to make exposures on electrically nonconductive substrates such as glass. 10 keV-100 keV are typical of the more common electro-optical systems used for lithographic processing. We study incident doses that vary over many orders of magnitude and find significant variations in the resulting dry-film thicknesses as a function if incident energy suggesting a rich interplay between chain scission and crosslinking. Importantly, proximity effects due to electrons backscattered from the underlying inorganic substrate can cause significant radiation chemistry in regions many tens of nanometres or more from the point of electron incidence leading to surface PEGylation sufficient to affect biointeractions but otherwise difficult to detect.

RESULTS AND DISCUSSION

Principles in EBL and physical properties of PEG gels

High resolution is one of the main concerns of EBL since its first application. It is limited by electron-optical aberrations and, more importantly, scattering of electrons in the resist and in the substrate. The main purpose of this chapter is to establish how beam broadening and backscattering affect PEG microgel formation.

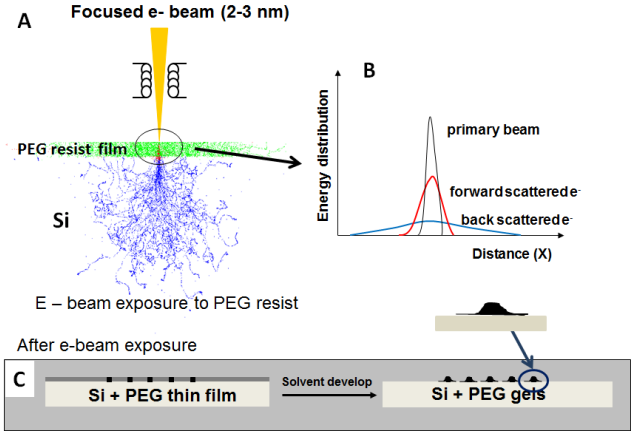

Figure 1 Schematic of the e-beam lithography process including: (A) Monte Carlo simulation of electron trajectories in the PEG resist and silicon substrate; (B) Energy distribution in e-beam resist; (C) Artificial structure generated by scattering after solvent development of the exposed resist.

A well-focused electron beam typically has a Gaussian intensity distribution with a full-width at half maximum of 1-3 nm. This primary beam is the energy source for resist exposure, and its exposure range is only a few nanometres. Figure 1A shows the results of a simple Monte Carlo simulation to illustrate the electron trajectories inside the PEG resist (red) and the Si substrate (blue) underneath. The energy distribution generated by these electrons is schematically shown in Figure 1B, that two major types of scattering could be treated separately and modelled by Gaussian distributions. Beam broadening due to forward scattering (red) is caused by small angle scattering of electrons as they penetrate the resist. It can be minimized by using a thinner resist (e.g. < 0.1 μm) and/or by applying higher accelerating voltages. Backscattering (blue) corresponds to the large-angle elastic scattering of electrons generated by electron collisions with the much heavier atomic nuclei of the substrate beneath the resist. These electrons retain most of their energy, which is also responsible for energy deposition inside the resist, but they can travel back through the resist at a significant distance from the incident beam and thus cause additional resist exposure. This backscattering phenomenon gives rise to the so-called proximity effect, which has received substantial attention in the lithography community. It

is not part of pattern features. However, after solvent development (Figure 1C), artefactual structure caused by the proximity effect can remain on the substrate. This structure can have a significant effect on the biointeractive properties of a surface, and we aim to find out how the energy deposited by the primary beam, the forward scattering and the backscattering control the protein adsorption on a patterned surface.

Besides the energy deposited by scattering, we can control the size of a single beam exposure by adjusting electron doses with respect to the dwell time. Figure 2 is acquired by SEM imaging after solvent development. The point dose ranges from 0.005 fC to 500 fC, the inter-gel spacing is 3 µm, and the squares outside serves as fiducial marks. At 2 keV, the minimum effective exposure point dose is 0.1 fC, which means enough PEG macromolecules have been crosslinked to form a gel and bind that gel onto the substrate. From the table inset in Figure 2, we can see that the minimum dose increased 10 times as the electron energy increased from 2 keV to 30 keV because electrons in the 1-3 keV regimes deposit most of their energy within the resist and create maximum density of crosslinking.

We further studied the swelling properties from both vertical and lateral directions by using Atomic Force Microscopy (AFM, Figure 3). Lower doses generate a lower crosslink density and, thus, a higher vertical swelling ratio. However lateral swelling is not as significant as vertical swelling. Krsko *et al*. [21] reported for the first time using e-beam lithography to pattern PEG, and similar swelling properties were found for a PEG gel pad of 5.4 µm × 5.4 µm. For PEG gel pad the swelling was much more significantly due to the more even distribution of low crosslinked region. PEG gels formed by a single point exposure do not have uniform crosslinking because of the uneven energy distribution. As shown in the Figure 3 inset, at 2 keV with a dose of 100 fC, the primary beam in the center caused higher crosslinking than the surrounding area cross-linked by scattered electrons. Backscattering may also contribute to the surrounding low crosslink density at such a high dose.

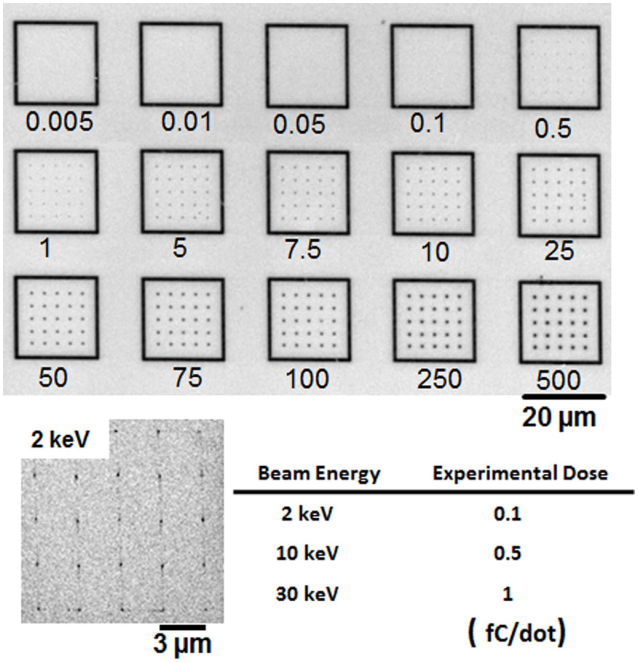

Figure 2 SEM image showing the microgel size dependence as a function of electron doses and the minimum effective exposure of 0.1 fC at 2 keV; The inset Table shows the experimental critical dose of single gel formation.

Scattering effect and Monte-Carlo simulations

To further understand the effects from forward scattering and backscattering on PEG cross-linking, we first compared the results generated by lateral force imaging and Monte-Carlo simulation. The AFM lateral force mode was used in conjunction with topographical images during one scan and allowed us to distinguish surfaces with different friction. Yao *et al*. [22] has shown that, measuring the local friction force, lateral force imaging could provide the atomic resolution on mica to investigate surface contamination, interaction forces and chemical speciation. As shown in the upper panel of Figure 4, PEG gel arrays (3x3) were generated with the same point dose of 100 fC but under different incident beam energies (2, 10, 30 keV). The lateral force images were obtained while the specimens were fully hydrated after immersing in deionized water for 10 min. The

different friction contrast from different lateral deflection signals represents variations in the hydrophobic forces (normally contribute to large contrast area) especially on the image of 10 keV gels. Hay et al. and Noy et al. demonstrated that the conditions under which the imaging is performed are important [23, 24], and a controllable environment can produce rationally-interpretable image contrast. Although image contrast can be affected by various controllable factors such as whether the samples are held in an aqueous environment, medium pH value and tip functionalization, it reflected different composition between regions. Similar with Rozsnyai and Wrighton observations that topographical image can fail to distinguish patterns with different functional groups [25], the image contrast could only be detected by lateral force imaging in our experimental results. The brighter regions surrounding PEG gels represent higher friction between normal AFM Si3N4 tip and the silicon surface, while the darker halo represents surface covered by a PEG thin layer. We do observe contrast in the middle of each gel which is the mostly significant in 2 and 10 keV images (Figure 4). The energy dissipation represented differences caused by crosslinking generated from different densities of energy deposited by the primary beam and forward scattered beam.

We used Monte Carlo simulations to calculate the energy deposition inside the PEG film in order to find out the different contributions from scattering. As shown in the lower panel of Figure 4, the exact cases of energy distributions in a 5 nm slice above the silicon surface were modelled for point exposure of 100 fC dose under different incident energies (2, 10, 30 keV). Assuming a threshold energy deposition for crosslinking of 5 eV nm^{-3} [26], only energy deposited enough for crosslinking were demonstrated here (> 5 eV nm^{-3}). We can see that at 2 keV, almost no backscattering was observed, and most of the energy deposited in this PEG layer was from primary beam and forward scattering. For 10 keV, there is significant elastic scattering in the Si substrate which extended the resist exposure distances when backscattered e^- emerge from the substrate and redeposit energy to the PEG film on the top. We can see that the energy deposition distance in Monte-Carlo simulations matched the AFM lateral force images for the case of 10 keV irradiation. In the

case of 30 keV irradiation, there is a slight contrast change in some regions surrounding the gels formed by primary beam crosslinking (forward scattering within the PEG resist can be largely reduced due to the high incident beam energy) in the AFM image. We can also see a much less dense distribution of energy scattered in the simulated modulation. However, it is still hard to say if there is enough energy deposited in PEG film to form enough crosslinking that finally affects the surface interactive events.

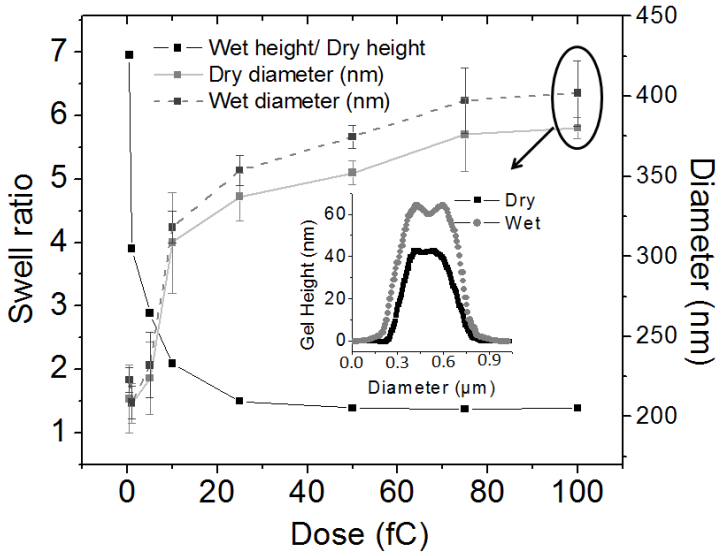

Figure 3 AFM topographical measurements give the vertical swell ratio (wet height/dry height) and diameter of gels at 2 keV. Inset figure shows the nonuniform crosslinking for a micro gel formed by single point expousre at 2 keV with a dose of 100 fC.

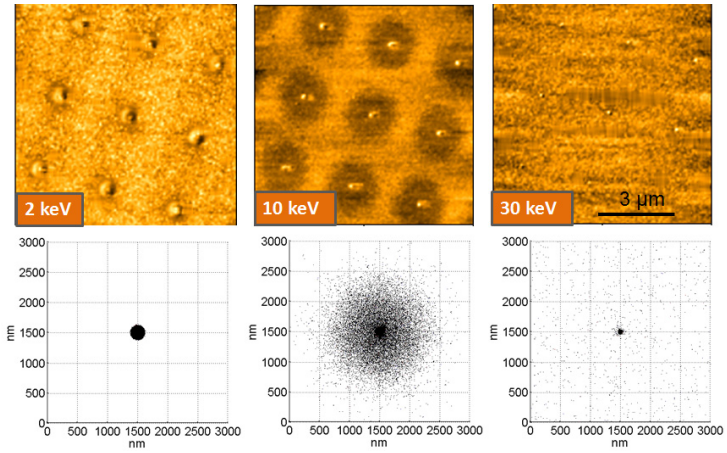

Figure 4 AFM lateral force images of PEG gel arrays (3x3) formed under different incident beam energies (2 keV, 10 keV, and 30 keV) with a point dose of 100 fC (upper panel). Monte Carlo simulation of energy deposition on a PEG resist-coated silicon substrate at corresponding incident energies (lower panel). Each dot represents energy deposition of larger than 5 eV nm^{-3} (crosslinking threshold).

Human fibronectin adsorption on PEG gels

We use confocal fluorescence imaging to further test protein adsorption on patterned PEG gels. Larger patterns of 200 µm × 200 µm arrays of gels were fabricated with point doses of 1, 10, 100, and 1000 fC at 2 keV, 10 keV and 30 keV incident beam energies on the same silicon substrate. In Figure 5, green area represents Fn adsorption and black represents PEGylated surface. We first notice that the lightly crosslinked regions repel Fn. This lower protein adsorption can be attributed to the repulsive steric forces toward the protein adsorption due to the large number of hydrogen bonds with water molecules [27, 28]. The lateral distribution of the protein adsorption depends on the minimum crosslinking caused by the energy deposited by the electrons, which related to both the energy of the primary electrons, the number of incident electrons, and the type of material the electrons traveling in.

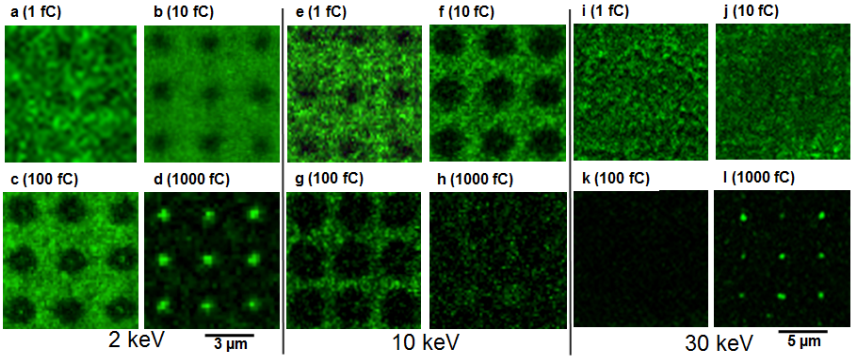

Figure 5 Immunofluorescent images showing the spatial distribution of adsorbed fibronectin (green) on surfaces with PEG microgel patterned with various incident electron eneries (2 keV, 10 keV and 30 keV) and doses (1, 10, 100, and 1000 fC).

In Figure 5, the lateral size of protein repulsion in 2 keV image increased from point dose of 1 fC (~ 300 to 400 nm) to 1000 fC (over 1500 nm). Furthermore, high-dose exposures created highly cross-linked cores in the center of each gel. Protein adsorption on the centers can be observed at point dose of 100 fC and is particularly clear at 1000 fC. We cannot detect the same high cross-linked cores in the 10 keV case, because, as shown in Figure 4, the forward scattering was reduced and may be beyond the detection limit. Also there was potential that at such high resolution, the relatively small fluorescent signal differences can easily be reduced during scanning. This is one of the common constraints with a laser scanning confocal microscopy [29]. This intensity limitation was further surpassed by much higher incident beam energy at 30 keV, as shown in Figure 5*l*, together with the effect of 1000 fC point dose. Most significant was that, as shown in Figure 5*k*, the protein repulsive region here was beyond 2500 nm. This confirmed that the small energy distribution as shown in the simulation (Figure 4) still caused low-crosslinking PEG layer which was protein repulsive. Both the AFM imaging and Monte-Carlo simulation at 30 keV (Figure 4) showed that primary electrons with high incident energy narrowed the size of forward scattering and can provide the final patterned features on the Si surface. But higher dose corresponds to longer dwelling time, together with high incident beam energy, both of them contribute to larger energy deposition by back scattering. This brings up the

awareness when using high incident beam energy in order to get ultra-fine surface features in the application of interacting with biological components such as protein, microbial and mammalian cells.

To achieve precisely controlled non-fouling features with protein repulsive properties, low incident beam energy (2 keV) with lower exposure dose (< 100 fC/dot) would be an appropriate choice for electron beam lithography, especially for a non-conductive substrate which could then largely reduce the charging problem.

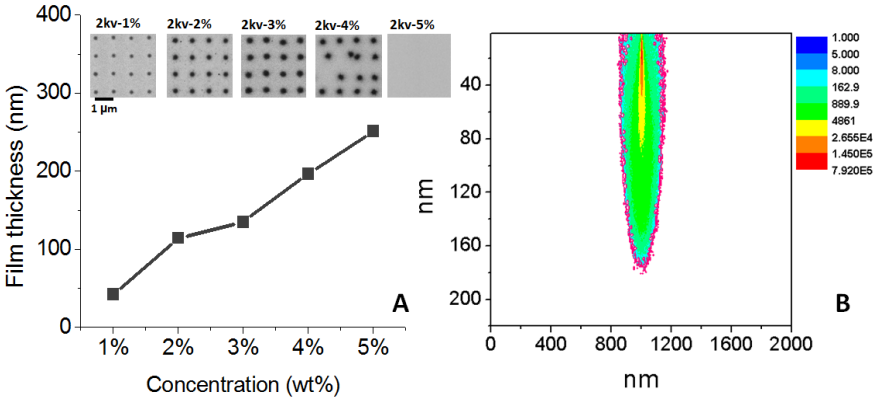

Figure 6 Electron penetration limitation at 2 keV with a dose of 100 fC on PEG film with different film thicknesses generated by different solvent concentration during spin casting (A); Monte Carlo simulation of energy deposition on a PEG resist of 200 nm thickness at 2 keV, purple represents energy deposition of larger than 5 eV nm^{-3} as crosslinking threshold.

Electron beam penetration limitation at 2 keV

Low incident beam energy reduce backscattering and provide PEG microgels with good swelling properties, uniform antifouling behavior, and relatively small size. These can be created at 2 keV with a point dose of < 100 fC. However, with lower incident energy, the penetration depth of the electrons is limited. As shown in Figure 6A, we varied the PEG film thickness by spin-casting PEG solution with different concentrations (1 wt% to 5 wt%). We tested the penetration depth of 100 fC dose at 2 keV and found that poor gel binding appeared at a film thickness of around 200 nm. If we increase the film thickness to 250 nm,

there is not enough energy to bind the PEG gels to the substrate. Figure 6B demonstrates the beam penetration limitation at 2 keV with dose of 100 fC in Monte-Carlo simulation. The purple color denotes the voxels in which the energy deposited per unit volume is 5 to 8 eV nm^{-3} corresponding to the threshold energy density for crosslinking. This simulation predicts a slightly smaller depth limitation of around 180 nm but nevertheless in reasonable agreement with the experimental results of around 200 nm.

CONCLUSIONS

We studied the effects of incident electron energy, exposure dose, and other parameters on the patterning of PEG resist used for bio-relevant applications such as protein adsorption. We found that low beam energy (2 keV) and lower exposure point dose (< 100 fC) were more suitable for bio-relevant patterning applications. With most of the energy deposited within the PEG resist, low beam energy helped to decrease the proximity effect (backscattering) dramatically while at the same time maximally preserved the bio-interactivities provided by low-crosslinking density.

EXPERIMENTAL

Preparation of Si substrates

A solution of 2 wt% PEG (6K Da; Fluka) in tetrahydrofuran was used to make thin films by spin casting on silicon wafers for 5 min (4000 rpm). Firstly, silicon substrates (10 mm x 10 mm) were cleaned and vinyl-silane modified using the same procedure as described before [9, 21]. Briefly, Si were sonicated in ethanol (96%) for 5 min and then dried with a nitrogen gas stream. In a second cleaning, Piranha etch solution (3:1 98% sulphuric acid and 30% H_2O_2) was used for deep cleaning, followed by rinsing in deionized water, nitrogen gas stream dried and then exposed to a low pressure O_2 plasma (~300 mTorr,1.75 W) for 10 min. The substrates were then spin cast with PEG solution. Samples were stored under vacuum (~10^{-3} Torr) before patterning. Film thicknesses varied from ~50 nm to ~250 nm by applying different concentrations of PEG solution (1wt% to 5wt%).

Ellipsometry

The thickness of dry PEG films after spin casting was measured with ellipsometry for multiple samples (> 3). Measurements of dry film thicknesses were performed using a custom-built, single-wavelength, phase-modulated ellipsometer at 65° angle of incidence. The refractive indices for the native silicon oxide layer and dry PEG films on a silicon substrate were assumed to be 1.456 and 1.500, respectively.

Electron beam patterning

Patterning was performed under the exposure of electron beam in a FEI Helios scanning electron microscope with Nanometer Pattern Generation System (Nabity) system [30]. This software controlled the properties of the surface-patterned PEG hydrogels by delivering radiative energy in terms of dwell time. The point dose (dose per single microgel) was calculated according to equation: Point dose $D=It$, where I represent the beam current, and t is the dwell time. A Faraday cup was used to measure the electron beam current. We used 3 different incident electron energies: 2 keV, 10 keV and 30 keV. After exposure, the substrates were developed in THF for 20 min to remove un-crosslinked PEG. In order to remove the solvent residues, samples were stored under vacuum (~10^{-3} Torr) for 2 h. Two sets of patterns were designed with DesignCAD. The one with dot arrays of 5 $\times$ 5 gels (3 µm apart) was for gel size measurement. With square fiducial mark outside the arrays of single gels, we can easily define the diameter of single gels by AFM after the solvent development and evaporation. The exposure point doses were from 0.005 to 500 fC. The other pattern was designed as 200 µm ×200 µm squares of dot arrays of also 3 µm apart for protein adsorption experiments and the immunofluorescence assays. For 30 keV we used 5 µm as intergel spacing to better define the backscattering edge because at 3 µm intergel spacing we observed overlap of black region surrounding single gel in the fluorescence assay.

Morphological analysis of PEG microgel

SEM (scanning electron microscope) imaging was done with same FEI Helios Dual-Beam FIB-SEM used to write the microgel patterns with fresh specimen fabricated only for the use of SEM imaging. Quantitative measurements of the gel height using a NanoScope IIIa scanning probe microscope in contact mode (Digital Instruments, Veeco Metrology Group) employed Veeco Nanoprobe tips (model NP-20). When making these height measurements, specimens were mounted in a Digital Instruments liquid cell. Gel heights were first determined from microgels in the dry state. The liquid cell was then filled with deionized water, and measurements of the gel height in the hydrated state were made after equilibrating the specimen in water for approximately 10 min. The AFM imaging force was minimized to limit the deformation of the gels by the AFM tip. Lateral force mode was used in conjunction with topographical mode, and both topographical and lateral force images were generated simutaneously.

Monte-Carlo simulations

A Monte-Carlo simulation based on references [26, 31, 32] was conducted to determine the interaction of incident electrons with PEG films. We modeled film thickness of 120 nm and 200 nm with a density of 1.05 g.cm^{-3} covering a semi-infinite Si substrate impacted at a single point, (0, 0, 0), by as many as 624, 000 electrons (about 100 fC), each with an energy of 2 keV. Single-electron trajectories were followed with decisions of scattering type—elastic or inelastic—scattering angle, and energy change due to electron–nuclei interactions made using a random-number generator weighted by a screened Rutherford elastic cross-section. We accounted for energy deposition using a modified expression for the Bethe stopping power [31, 33]:

$$S = \frac{dE}{dx} = \frac{-78500Z}{AE}\ln\left[\frac{1.166(E+KJ)}{J}\right] \quad (1)$$

where K =0.734$Z^{0.037}$ and S, Z, A, E, and J are the stopping power, atomic number, atomic weight, instantaneous energy, and mean ionization potential, respectively. Individual electron trajectories were followed until the electron energy fell below a threshold of 50 eV or until an electron reached the top surface of the specimen, (x, y, z = 0), where it escaped into the surrounding vacuum. The coordinates of each electron trajectory were recorded in one of the three different arrays: (1) as a primary electron in the PEG film; (2) as a primary electron in the Si; and (3) as an electron backscattered from the Si substrate into the PEG film. Energy deposition in the Si substrate was ignored, since the semi-infinite Si is a good heat sink. Energy deposition in the PEG film was accumulated in 1 nm^3 voxels.

Human fibronectin adsorption on patterned surfaces

Samples were rinsed with PBS buffer. The Fn and antibodies were processed to deposit on the PEG gel patterns as described before [21]. Briefly, patterned surfaces were exposed to human plasma Fn fragments at 37 °C for 2 h with a Fn concentration of 0.1 mg/mL in PBS buffer. Samples were then rinsed 3 times with PBS for 5 min each time. Mouse antihuman primary antibody of 5 µl/mL in PBS was applied to the cleaned surfaces for 30 min at room temperature followed by rinsing with PBS for 3 iterations of 5 min each. The specimens were then immersed in the FITC-conjugated goat anti-mouse secondary antibody (0.1 mg/mL) for 30 min at room temperature. They were then rinsed with PBS for 3 times each for 5 min, the fourth rinse of DI water for 30 s, and finally dried under nitrogen gas stream. Immunofluorescence images were taken immediately after the protein deposition process with a Confocal Laser Scanning Microscopy (Nikon E1000 upright microscope with C1 confocal capabilities).

ACKNOWLEGEMENTS

This project was supported by the U.S. Army Research Office *via* grant W911NF-07-0543 (Y. Wang, E. Firlar, X. Dai and M. Libera). E-beam patterning was done at the Center for Functional Nanomaterials, Brookhaven Nat. Lab. (U.S. DOE, Basic Energy Sciences, Contract #DE-AC02-98CH10886).

REFERENCES

1. Yim EK, Leong KW. Significance of synthetic nanostructures in dictating cellular response. Nanomedicine 2005;1:10-21.
2. Zajtchuk R. New technologies in medicine: biotechnology and nanotechnology. Dis Mon 1999;45:449-95.
3. Murphy J, Carr B, Atkinson T. Nanotechnology in medicine and the biosciences. The UK National Symposium on Nanotechnology in Medicine and the Biosciences, London, UK, 1994. Trends Biotechnol 1994;12:289-90.
4. Patel N, Padera R, Sanders GH, Cannizzaro SM, Davies MC, Langer R, et al. Spatially controlled cell engineering on biodegradable polymer surfaces. FASEB J 1998;12:1447-54.
5. Britland S, Perez-Arnaud E, Clark P, McGinn B, Connolly P, Moores G. Micropatterning proteins and synthetic peptides on solid supports: a novel application for microelectronics fabrication technology. Biotechnol Prog 1992;8:155-60.
6. McDonald JC, Duffy DC, Anderson JR, Chiu DT, Wu H, Schueller OJ, *et al*. Fabrication of microfluidic systems in poly(dimethylsiloxane). Electrophoresis 2000;21:27-40.
7. Khademhosseini A, Langer R, Borenstein J, Vacanti JP. Microscale technologies for tissue engineering and biology. Proc Natl Acad Sci USA 2006;103:2480-7.
8. Russell MT, Pingree LS, Hersam MC, Marks TJ. Microscale features and surface chemical functionality patterned by electron beam lithography: a novel route to poly(dimethylsiloxane) (PDMS) stamp fabrication. Langmuir 2006;22:6712-8.
9. Krsko P, Saaem I, Clancy R, Geller H, Soteropoulos P, Libera M. E-beam-patterned hydrogels to control nanoscale surface bioactivity. Proc SPIE 2005;6002.
10. Krsko P, Libera M. Biointeractive hydrogels. Materials Today 2005;8:36-44.
11. Krsko P, Kaplan JB, Libera M. Spatially controlled bacterial adhesion using surface-patterned poly(ethylene glycol) hydrogels. Acta Biomater 2009;5:589-96.
12. Lussi JW, Tang C, Kuenzi P-A, Staufer U, Csucs G, Vörös J, *et al*. Selective molecular assembly patterning at the nanoscale: a novel platform for producing protein

patterns by electron-beam lithography on SiO2/indium tin oxide-coated glass substrates. Nanotechnology 2005;16.

13. Burkert S, Schmidt T, Gohs U, Mönch I, Arndt K-F. Patterning of thin poly(N-vinyl pyrrolidone) films on silicon substrates by electron beam lithography. J Appl Polym Sci 2007;106:534-9.
14. Lee BM, Kang DW, Jung CH, Choi JH, Hwang IT, Hong SK, *et al*. Patterning of polymer nanocomposite resists containing metal nanoparticles by electron beam lithography. J Nanosci Nanotechnol 2011;11:7390-3.
15. Saaem I, Tian J. E-Beam nanopatterned photo-responsive bacteriorhodopsin-containing hydrogels. Adv Mater 2007;19:4268-71.
16. Hong Y, Krsko P, Libera M. Protein surface patterning using nanoscale PEG hydrogels. Langmuir2004;20:11123-6.
17. Krsko P, McCann TE, Thach TT, Laabs TL, Geller HM, Libera MR. Length-scale mediated adhesion and directed growth of neural cells by surface-patterned poly(ethylene glycol) hydrogels. Biomaterials 2009;30:721-9.
18. Christman KL, Schopf E, Broyer RM, Li RC, Chen Y, Maynard HD. Positioning multiple proteins at the nanoscale with electron beam cross-linked functional polymers. J Am Chem Soc 2009;131:521-7.
19. Kolodziej CM, Chang C-W, Maynard HD. Glutathione S-transferase as a general and reversible tag for surface immobilization of proteins. J Mater Chem 2011;21:1457-61.
20. Broyer RM, Schopf E, Kolodziej CM, Chen Y, Maynard HD. Dual click reactions to micropattern proteins. Soft Matter 2011;7:9972-7.
21. Krsko P, Sukhishvili S, Mansfield M, Clancy R, Libera M. Electron-beam surface-patterned poly(ethylene glycol) microhydrogels. Langmuir 2003;19:5618-25.
22. Nan Yao ZW, editor. Handbook of microscopy for nanotechnology: Springer - Verlag; 2005.
23. Hay MB, Workman RK, Manne S. Mechanisms of metal ion sorption on calcite: Composition mapping by lateral force microscopy. Langmuir 2003;19:3727-40.

24. Noy A, Sanders CH, Vezenov DV, Wong SS, Lieber CM. Chemically-sensitive imaging in tapping mode by chemical force microscopy: relationship between phase lag and adhesion. Langmuir 1998;14:1508-11.
25. Rozsnyai LF, Wrighton MS. Selective electrochemical deposition of polyaniline *via* photopatterning of a monolayer-modified substrate. J Amer Chem Soc 1994;116:5993-4.
26. Dai X, Yang W, Firlar E, Marras SAE, Libera M. Surface-patterned microgel-tethered molecular beacons. Soft Matter. 2012, in press.
27. Banerjee I, Pangule RC, Kane RS. Antifouling coatings: recent developments in the design of surfaces that prevent fouling by proteins, bacteria, and marine organisms. Adv Mater 2011;23:690-718.
28. Zheng J, Li L, Tsao H-K, Sheng Y-J, Chen S, Jiang S. Strong repulsive forces between protein and oligo (Ethylene Glycol) self-assembled monolayers: a molecular simulation study. Biophys J 2005;89:158-66.
29. Claxton NS, Fellers TJ, Davidson MW. Microscopy, Confocal. Encyclopedia of medical devices and instrumentation: John Wiley & Sons, Inc.; 2006.
30. Nabity JC. NPGS Lithography Systems, PO Box 5354, Bozeman, MT 59717 USA, (406-587-0848), jcnabity@aol.com.
31. Eades A. Monte Carlo modeling for electron microscopy and microanalysis, by D. C. Joy. Oxford University Press, Microscopy Research and Technique. 1996;35:413.
32. Shimizu R, Ze-Jun D. Monte Carlo modelling of electron-solid interactions. Rep Prog Phys 1992;55:487-531.
33. Han G, Khan M, Fang Y, Cerrina F. Comprehensive model of electron energy deposition. J Vac Sci Technol. 2002;20:2666-2671.

Chapter 3

Length-Scale Mediated Differential Adhesion of Mammalian Cells and Microbes

Reproduced with permission of Wiley VCH from: Yi Wang, Guruprakash Subbiahdoss, Jan Swartjes, Henny C. van der Mei, Henk J. Busscher, and Matthew Libera, Advanced Functional Materials 2011:21:3916-23

ABSTRACT

Surfaces of implantable biomedical devices are increasingly engineered to promote their interactions with tissue. However, surfaces that stimulate desirable mammalian cell adhesion, spreading, and proliferation also enable microbial colonization. The biomaterials-associated infection that can result is now a critical clinical problem. We have identified an important mechanism to create a surface that can simultaneously promote healing while reducing the probability of infection. We created surfaces with submicron-sized, non-adhesive microgels patterned on an otherwise cell-adhesive surface. Quantitative force measurements between a staphylococcus and a patterned surface show that the adhesion strength decreases significantly at inter-gel spacings comparable to bacterial dimensions. Time-resolved flow-chamber measurements show that the microbial deposition rate dramatically decreases at these same spacings. Importantly, the adhesion and spreading of osteoblast-like cells is preserved despite the sub-cellular non-adhesive surface features. Since such length-scale-mediated differential interactions do not rely on antibiotics, this mechanism can be particularly significant in mitigating biomaterials-associated infection by antibiotic-resistant bacteria such as MRSA.

INTRODUCTION

Restoration of human function using implantable biomedical devices and prostheses is indispensable to modern medicine, and the surfaces of modern biomaterials are now highly engineered to regulate their interactions with physiological systems. However, many of the same surface properties that influence mammalian cell interactions also enable bacterial adhesion (Figure 1A). The subsequent biomaterials-associated-infection that can occur is now recognized as a major clinical problem. When bacteria win the race with mammalian cells to colonize an implant surface [1-4], they can develop into biofilms where they are both extremely resistant to antibiotics and able to evade the host immune system [5-9]. While antibiotics can mitigate the short-term symptoms of systemic infection, they are usually unable to resolve the localized biomaterials-associated infection. In such cases, the implant is removed, the infection is resolved over periods of week to months, and a revision surgery, with a higher probability of re-infection, is performed in a site with less native tissue [10-12]. Biomaterials-associated infection is a concern with all biomedical devices that contact tissue and is usually assumed as a given in cases involving, for example, long-term percutaneous structures or serious trauma involving large and contaminated wounds. The general problem is being increasingly exacerbated by the growing preponderance of antibiotic-resistant bacteria and the concomitant decline of new antibiotic development [13, 14].

Surface modification to mitigate bacterial colonization has largely followed one of two routes. The first incorporates antimicrobials by various drug-delivery mechanisms [15-17]. Such an approach, however, must determine *a priori* the appropriate antimicrobial and often delivers it when not needed, thus promoting antibiotic resistance. Consequently there is a growing focus on alternatives involving, for example, metal ions, cationic peptides, and quorum-sensing targets. A second route concentrates on the modification of the surface itself, much of which has focused on antifouling coatings. Among these, surfaces that incorporate poly(ethylene glycol) [PEG] have been extensively studied because of their ability to resist both protein adsorption and cell adhesion [18, 19]. These

have served as a model for the development of other highly hydrophilic non-adhesive and multi-functional surfaces [20-23]. Such surfaces protect against microbial colonization, but they also resist mammalian cell adhesion (Figure 1B). Thus, while they can mitigate biomaterials-associated infection, they simultaneously compromise healing.

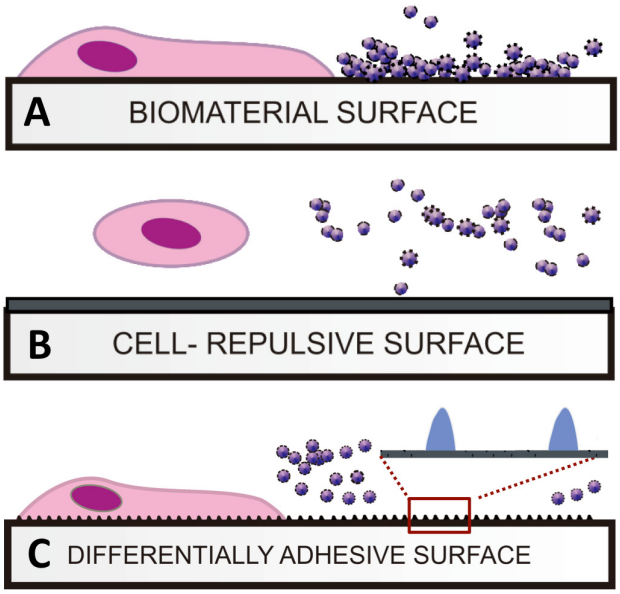

Figure 1 (A) Both mammalian cells and microbes can adhere to a fully cell-adhesive biomaterial surface; (B) Neither mammalian cells nor microbes can adhere to a fully non-adhesive biomaterial coating; (C) A surface patterned with submicron-sized, non-adhesive features on an otherwise cell-adhesive surface can enable mammalian-cell adhesion but reduce microbial adhesion due to their smaller size.

A fundamental problem in biomaterials science centers on how to create surfaces that differentially interact with different cell types. In the case of biomaterials-associated infection, this problem sharpens to the question of how to create a surface that differentially promotes interactions with desirable mammalian cells while simultaneously inhibiting microbial colonization [24, 25]. Significantly, there are important physico-chemical differences between mammalian cells and bacteria around which differentially interactive surfaces can be designed. For example, mammalian cells, such as osteoblasts, are typically 10-100 µm in diameter, have flexible cell membranes that can conform to a

substratum, and adhere to surfaces through multiple, integrin-mediated submicron-sized focal contacts [26]. In contrast, microbes have well-defined shapes and are a few micrometers or less in size. In particular, the staphylococci most often implicated in biomaterials-associated infection – *Staphylococcus epidermidis* and *Staphylococcus aureus* - are spherically shaped with diameters of about 1 μm and have relatively rigid cell walls. Combining these differences with emerging concepts of surface patterning and compartmentalization [27, 28], we hypothesize that a surface whose cell adhesiveness is laterally modulated at microscopic length scales will enable mammalian cell adhesion while reducing microbial adhesion (Figure 1C). Using a combination of electron-beam surface patterning, quantitative staphylococcal-surface adhesive force measurement, and *in situ* characterization of microbe/osteoblast surface colonization, we show this hypothesis to be true: laterally modulated adhesiveness significantly reduces microbial colonization, in the absence of antibiotics, when the spacing between non-adhesive features is comparable to microbial dimensions (1-2 μm), while osteoblast-like cells can nevertheless adhere to and spread over these surfaces. Such a differentially adhesive surface is one that can promote healing while simultaneously reducing the risk of infection.

RESULTS AND DISCUSSION

Surface-patterned PEG gels

To test the concept of length-scale-mediated differential adhesion, we created submicron-sized PEG hydrogels patterned in square arrays on an otherwise cell-adhesive substratum. We assessed the response of various microbes and an osteoblast-like cell line to these as a function of inter-gel spacing, δ. Focused electron beams (e-beams) can locally crosslink PEG films to form surface-bound microgels [29-31]. We have shown that such gels resist nonspecific protein adhesion [30, 31] as well as the adhesion of *S. epidermidis* [32], astrocytes, and neurons [33]. We have also previously shown that the exposed surface between microgels remains adhesive to protein adsorption [31, 33]. Because of the flexibility afforded by e-beam patterning, the spatial distribution of these discrete microgels can be easily varied. Figure 2A shows atomic force microscopy (AFM) images of

surface-patterned PEG microgels in the dry and hydrated states for three intergel spacings (δ = 0.5, 1.5, and 3.0 μm). When hydrated, each microgel is about 400 nm in diameter and about 120 nm in height. They swell from the dry state by a factor of about 2, primarily in the direction perpendicular to the substratum. Importantly, the irradiation conditions used to create each microgel are identical, so their size and swelling behaviour are very reproducible.

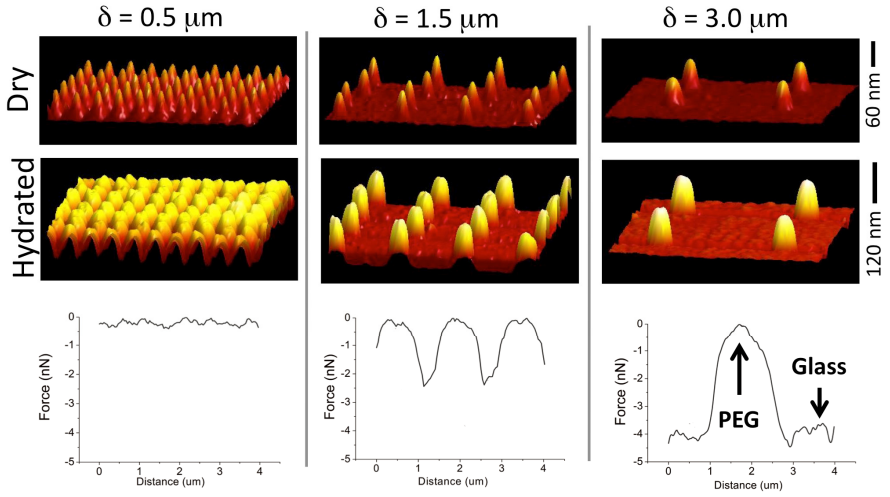

Figure 2 Surface-patterned PEG microgels modulate the adhesion force experienced by an individual *S. aureus* bacterium. AFM images (upper) of patterned surfaces in the dry and hydrated states for three inter-gel spacings (δ). These images were collected in non-contact mode using a Si_3N_4 tip. The surfaces were hydrated in PBS buffer. The lower plots show examples of the spatially resolved adhesion force between a *S. aureus* bacterial probe and the three patterned surfaces. The adhesion force is minimal for δ = 0.5 μm and develops a substantial spatial dependence as δ is increased to dimensions comparable to or larger than the size of an individual bacterium.

By immobilizing bacteria on an AFM cantilever in place of a typical Si or Si_3N_4 AFM tip, an atomic force microscope was used to measure the adhesion force that an *S. aureus* bacterium feels as it interacts with a silanized glass surface modulated by PEG microgels. The probe was made by adhering *S. aureus* to a poly-L-lysine-treated AFM cantilever. In contrast to a typical AFM tip, this bacterial tip is substantially larger and provides a

biochemical interaction of bacterial origin. Single-bacterium probes were rastered across patterned surfaces, and the adhesion force was determined at each point in the raster. Figure 2 (lower plots) illustrates the adhesion force as a function of lateral distance for surfaces with δ = 0.5, 1.5, and 3.0 μm. The force is negligible between the bacterium and the PEG microgels, consistent with the non-adhesive characteristics of highly hydrated PEG. The magnitude of the adhesive force increases between the gels. The maximum force is tabulated in Table I as a function of inter-gel spacing. It is lowest for δ = 0.5 μm where the individual gels almost overlap. In this case, the bacterium is shielded from the glass surface by the intervening PEG. As δ increases, the maximum adhesion force increases. For δ between 1.0 and 1.5 μm, the adhesion force increases substantially. It further increases as δ increases to 3.0 μm. This finding confirms that: (i) an individual bacterium experiences an adhesive interaction with the patterned substrates despite the non-adhesive features; and (ii) the magnitude of the adhesive interaction increases as the spacing between the non-adhesive features increases.

Table 1 Maximum adhesion force of *S. aureus* on patterned glass surfaces with different inter-gel spacing (δ). Each data point represents the average ± the standard deviation from at least nine values of maximum and minimum adhesive force.

Inter-gel spacing (μm)	0.5	1.0	1.5	2.0	2.5	3.0
Adhesion Force (nN)	-0.04 ± 0.04	-0.3 ± 0.0	-2.2 ± 0.2	-2.8 ± 0.3	-2.5 ± 0.8	-3.6 ± 0.3

Microbial adhesion

We used a parallel-plate flow chamber to measure the initial deposition rate of various microbes. Glass slides were prepared with square arrays of patterned gels, each array having a fixed δ. Triplicate arrays with δ ranging from 0.5 μm to 8 μm were patterned on the same substratum. Thus, the interactions of a given microbe with a range of patterns could be evaluated in a single flow-chamber experiment. Inocula with fixed microbial concentrations were passed over the surface for 3 h, and we measured the number of adhering bacteria on each patterned array as a function of time. Nutrient-free media were used to isolate microbial adhesion from growth.

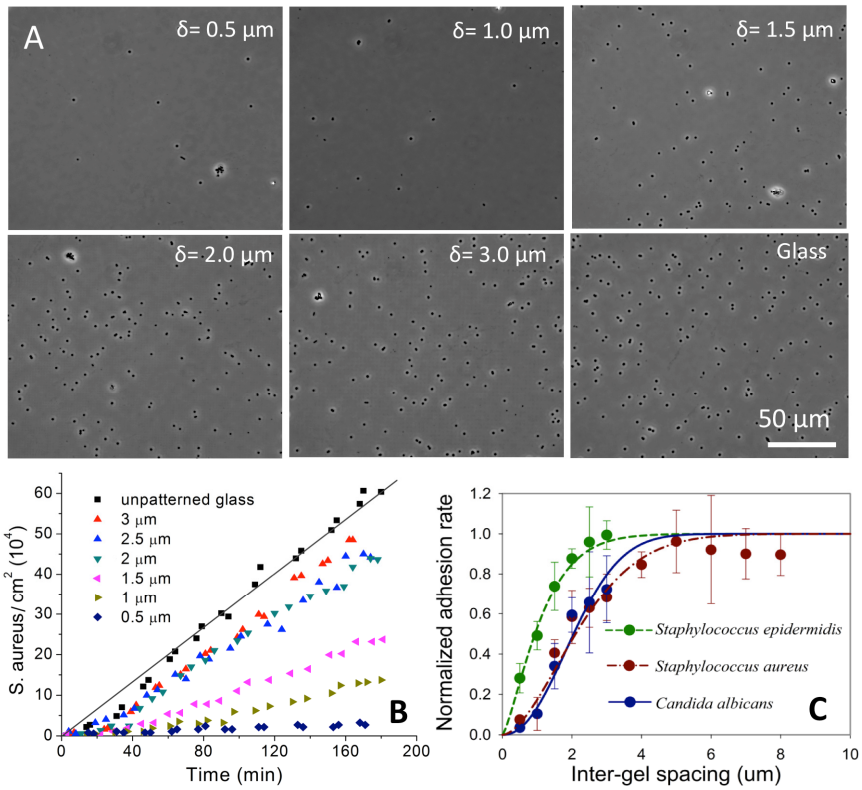

Figure 3 The microbial deposition rate decreases as δ approaches microbial dimensions. (A) Representative optical micrographs of *S. aureus* adhered to various surfaces after 180 min deposition time from an inoculum of 3x10^6 bacteria/mL at a shear rate of 11/s. (B) The number of adhering *S. aureus* increases linearly with time for a given δ. The solid line is a linear least squares fit to one data set. (C) A Weibull model (lines) of normalized microbial deposition rate shows that surfaces with cell adhesiveness laterally modulated over microscale distances resist microbial adhesion. Each data point represents the average, and the error bars represent the standard deviation, of slopes of linear least squares fits to data from three independent bacterial culture experiments.

Typical image data are presented in Figure 3A for *S. aureus* adhesion after 180 min. Note that the bacteria appear primarily as individuals rather than as multi-bacteria clusters. Figure 3B plots the number of adherent bacteria per unit area over 180 min. For all inter-gel spacings, the number of adhering *S. aureus* increases linearly with time, indicating that the surface fraction covered by bacteria remains small during the experiment. Interactions

between incoming and adhering bacteria can thus be neglected. We determined the initial deposition rate from the slope of straight lines fit to such data (Figure 3B). The initial deposition rate on the unpatterned glass surface, $j_{o,glass}$, was always the highest. The deposition rate on a surface with a particular inter-gel spacing, $j_{o,\delta}$, decreased as δ decreased. For a given microbial species, we defined a normalized initial deposition rate as:

$$F(\delta) = \left[\frac{j_{o,\delta}}{j_{o,glass}} \right] \quad (1)$$

Normalized rates are presented in Fig. 3C. We used a cumulative Weibull function to model these rates as a function of inter-gel spacing according to:

$$F(\delta) = 1 - \exp\left[-\left(\frac{\delta}{\alpha} \right)^{\beta} \right] \quad (2)$$

The solid lines (Figure 3C) represent Weibull fits, and Table II reports values of α and β for the three data sets. The Weibull function has historically been used to model statistical phenomena associated with random events, most notably for instances of failure in engineered systems, and it provides two parameters, α and β, which give further insight into the microbial adhesion process. The scale parameter, α, represents the δ value at which the initial deposition rate is 63.2% of that for unpatterned glass. The different α values indicate that *S. aureus* and *C. albicans* are affected more strongly by the gels than *S. epidermidis*. The shape factor, β, exceeds 1 for all three microbes, consistent with our finding that the deposition rates increase with increasing δ. The fact that β is close to 2 is consistent with the idea that the adhesion rate is related to the available area of adhesive surface, since from eq. [2] it follows that $j_{o,\delta} \approx (\delta/\alpha)^{\beta}\ j_{o,glass}$. Deviations from β=2 again indicate species-specific differences in the nature of the microbe-surface adhesive interaction.

Table 2 The initial deposition rates on unpatterned glass of the different microbial strains, together with Weibull scale (α) and shape (β) factors describing initial deposition rates on patterned surfaces as a function of inter-gel spacing.

Microbial strain	$j_{o,\,glass}$ ($cm^{-2}\,sec^{-1}$)	α (μm)	β
S. epidermidis	15 ± 3	1.2 ± 0.2	1.3 ± 0.06
S. aureus	46 ± 20	2.6 ± 0.2	1.7 ± 0.02
C. albicans	76 ± 35	2.4 ± 0.2	2.2 ± 0.1

Mammalian cell adhesion and spreading

We studied surface interactions with an osteoblast-like cell line (U2OS) in the same flow-chamber system in which the microbial studies were performed. U2OS is an immortalized human cell line derived from osteosarcoma cells [34] and was chosen from a broad selection of human osteoblastic cell lines used previously [4, 35]. Though there are well-known differences between cancerous and primary osteoblastic cells, Clover *et al*. [36] have demonstrated that osteosarcoma cell lines exhibit meaningful osteoblastic phenotypes. For our experiments, these mammalian cells were suspended in culture medium to enable both adhesion and spreading. After a deposition period of 1.5 h to allow for static U2OS binding, cell-free medium was passed through the chamber. Our analysis concentrated on 1.5 h and 48 h to assess the initial adhesion and cell spreading, respectively. Figure 4 shows typical image data'' demonstrating the very different U2OS behaviour when interacting with surfaces patterned with microgels at different inter-gel spacings. The cells clearly adhere to the surrounding unpatterned surface. They are completely absent from surface with δ = 0.5 μm. SEM imaging (Figure 5A) confirms this behavior and further illustrates that U2OS cells spread nicely on adjacent unpatterned surface.

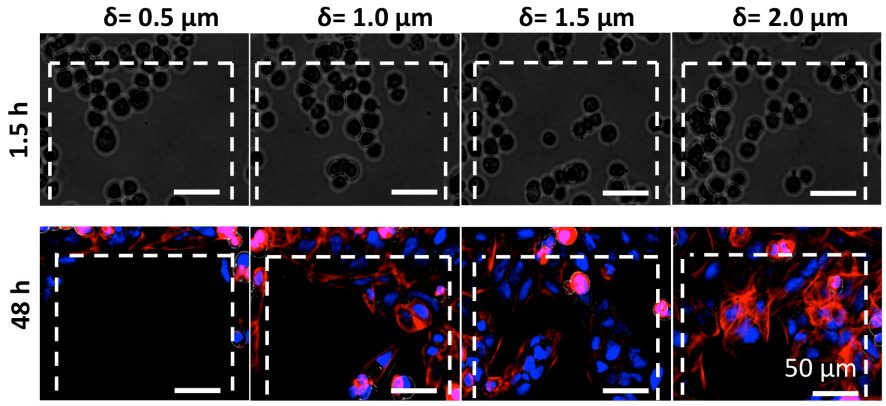

Figure 4 Osteoblast-like U2OS cells are able to adhere and spread on microgel-patterned surfaces with an inter-gel spacing of 1.0 µm or more.
Top: phase-contrast microscope images collected *in situ* during cell culture within a flow chamber; Bottom: fluorescent microscope images showing the nuclei (blue) and cytoskeletal actin (red).

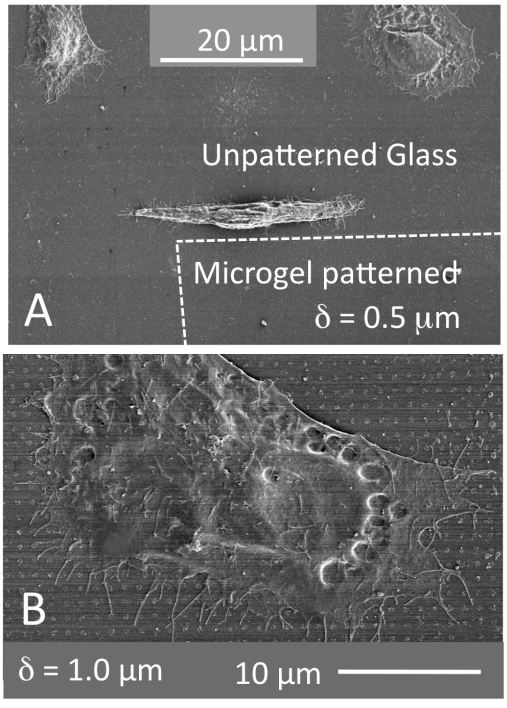

Figure 5 Scanning electron micrographs showing that osteoblast-like U2OS cells are able to (A) adhere and spread on unpatterned glass but not on microgel-patterned surface with an inter-gel spacing of δ=0.5 µm located in the right bottom corner of this micrograph; and (B) adhere and spread on microgel-patterned surface with an inter-gel spacing of δ=1.0 µm despite the presence of non-adhesive PEG microgels at sub-cellular length scales. Note that lamellapodia extend over and between non-adhesive microgels to reach the adhesive glass surface.

A significant number of cells can be seen on the patterned δ = 1 μm surface (Figure 4) for both 1.5 and 48 h. SEM imaging (Figure 5B) shows that the cells are able to grow and spread over the non-adhesive microgels.

Time-resolved measurements further capture the dynamics of mammalian-cell interactions with the various surfaces. Fig. 6A describes the number of adhering U2OS cells as a function of δ after 1.5 and 48 h. At 1.5 h, we calculated the number of cells and total coverage of cells from the phase contrast images. Whereas at 48 h, the number of cells and surface coverage of adhering U2OS cells were obtained from fluorescent stained CLSM images. The number of cells decreases with time for δ = 0.5 μm, indicating that the cells have a high motility on this surface and migrate to the adjacent unpatterned surface. In contrast, the number of cells on the δ = 1.0 μm surface remains high after 48 h. The effect is even more pronounced for surfaces with δ = 1.5 μm and above, indicating that both the fraction of adhesive area and its spatial distribution are sufficient to promote stable cell adhesion. Note that the number of cells per unit area on unpatterned and patterned surfaces with $\delta \geq 1$ μm do not change significantly over 48 h indicating that only cell spreading and no proliferation takes place during this time period. Data on the area fraction of the patterned square arrays covered after 1.5 h and 48 h (Figure 6B) provide insight into the spreading behaviour. The fraction for δ = 0.5 μm decreases with time, because the cells migrate away from this surface. For larger δ, however, the fraction covered increases significantly with time despite the fact that the number of cells does not change (Figure 6B). This finding indicates that the cells spread on these surfaces, and, for δ = 1.5 μm or more, do so in a manner similar to that on unpatterned surface.

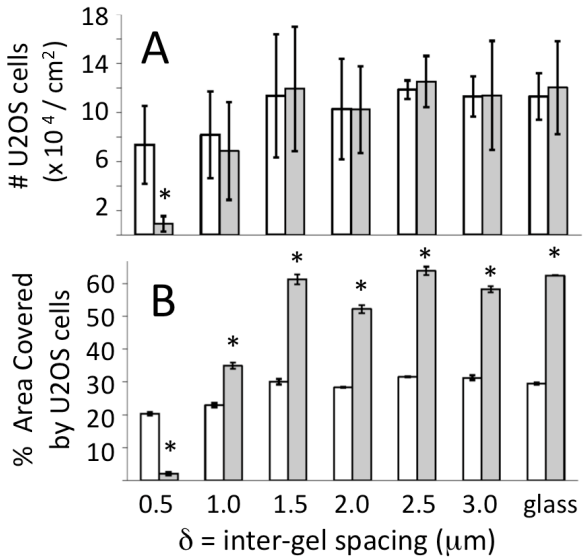

Figure 6 Osteoblast-like U2OS cells adhere to and spread on surfaces with $\delta \geq 1$ μm: (A) the number of adhering U2OS cells 1.5 h (white) and 48 h (grey) after seeding; and (B) the percent surface coverage by adhering U2OS cells immediately after seeding at 1.5 h (white) and after 48 h (grey) of growth on gel-patterned glass. *Indicates a significant difference ($p<0.05$) from 1.5 h.

Our findings that osteoblast-like cells are able to adhere to a surface with modulated adhesiveness are consistent with a number of studies showing similar results involving different mammalian cells and different patterning methods. For example, Chen *et al*. [37] used soft lithography to pattern circular fibronectin patches 5 μm in diameter and separated from each other by PEGylated thiols at inter-patch distances of 10 μm. Fibroblasts could adhere to these modulated surfaces and cellular vinculin was co-localized with the patterned fibronectin, indicating that focal adhesions could form on the adhesive patches and the cells could bridge the intervening non-adhesive regions. More recently, Spatz *et al*. [38, 39] have studied the dynamics of integrin-mediated mammalian-cell binding and focal-contact formation on surfaces with nanoscale modulations of adhesiveness provided by RGD-functionalized gold nanoparticles in clusters of controllable size and spacing on an otherwise non-adhesive surface. Despite the fact that these

experimental configurations are the inverse of ours i.e. adhesive patches on a largely non-adhesive background rather than non-adhesive patches on an adhesive background, this and other work [40-43] again clearly demonstrates that mammalian cells are able to efficiently bind to 2-D surfaces with sub-cellular modulations of adhesiveness.

Length-scale mediated differential adhesion

We have studied both mammalian cell and microbe response to surfaces intermediate between the two extremes of fully adhesive and fully repulsive. Our experimental platform provides for a controllable area fraction and spatial distribution of non-adhesive microgels on an otherwise cell-adhesive surface. We attribute the differential response exhibited by these mammalian cells and microbes to differences in their size, their adhesion mechanism(s), and the relative mechanical rigidity/fluidity of bacterial cell walls and mammalian cell membranes.

Flow-chamber measurements indicate that microbial adhesion is very strongly reduced when the spacing between microgels is approximately 1.5 μm or less. AFM force measurements show that this spacing is a critical one, below which the adhesion force between the surface and an individual bacterium substantially decreases. Staphylococci are approximately 1 μm in diameter and spherical, and they have highly crosslinked and relatively rigid cell walls. The fact that staphylococcal adhesion decreases substantially when they sense non-adhesive features at spacings comparable to their own dimension is consistent with the idea that reconfiguring their shape to better access exposed patches of cell-adhesive surface is energetically unfavorable. Interestingly, *Candida albicans* exhibits similar adhesive behavior despite the fact that it is physically larger than *S. epidermidis* and *S. aureus* and could be perhaps expected to show a decreased adhesion rate at correspondingly larger microgel spacings. We attribute this behavior to the fact that the surface of *C. albicans* is decorated with cell surface structures [44] that afford a degree of conformational flexibility and an adhesion mechanism unavailable to staphylococci.

Significantly, we find that osteoblast-like cells can adhere to and spread on surfaces with microgels patterned at inter-gel spacings of 1 μm or more, including the range where staphylococcal adhesion is substantially reduced. In contrast to the highly crosslinked cell walls of Gram-positive bacteria, the membranes of mammalian cells are highly fluid. Furthermore, such cells adhere to surfaces via clusters of transmembrane integrins that ultimately develop into focal contacts and focal adhesions whose dimensions can be in the range of tens to hundreds of nanometers. Consistent with published reports establishing mammalian cell adhesion and spreading on surfaces with modulated adhesiveness, we speculate that the osteoblast-like cells studied are able to adhere to the adhesive patches in between non-adhesive microgels by sub-micron focal contacts/adhesions. The energetic price to extend cell membranes over the nonadhesive microgels is apparently insufficient to prevent adhesion except in the case of microgels spaced at 0.5 μm intervals, which corresponds to a pseudo-continuous PEG film.

The finding of length-scale-mediated differential cell adhesion is important, because it is a non-specific mechanism by which a surface can differentially interact with different types of cells. By reducing the probability of microbial adhesion, such a surface can both minimize biofilm formation and force bacteria at a wound site to reside planktonically where they can be effectively cleared by the innate immune system. In the particular case of osteoblast-like mammalian cells and staphylococci, this finding has important technological implications for a broad range of orthopedic implant materials, which must promote tissue integration necessary for healing while simultaneously reducing the bacterial colonization that leads to infection.

MATERIALS AND METHODS

PEG hydrogel surface patterning

Patterned glass slides were prepared using established procedures [31, 45]. Slides were sonicated in ethanol for 5 min and dried with N_2 gas. Piranha etch (3:1 98% sulphuric acid and 30% H_2O_2) was used for a second cleaning. After a water rinse and N_2 dry, the slides

were exposed to an O_2 plasma (300 mTorr, 1.75 W) for 10 min and silanized with 2% [v/v] vinyl-methoxy siloxane (Gelest) in ethanol for 10 min, rinsed with ethanol and baked at 110°C (2 h). A solution of 2 wt% PEG (6 kDa; Fluka) in tetrahydrofuran was used to make thin films by spin casting on these slides. The film thickness after solvent evaporation was ~60 nm.

E-beam patterning used an FEI Helios SEM controlled by a Nanometer Pattern Generation System (Nabity). A typical point dose (dose per single microgel) was 10 fC (2 keV) to locally crosslink the PEG. The crosslinking of PEG under such e-beam irradiation has been attributed to a free-radical polymerization mechanism after ionization of C-H bonds [[27, 45]]. After exposure, the slides were washed in de-ionized water (30 min) to remove unexposed PEG. The resulting surface consisted of surface-bound microgels separated from each other by silanized glass. Patterns were made as 200 µm × 200 µm microgel arrays. Within a given array, δ was fixed. Three identical copies with a particular δ were created on each substratum. Arrays sampling inter-gel spacings from 0.5 - 8 µm were patterned on the same substratum. Each array was separated from an adjacent array by 100 µm. After patterning, substrata were stored under vacuum (50 mTorr). Prior to adhesion experiments, the substrates were placed in phosphate buffered saline (PBS) for at least 30 min.

Experiments with bacteria and yeast

Bacterial inoculum

Two different staphylococcal strains were used: *S. aureus* ATCC 12600 and *S. epidermidis* ATCC 35983. For each flow-chamber experiment a colony from an agar plate was inoculated into 10 mL of tryptone soya broth (TSB), cultured for 24 h at 37 ºC, and used to inoculate a second culture grown for 17 h in 200 mL TSB. Bacteria were harvested by centrifugation (6500 g) for 5 min at 10 ºC and washed twice in sterile phosphate-buffered saline (PBS; 10 mM potassium phosphate and 0.15 M NaCl, pH 7). Bacterial aggregates were broken by mild sonication on ice for 3 × 10 s at 30 W (Wibra Cell model 375, Sonics

and Materials Inc., Danbury, Connecticut, USA) and then resuspended to a concentration of 3×10^6 bacteria/mL in sterile PBS.

Yeast cell inoculum

Candida albicans GB1/2 yeast cells were used. A colony from a brain heart infusion (BHI) agar plate was inoculated in 10 mL BHI, cultured for 24 h at 37 ^{o}C, and used to inoculate a second culture grown for 17 h in 200 mL BHI. Yeast cells were harvested by centrifugation (5000 g) for 5 min at 10 ^{o}C and washed twice in sterile PBS. The harvested cells were resuspended in 10 mL sterile PBS and diluted to 3×10^6 cells/mL in PBS.

Time-resolved microbial adhesion

Microbial adhesion was studied by incorporating patterned slides into a parallel-plate flow chamber [4]. Microbial deposition was monitored by digital phase-contrast microscopy (Olympus BH-2; 40x). After removing air bubbles by flowing PBS, bacteria or yeast cells in PBS were perfused through the chamber (11 s^{-1} shear rate) for 3 h at room temperature. Images were taken from each patterned array, and from the unpatterned silanized glass (control), at 1 min intervals. From these, the number of adhering bacteria or yeast on each array was determined. Since yeast tended to sediment, the yeast inoculum reservoir was gently stirred.

Mammalian cell experiments

Mammalian cell culturing and harvesting

U2OS osteosarcoma cells were cultured in low-glucose Dulbecco's Modified Eagles Medium (DMEM) supplemented with 10% fetal calf serum (FBS) and 0.2 mM of ascorbic acid-2-phosphate. U2OS cells were maintained in T75 culture flasks at 37 ^{o}C in humidified 5% CO_2 and harvested at 90% confluency using trypsine/ethylenediamine–tetraacetic acid. The harvested cells were diluted to 6×10^5 cells/mL.

Time-resolved mammalian cell adhesion

U2OS adhesion and spreading on patterned substrata were studied by *in situ* imaging in the parallel-plate flow chamber and by *ex situ* immunofluorescence/SEM imaging. The flow chamber was kept at 37 °C. Once fully filled and bubble free, a U2OS cell suspension in modified medium (DMEM + 10% FBS and 2% TSB [4]) was introduced. After filling the chamber, flow was stopped (1.5 h) to allow for U2OS adhesion. Modified culture medium supplemented with 2% HEPES buffer was then flowed at 0.14 s^{-1} shear rate for 48 h. Phase-contrast images were taken from each patterned array and from the silanized-glass control at 1.5 h to determine the number of adhering cells per unit area and total surface coverage of spread U2OS cells. Statistical analysis of variance used Tukey's HSD post hoc test and a p-value of <0.05 was considered significant.

After 48 h the substratum was removed. Substrata were fixed in 30 mL of 3.7% formaldehyde in cytoskeleton stabilization buffer (CS; 0.1 M Pipes, 1 mM EGTA, 4% (w/v) PEG 8000, pH 6.9). After 5 min, this fixation step was repeated. Slides were then incubated in 0.5% Triton X-100 (3 min), rinsed with PBS, and stained for 30 min in 5 mL PBS containing 49 µL DAPI and 2 µg/mL of TRITC–Phalloidin. After 4x wash in PBS, the slides were examined by fluorescence microscopy (Leica DM 4000B). The number of adhering cells per unit area and the total surface coverage of adhered cells on the patterned surface were determined using Scion image software. To further visualize cell morphology after 48 h, cells were fixed with 2% glutaraldehyde in 0.1 M cacodylate buffer, post fixed with OsO_4 (1% in 0.1 M cacodylate buffer) for 1 h and dehydrated using an ethanol series. Cells were incubated in tetramethylsilane for 15 min, air dried and sputter coated with Au/Pd. Secondary electron imaging was done using a JEOL JSM 6301F SEM at 2 kV.

AFM force measurement

Bacterial probe preparation

S. aureus ATCC 12600 was immobilized on tipless V-shaped cantilevers (VEECO, DNP-0) via electrostatic interaction with poly-L-lysine (PLL). A drop of PLL solution was placed on a

glass slide and the tip of the cantilever was dipped in the droplet for 1 min. After air drying, the cantilever was dipped in bacterial suspension (1 min). Bacterial probes were freshly prepared for each experiment. The bacterial probes usually yielded single-cell contact with a substratum. Images with double contour lines indicated double cell contacts, and a probe exhibiting such behavior was discarded. Each patterned surface was interrogated by at least nine different *S. aureus* bacterial AFM probes. Three probes were made from each of three different cultures of *S. aureus*.

Atomic force microscopy

Force measurements were done at room temperature in PBS (pH 7) using a Bioscope Catalyst AFM with PeakForce^{TM} Quantitative NanoMechanical Mapping software (Bruker). Each curve was analyzed to produce the maximum adhesion force as the control feedback signal and the mechanical properties of the sample (Adhesion, Modulus, Deformation, and Dissipation). By collecting data from different specimen locations, comparative values were derived by subtracting the most adhesive (glass) and most repulsive (gel). Calibration of bacterial probes was done using by thermal tuning to yield spring constants of 0.044 ± 0.008 Nm^{-1}.

ACKNOWLEDGEMENTS

We thank Joop de Vries (W.J. Kolff Institute, University Medical Center Groningen, The Netherlands) for assisting with the AFM force measurements. Y. Wang and M. Libera thank the U.S. Army Research Office for support (grant W911NF-07-0543). E-beam patterning was done at the Center for Functional Nanomaterials, Brookhaven Nat. Lab. (U.S. DOE, Basic Energy Sciences, Contract #DE-AC02-98CH10886).

REFERENCES

1. Gristina AG, Hobgood CD, Webb LX, Myrvik QN. Adhesive colonization of biomaterials and antibiotic resistance. Biomaterials 1987;8:423-6.
2. Lee JH, Wang H, Kaplan JB, Lee WY. Effects of *Staphylococcus epidermidis* on osteoblast cell adhesion and viability on a Ti alloy surface in a microfluidic co-culture environment. Acta Biomater 2010;6:4422-9.
3. Subbiahdoss G, Kuijer R, Busscher HJ, Van der Mei HC. Mammalian cell growth *versus* biofilm formation on biomaterial surfaces in an in vitro post-operative contamination model. Microbiology 2010;156:3073-8.
4. Subbiahdoss G, Kuijer R, Grijpma DW, Van der Mei HC, Busscher HJ. Microbial biofilm growth *vs.* tissue integration: "the race for the surface" experimentally studied. Acta Biomater 2009;5:1399-404.
5. Bryers JD. Medical biofilms. Biotechnol Bioeng 2008;100:1-18.
6. Costerton JW, Stewart PS, Greenberg EP. Bacterial biofilms: A common cause of persistent infections. Science 1999;284:1318-22.
7. Hall-Stoodley L, Costerton JW, Stoodley P. Bacterial biofilms: From the natural environment to infectious diseases. Nat Rev Microbiol 2004;2:95-108.
8. Mah T-FC, O'Toole GA. Mechanisms of biofilm resistance to antimicrobial agents. Trends Microbiol 2001;9:34-9.
9. Sauer K, Rickard AH, Davies DG. Biofilms and biocomplexity. Microbe 2007;2:347-53.
10. Campoccia D, Montanaro L, Arciola CR. The significance of infection related to orthopedic devices and issues of antibiotic resistance. Biomaterials 2006;27:2331-9.
11. Engelsman AF, Saldarriaga-Fernandez IC, Nejadnik MR, Van Dam GM, Francis KP, Ploeg RJ, *et al*. The risk of biomaterial-associated infection after revision surgery due to an experimental primary implant infection. Biofouling 2010;26:761-7.
12. Tetsworth K, Dennis J. Contemporary management of infected total knee replacement. Curr Orthopaed Pract 2008;19:175-80.
13. Douthwaite S. Designer drugs for discerning bugs. Proc Nat Acad Sci U S A 2010;107:17065-6.

14. Projan SJ. Why is big Pharma getting out of antibacterial drug discovery? Curr Opin Microbiol 2003;6:427-30.
15. Richards RG, Harris LG, Schneider E, Haas N. Antiseptics and antibiotics on implants. Injury 2006;37:S113-S6.
16. Tiller JC, Lioa C-J, Lewis K, Klibanov A, M. Designing surfaces that kill bacteria on contact. Proc Nat Acad Sci U S A 2001;98:5981-5.
17. Vasilev K, Cook J, Griesser HJ. Antibacterial surfaces for biomedical devices. Expert Rev of Med Devic 2009;6:553-67.
18. Israelachvili J. The different faces of poly(ethylene glycol). Proc Nat Acad Sci U S A 1997;94:8378-9.
19. Prime KL, Whitesides GM. Adsorption of proteins onto surfaces containing end-attached oligo(ethylene oxide): A model system using self-assembled monolayers. J Am Chem Soc 1993;115:10714-21.
20. Hucknall A, Rangarajan S, Chilkoti A. In pursuit of zero: Polymer brushes that resist the adsorption of proteins. Adv Mater 2009;21:2441-6.
21. Lichter JA, Van Vlietpa KJ, Rubner MF. Design of antibacterial surfaces and interfaces: Polyelectrolyte multilayers as a multifunctional platform. Macromolecules 2009;42:8573-86.
22. Magin CM, Cooper SP, Brennan AB. Non-toxic antifouling strategies. Mater Today 2010;13:36-44.
23. Wagner VE, Koberstein JT, Bryers JD. Protein and bacterial fouling characteristics of peptide and antibody decorated surfaces of PEG-poly(acrylic acid) co-polymers. Biomaterials 2004;25:2247-63.
24. Hu X, Neoh KG, Shi Z, Kang ET, Poh C, Wang W. An *in vitro* assessment of titanium functionalized with polysaccharides conjugated with vascular endothelial growth factor for enhanced osseointegration and inhibition of bacterial adhesion. Biomaterials 2010;31:8854-63.
25. Vasilev K, Sah V, Anselme K, Ndi C, Mateescu M, Dollmann B, *et al*. Tunable antibacterial coatings that support mammalian cell growth. Nano Lett 2010;10:202-7.

26. Dubash AD, Menold MM, Samson T, Boulter E, Garcia-Mata R, Doughman R, *et al.* Focal Adhesions: New Angles on Old Structures. Intern Rev Cell Mol Biol 2009;277:1-65.
27. Christman KL, Enrique-Rios VD, Maynard HD. Nanopatterning proteins and peptides. Soft Matter 2006;2:928-39.
28. Mitragotri S, Lahann J. Physical approaches to biomaterial design. Nat Mater 2009;8:15-23.
29. Christman KL, Schopf E, Broyer RM, Li RC, Chen Y, Maynard HD. Positioning multiple proteins at the nanoscale with electron beam cross-linked functional polymers. J Am Chem Soc 2009;131:521-7.
30. Hong Y, Krsko P, Libera M. Protein surface patterning using nanoscale poly(ethylene glycol) nanohydrogels. Langmuir 2004;20:11123-6.
31. Krsko P, Mansfield M, Sukhishvili S, Clancy R, Libera M. Electron-beam patterned poly(ethylene glycol) microhydrogels. Langmuir 2003;19:5618-25.
32. Krsko P, Kaplan J, Libera M. Spatially controlled bacterial adhesion using surface-patterned poly(ethylene glycol) hydrogels. Acta Biomater 2009;5:589-96.
33. Krsko P, McCann T, Thach T-T, Laabs T, Geller H, Libera M. Length-scale mediated adhesion and directed growth of neural cells by surface-patterned poly(ethylene glycol) hydrogels. Biomaterials 2009;30:721-9.
34. Pautke C, Schieker M, Tischer T, Kolk A, Neth P, Mutschler W, *et al*. Characterization of osteosarcoma cell lines MG-63, Saos-2 and U-2 OS in comparison to human osteoblasts. Anticancer Res 2004;24:3743-8.
35. De Ruijter JE, Ter Brugge PJ, Dieudonne SC, Van Vliet SJ, Torensma R, Jansen JA. Analysis of integrin expression in U2OS cells cultured on various calcium phosphate ceramic substrates. Tissue Eng 2001;7:279-89.
36. Clover J, Gowen M. Are MG-63 and HOS TE85 human osteosarcoma cell lines representative models of the osteoblastic phenotype? Bone 1994;15:585-91.
37. Chen CS, Mrksich M, Huang S, Whitesides GM, Ingber DE. Geometric control of cell life and death. Science 1997;27:1425-8.

38. Arnold M, Schwieder M, Blommel J, Cavalcanti-Adam EA, Lopez-Garcia M, Kessler H, *et al*. Cell interactions with hierarchically structured nano-patterned adhesive surfaces. Soft Matter 2009;5:72-7.
39. Cavalcanti-Adam EA, Volberg T, Micoulet A, Kessler H, Geiger B, Spatz JP. Cell spreading and focal adhesion dynamics are regulated by spacing of integrin ligands. Biophys J 2007;92:2964-74.
40. George PA, Doran MR, Croll TI, Munro TP, Cooper-White JJ. Nanoscale presentation of cell adhesive molecules via block copolymer self-assembly. Biomaterials 2009;30:4732-7.
41. Jaehrling S, Thelen K, Wolfram T, Pollerberg GE. Nanopatterns biofunctionalized with cell adhesion molecule dm-grasp offered as cell substrate: Spacing determines attachment and differentiation of neurons. Nano Lett 2009;9:4115-21.
42. Lehnert D, Wehrle-Haller B, David C, Weiland U, Ballestrem C, Imhof BA, *et al.* Cell behaviour on micropatterned substrata: Limits of extracellular matrix geometry for spreading and adhesion. J Cell Sci 2004;117:41-52.
43. Malmstrom J, Christensen B, Jakobsen HP, Lovmand J, Foldbjerg R, Sorensen ES, *et al*. Large area protein patterning reveals nanoscale control of focal adhesion development. Nano Lett 2010;10:686-94.
44. Chaffin WL. *Candida albicans* cell wall proteins. Microbiol Mol Biol Rev 2008;72:495-544.
45. Krsko P, Saaem I, Clancy R, Geller H, Soteropoulos P, Libera M. E-beam patterned hydrogels to control nanoscale surface bioactivity In: Lai WY, Ocola LE, Pau S, editors. Nanofabrication: Technologies, Devices, and Applications II. Bellingham: SPIE; 2005; p. 600201.

Chapter 4

The Effect of Adsorbed Fibronectin on the Length-Scale-Mediated Differential Adhesion of Bacteria and Mammalian Cells

Submitted to European Cells and Materials

Yi Wang, Guruprakash Subbiahdoss, Joop de Vries, Mattew Libera, Henny C. van der Mei, Henk J. Busscher

ABSTRACT

The period shortly after a biomaterials-implant surgery has been depicted as a race for the implant surface between bacteria and mammalian cells, and a paradigm shift is occurring to not simply create surfaces adhesive or repulsive to all cells but to instead develop surfaces that simultaneously resist bacterial adhesion and promote mammalian cell adhesion/spreading. Such differentially adhesive surfaces are possible by laterally modulating cell adhesiveness over length scales comparable to bacterial dimensions. Here we advance this concept under the more rigorous condition where modulated surfaces were pre-exposed to fibronectin (Fn) and probed by a Fn-binding *Staphylococcus aureus*. Non-adhesive poly(ethylene glycol) microgels were patterned at inter-gel spacings between 0.5 ~ 3.0 μm on glass, and Fn adsorbed to the exposed glass surface. Quantitative measurements using an atomic force microscope with a single-bacterium probe showed that the adhesion force between *S. aureus* and a modulated surface increased substantially when the surface was coated with Fn but still decreased with decreasing inter-gel spacing. Time-resolved flow-chamber measurements also showed a decrease in bacterial adhesion rate with decreasing inter-gel spacing. Nevertheless, osteoblasts could bind to modulated surfaces despite the non-adhesive microgels. Pre-exposure to Fn substantially amplified this effect. In a 48 h culture, Fn enabled osteoblasts to both adhere to and spread on surfaces with microgels patterned as closely as 1 μm. Thus, even when the adhesiveness of a modulated biomaterials surface is increased, a window of modulation length scales around 1 μm remains that can promote implant healing while simultaneously reducing the risk of infection.

INTRODUCTION

Infection is a primary risk factor during surgery, and it is a particular concern when the surgery involves an implanted biomaterial. Biomaterials-associated infection (BAI) occurs when bacteria colonize the surface of an implanted biomaterial and develop into biofilms. Biomaterials-associated infections are difficult to eradicate, because the biofilm mode of growth provides protection against both the host immune system and antibiotic therapy [1, 2]. BAI occurs despite the use of aseptic surgical techniques and systemic antibiotics, and these infections are ultimately related to how a biomaterials surface interacts with the host tissue cells and with potentially harmful microbes. Consequently, the fate of a biomedical device implanted into the human body has been described as a race between bacteria and mammalian cells to colonize a surface [3]. If mammalian cells win this race and develop robust tissue integration with an implanted device, they can provide a strong barrier against bacterial colonization. If bacteria win this race, their secreted toxins are sufficient to hinder good tissue integration, and the offspring of mature biofilms are able to chronically infect the surrounding tissue.

Realizing that BAI is initiated by bacterial surface adhesion, a number of different surface coatings have been developed that prevent or reduce bacterial adhesion [4-6]. However, these coatings very often, if not always, inhibit not only bacterial adhesion but also allow for little or no tissue integration. This implies that modifying a biomaterials surface with non-adhesive surface functionalities, in general, is not sufficient to both inhibit infection and simultaneously promote healing, and it explains the general lack of success of this approach for totally internal implants or devices. In the absence of such coatings, conditioning protein films adsorb onto implant surfaces from the physiological milieu, and these are able to mediate the adhesion of mammalian cells [7]. Adsorbed fibronectin, for instance, is well recognized for the important role its RGD moieties can play in mammalian cell adhesion and spreading largely through the transmembrane integrin-receptor pathway. However, many bacterial strains use the same ligand-receptor moieties provided by adsorbed serum proteins that mammalian cells require for their adhesion and

spreading [8]. Hence, surfaces that are adhesive to mammalian cells are also adhesive to bacteria. There is thus increasing interest in creating surfaces between these two extremes of fully repulsive and fully adhesive as a means by which to promote differential cell-surface interactions. For example, PEGylated surfaces functionalized with a low concentration of RGD oligopeptides are sufficiently non-adhesive to repel bacteria but at the same time provide sufficient footholds for mammalian cells to adhere and spread [9].

Recently we have realized a bi-functional coating based on the concept of length-scale-mediated differential cell adhesion [10]. Using electron-beam lithography, submicron-sized, non-adhesive poly(ethylene glycol) (PEG) microgels were patterned on glass surfaces. Time-resolved flow-chamber measurements showed that, relative to unpatterned controls, microbial deposition rates and adhesion forces dramatically decreased at inter-gel spacings comparable to the microbial dimensions. Importantly, the adhesion and spreading of much larger osteoblast-like cells was preserved at these inter-gel spacings, despite the presence of sub-cellular, non-adhesive surface features. While this previous work was able to successfully demonstrate differential mammalian cell and microbial interactions with a surface whose cell adhesiveness was laterally modulated by non-adhesive microgels, it did not address how these interactions would be affected by simultaneous modulations in the cell adhesiveness of the underlying glass substratum. Because of the conditioning films that form from the adsorption of proteins from plasma or serum, the surfaces of implanted biomaterials provide a range of adhesion sites for both bacteria and mammalian cells in their race for the surface [7].

This study investigates whether the mechanism of length-scale-mediated differential adhesion, as constituted by PEG–microgel patterns, is sufficiently robust to discourage bacterial adhesion, yet still promote interactions with mammalian cells, in the presence of an adsorbed Fn film. We study surfaces patterned with electron-beam processed PEG microgels over a range of inter-gel spacings, but, in contrast to our earlier work [10], here we use a *S. aureus* strain known to possess Fn binding proteins (FnBPs). We compare the

response of this *S. aureus* strain, as well as that of an osteoblast-like cell line, to microgel-patterned surfaces with and without exposure to fibronectin. Note that the use of a staphylococcus strain with Fn-binding proteins constitutes a most rigorous evaluation of the concept of length-scale mediated differential adhesion when the effects of adsorbed protein are included.

MATERIALS AND METHODS

PEG microgel surface patterning

PEG-microgel patterned glass slides were prepared using established procedures [11, 12]. Briefly, glass slides were sonicated in ethanol, deep cleaned in a Piranha solution, water rinsed and exposed to an O_2 plasma prior to silanization with 2% [v/v] vinyl-methoxy siloxane (Gelest, Morrisville, PA, USA). A solution of 2 wt% PEG (6 kDa; Fluka, Sigma-Aldrich, USA) in tetrahydrofuran was used to make thin films by spin casting on the glass slides. The film thickness after solvent evaporation was measured to be ~120 nm by ellipsometry.

PEG was locally crosslinked during e-beam lithography [12, 13] using a Zeiss Auriga scanning electron microscope (SEM) operated at 2 kV. After e-beam exposure, the slides were washed in Milli-Q water for 30 min to remove unexposed PEG. The resulting surface consisted of surface-bound microgels separated from each other by silanized glass. Patterns were made as 200 µm × 200 µm microgel arrays. Three identical arrays with a particular inter-gel spacing (δ) ranging from 0.5 to 3 µm were patterned on each substratum. This range of inter-gel spacings has previously [10] been shown to encompass, in the absence of pre-adsorbed Fn, a range of inter-gel spacings at which bacterial adhesion was discouraged while leaving mammalian cell adhesion and spreading unaffected. Each array was separated from an adjacent array by a 100 µm wide strip of silanized glass. Some samples were imaged using the same Zeiss SEM used for patterning. These samples were then discarded. The remaining samples were stored under vacuum (50 mTorr).

Fibronectin pre-adsorption on PEG-microgel patterns

A 0.05 mL droplet of Fn (25 µg/mL human Fn; Sigma-Aldrich BV, Zwijndrecht, The Netherlands) was placed on the patterned region of a glass slide for 30 min at room temperature. Subsequently, the entire slide was immersed in phosphate buffered saline (PBS; 10 mM potassium phosphate and 0.15 M NaCl, pH 7) containing 1% BSA for 1 min to block non-specific adsorption of proteins. It was then rinsed three times (5 min for each rinse) with PBS containing 1% BSA solution after which primary antibody (rabbit-anti-human fibronectin Ab, polyclonal, dilution 1:400) was adsorbed for 30 min and slides were again rinsed three times (5 min for each rinse). Finally, a second, fluorescent antibody (FITC conjugated Donkey anti-rabbit IgG, dilution 1:100) was adsorbed and slides were rinsed as described above. The patterned glass slide was put in a petri dish filled with PBS and examined by confocal laser scanning microscopy (CLSM, Leica DMRXE with confocal TCS SP2 unit) equipped with a 40x water immersion lens

Bacterial strain, growth and harvesting

Staphylococcus aureus 8325-4, which possesses FnBPs (provided by T.J. Foster, Moyne Institute of Preventive Medicine, Dublin, Ireland), was used in this study. The staphylococci were maintained at -80 °C in tryptone soy broth (TSB) (Oxoid, Basingstoke, United Kingdom) containing 7% dimethyl sulfoxide (Merck, Germany). *S. aureus* were incubated on TSB agar plates overnight at 37 °C. Subsequently, bacterial colonies were pre-cultured in 10 mL TSB overnight under constant rotation. Each pre-culture was used to inoculate a main culture in 190 mL TSB. After approximately 2 h, representing early stationary phase bacteria with peak expression of FnBPs in *S. aureus* 8325-4 [14], staphylococci were harvested by centrifugation at 6500g for 5 min at 10 °C and washed twice in sterile PBS. Bacterial aggregates were broken by mild, intermittent sonication on ice for 3 times 10 s each at 30 W (Wibra Cell model 375, Sonics and Materials Inc., Danbury, Connecticut, USA) and resuspended to a concentration of 3×10^6 bacteria/mL in sterile PBS.

Atomic force microscopy

S. aureus 8325-4 was immobilized on tipless atomic force microscopy (AFM) V-shaped cantilevers (VEECO, DNP-0) via electrostatic interactions with poly-L-lysine (PLL) using a method described previously [15]. A drop of PLL solution was placed on a glass slide, and the tip of the cantilever was dipped in the droplet for 1 min. After air-drying, the cantilever was dipped in a staphylococcal suspension for 1 min to enable bacteria to adhere to the PLL-treated cantilever. These bacterial probes were freshly prepared for each experiment. The bacterial probes usually yielded single-cell contact with a sample of interest. Images with double contour lines indicated that two bacteria adsorbed on the cantilever were simultaneously contacting the surface, and any probe exhibiting such behaviour was discarded. Patterned surfaces, in the absence and presence of a 30 min, adsorbed Fn film, were interrogated by at least nine different *S. aureus* bacterial probes. Three probes were made from each of three different cultures of *S. aureus*.

Force measurements were done at room temperature in PBS (pH 7.0) using a Bioscope Catalyst AFM with PeakForce^{TM} Quantitative NanoMechanical Mapping software (Bruker). Each curve was analyzed for its maximum adhesion force. By collecting data from different specimen locations, comparative values were derived by subtracting the forces found at the most adhesive (inter-gel regions of surface) from those measured on the least adhesive (PEG-microgel) sites. Calibration of the bacterial probes was done using by thermal tuning to yield spring constants of 0.044 ± 0.008 Nm^{-1}.

Staphylococcal adhesion

Bacterial adhesion was studied in a parallel-plate flow chamber [16] on PEG-microgel patterned glass slides, prior to and after 30 min Fn adsorption. Bacterial adhesion was monitored by digital phase-contrast microscopy (Olympus BH-2; 40x objective). After removing air bubbles by flowing PBS, *S. aureus* in PBS were perfused through the chamber at a shear rate of 11 s^{-1} for 3 h at room temperature. Images were taken from each PEG-microgel patterned array and from unpatterned, silanized glass at 1 min intervals. From

these, the number of adhering bacteria on each array was determined as a function of time. Straight lines were fit to these data to obtain the initial bacterial adhesion rate on each pattern with specific δ, $j_{o,\delta}$. The initial adhesion rate on the unpatterned glass surface, $j_{o,glass}$, served as a control. We defined the normalized initial deposition rate as:

$$F(\delta) = \left[\frac{j_{o,\delta}}{j_{o,glass}} \right] \quad (1)$$

A cumulative Weibull function was used to model these rates as a function of inter-gel spacing according to:

$$F(\delta) = 1 - \exp\left[-\left(\frac{\delta}{\alpha} \right)^{\beta} \right] \quad (2)$$

where the parameters α and β represent the so-called scale factor and shape factor, respectively [10].

Mammalian cell culturing, harvesting and adhesion

U2OS osteosarcoma cells were cultured in low-glucose Dulbecco's Modified Eagles Medium (DMEM) supplemented with 10% fetal calf serum (FBS) and 0.2 mM of ascorbic acid-2-phosphate. U2OS cells were maintained in T75 culture flasks at 37 °C in humidified 5% CO_2 and harvested at 90% confluency using trypsine/ethylenediamine–tetra-acetic acid. The harvested cells were diluted to 6 x 10^5 cells/mL. U2OS is an immortalized human cell line derived from osteosarcoma cells and was chosen from a broad selection of human osteoblastic cell lines used previously [17]. It has been demonstrated that osteosarcoma cell lines exhibit meaningful osteoblastic phenotypes [18].

U2OS adhesion and spreading on PEG-microgel patterned surfaces in the absence and presence of a 30 min, pre-adsorbed Fn treatment were studied by *in situ* imaging in the parallel-plate flow chamber and by *ex situ* immunofluorescence and SEM imaging. The flow chamber was kept at 37 °C during these experiments. Once fully filled and free of air-bubbles, a U2OS cell suspension in modified medium (DMEM + 10% FBS and 2% TSB [16]

was introduced. After filling the chamber, flow was stopped after 1.5 h to allow for U2OS adhesion. Phase-contrast images were taken from each patterned array and from the surrounding silanized glass to determine the initial number of adhering cells per unit area and the total surface coverage of spread U2OS cells. Modified culture medium supplemented with 2% HEPES buffer was then flowed at 0.14 s^{-1} shear rate for 48 h. After 48 h the substrata were removed, fixed twice in 30 mL of 3.7% formaldehyde in cytoskeleton stabilization buffer (CS; 0.1 M Pipes, 1 mM EGTA, 4% (w/v) PEG 8000, pH 6.9), incubated in 0.5% Triton X-100 (3 min), rinsed with PBS, and stained for 30 min in 5 mL PBS containing 49 µL DAPI and 2 µg/mL of TRITC–Phalloidin. After four washes in PBS, the slides were examined by fluorescence microscopy (Leica DM 4000B). The total surface coverage of adhering cells on the patterned surface was determined by Scion image software.

Statistical analysis

Staphylococcal adhesion forces, bacterial and mammalian cell adhesion were performed with triplicate cultures and presented as means with standard deviations. For statistical analysis, ANOVA was employed with Tukey's HSD post hoc test, considering $p < 0.05$ as statistically significant.

RESULTS

Fn adsorption on patterned surfaces

SEM micrographs (Figure 1 insets) illustrate typical surface morphologies of the PEG-microgel patterns at different inter-gel spacings. The upper CLSM images indicate that Fn hardly adsorbs to the patterns with an inter-gel spacing of 0.5 µm (dark contrast). Instead, Fn adsorbs to the silanized glass surrounding the PEG microgels (green fluorescence).

Staphylococcal adhesion forces

The force of adhesion between a *S. aureus* bacterium and the patterned surfaces depends both on the inter-gel spacing and on the absence or presence of pre-adsorbed Fn. *S.*

aureus 8325-4 exhibits an extremely small adhesion force (< 1 nN) with microgel-patterned surfaces that have an inter-gel spacing of 0.5 µm irrespective of the absence or presence of adsorbed Fn (see Figure 2).

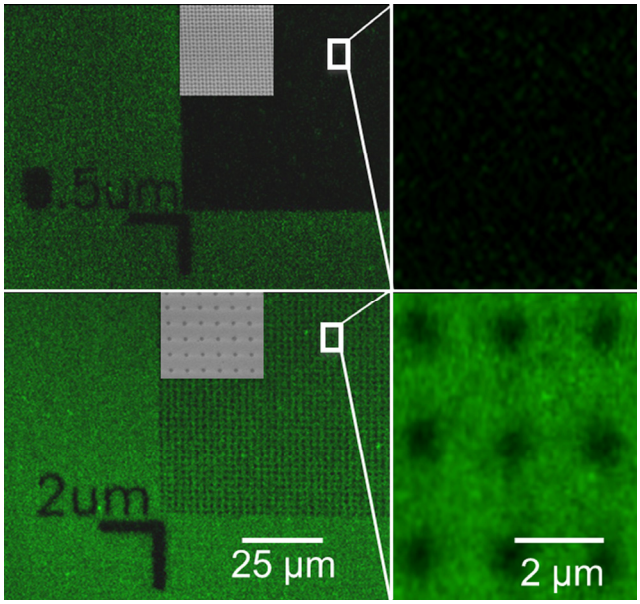

Figure 1 Fn adsorption (bright, green fluorescence) on PEG-microgel patterned surfaces with inter-gel spacings of 0.5 µm (upper row) and 2 µm (lower row) at low (left panels) and higher magnifications (right panels). The insets are SEM images of the patterned surfaces in the absence of adsorbed fibronectin.

In the absence of adsorbed Fn, the adhesion force slightly increases with increasing inter-gel spacing, but it remains relatively small even at an inter-gel spacing of 3 µm. In the presence of adsorbed Fn, however, the adhesion force increases strongly with increasing inter-gel spacing. Notably, the adhesion force to the pattern with the 3 µm inter-gel spacing in the presence of adsorbed Fn is around five times higher than that in the absence of Fn. Scanned-probe topographic images generated using a bacterial AFM probe confirmed that the interaction force was generated from a single bacterium interaction (see insets in Figure 2).

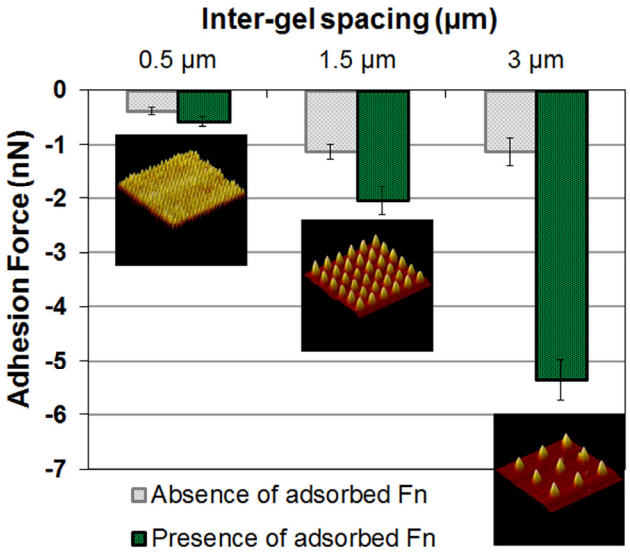

Figure 2 Adhesion forces between *S. aureus* 8325-4 and microgel-patterned surfaces with different inter-gel spacings in the absence and presence of adsorbed Fn. Error bars indicate the standard deviations of measurements using three different patterned substrata probed by bacteria from different cultures. The insets are scanned-probe AFM images (10 μm ×10 μm) taken of PEG-microgel patterns in the presence of adsorbed Fn using a bacterial probe.

Staphylococcal adhesion to microgel-patterned surfaces

Figure 3 summarizes the kinetics of *S. aureus* 8325-4 adhesion on microgel-patterned surfaces. These experiments were performed in triplicate for specimens in the absence and presence of pre-adsorbed Fn. Irrespective of the inter-gel spacing and the presence or absence of Fn, the number of adhering staphylococci increases linearly with time, and linear least squares fitting was used to determine the rate of staphylococcal adhesion. Staphylococcal adhesion rates were highest on unpatterned glass and decreased with decreasing inter-gel spacing. The normalized adhesion rates obeyed the cumulative Weibull function. Values of j_0 on glass in the absence and presence of adsorbed Fn and α and β for patterned surfaces are summarized in Table 1. The scale parameter, α, represents the δ value at which the initial deposition rate is 63.2% of that for unpatterned glass, and the higher scale factor in the absence of adsorbed Fn indicates that adhesion is

more strongly affected than in the presence of adsorbed Fn. The shape factor, β, exceeds 1 in the absence of adsorbed Fn, while it is close to unity in the presence of adsorbed Fn.

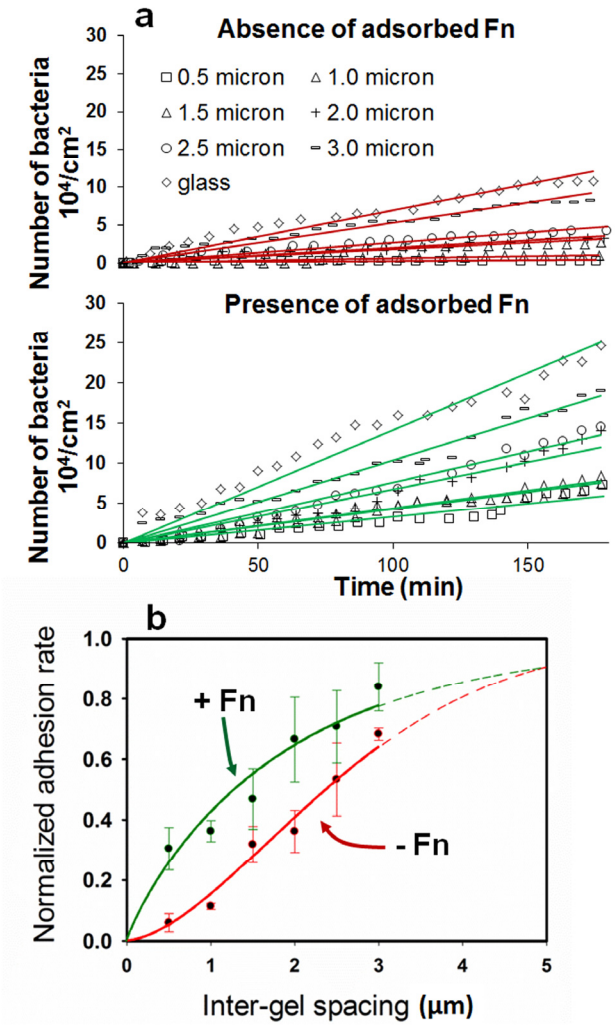

Figure 3 (a) Example describing the number of *S. aureus* 8325-4 adhering to microgel-patterned surfaces with different inter-gel spacings in absence (upper) and presence (lower) of adsorbed Fn as a function of time.
(b) The *S. aureus* 8325-4 adhesion rate, normalized to the rate on glass as a function of inter-gel spacing. The error bars correspond to the standard deviation of three separate experiments. The solid curves correspond to a Weibull model of each dataset.

Table 1 Initial *S. aureus* 8325-4 adhesion rates on bare glass in the absence (-Fn) and presence (+Fn) of adsorbed Fn at a shear rate of 11 s^{-1} together with scale and shape factors derived from Weibull fitting of normalized adhesion rates as a function of the inter-gel spacing. ± indicates the standard deviation of three different experiments.

S. aureus	$j_{o,\,glass}$ (cm^{-2} sec^{-1})	α (μm)	β
8325-4 (- Fn)	24 ± 5	2.9	1.7
8325-4 (+ Fn)	36 ± 11	1.9	0.9

Mammalian cell adhesion and spreading

Phase-contrast micrographs of U2OS cells adhering to and spreading on microgel-patterned surfaces with different inter-gel spacings and in the absence or presence of pre-adsorbed Fn immediately after cell adhesion are shown in Figure 4 (panel A). Both in the absence and presence of pre-adsorbed fibronectin, the number of adhering cells increases with increasing inter-gel spacing up to 1.5 μm, above which there is no noticeable further increase in cell number. Cells adhering to surfaces with no pre-adsorbed Fn are all rounded and are not well attached irrespective of the inter-gel spacing. In contrast, almost all cells on surfaces with pre-adsorbed Fn are well spread after 1.5 h, except on patterns with an inter-gel spacing of 0.5 μm. The percentage of surface covered by cells at both 1.5 h, $X_{1.5}$, and at 48 h, X_{48}, increases steadily with increasing inter-gel spacing, as shown in Figure 5A.

After 48 h, the U2OS cells were fixed, stained with DAPI and Phalloidin, and imaged by CLSM (Figure 4, panel B) to derive the cell surface coverage on the microgel-patterned surfaces after growth (Figure 5A). Surface coverage after 48 h is low on the surface with microgels patterned at a 0.5 μm inter-gel spacing, but readily reaches 50% to 60% for the higher inter-gel spacings, including the glass surface. Since the number of U2OS cells does not change significantly over the 48 h time period, the increase in surface coverage provides a measure of cell spreading. The fractional change in surface coverage in the

presence of pre-adsorbed Fn was highest for the 1 µm inter-gel spacing. Figure 6 presents a typical SEM image showing that U2OS cells are able to grow over microgels on Fn-treated surfaces with microgels patterned at 1 µm spacings. The U2OS filopodia are clearly able to thread their way between microgels.

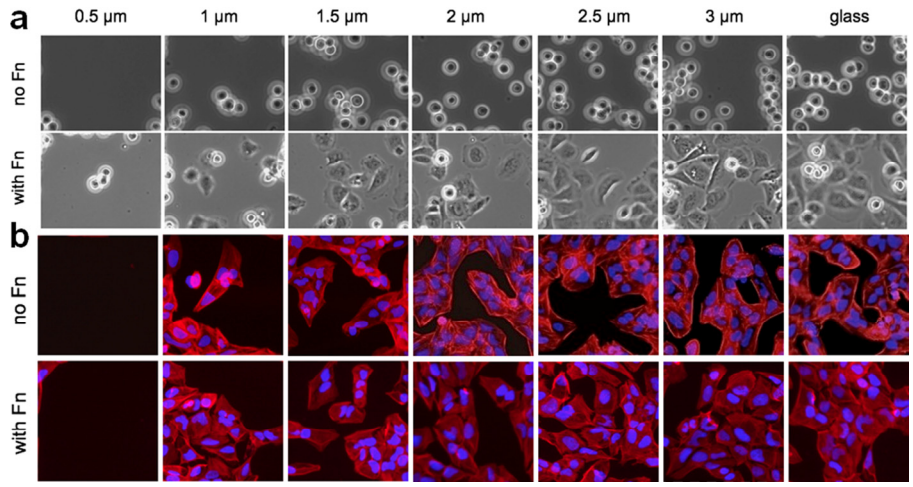

Figure 4 Phase-contrast (panel a, 200 µm × 150 µm, after 1.5 h of U2OS adhesion) and fluorescent (panel b, 150 µm × 150 µm, after 48 h of U2OS culture) micrographs of U2OS cells adhering to and spreading on microgel-pattern surfaces with different inter-gel spacings in the absence and presence of adsorbed Fn.

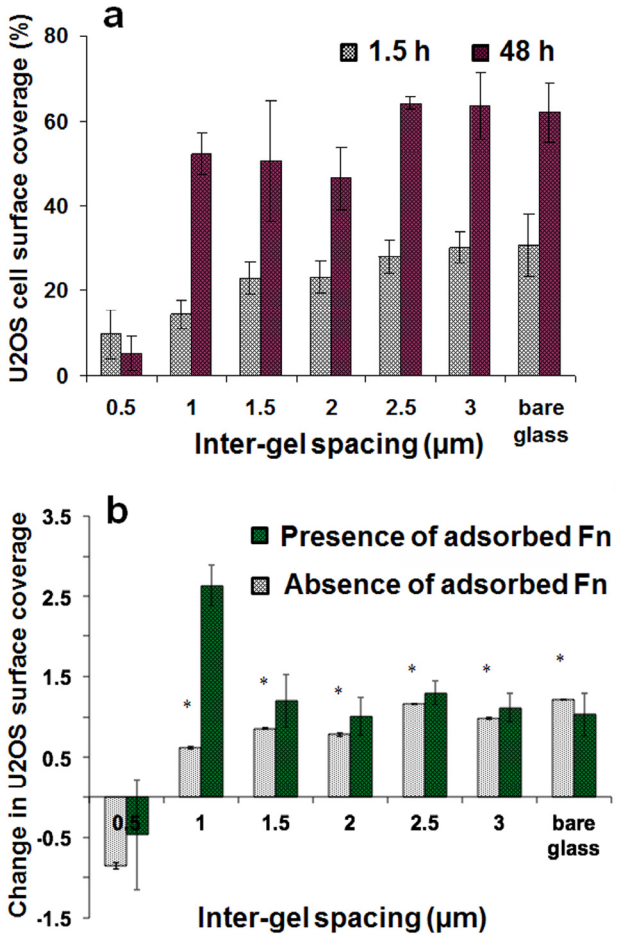

Figure 5 (a) U2OS cell surface coverage after 1.5 h seeding and after 48 h of growth on microgel-patterned surfaces in the presence of Fn. (b) Fractional change in U2OS surface coverage from its initial value at 1.5 h to its value after 48 h of growth in the absence (data taken from (10)) and presence (current measurements) of pre-adsorbed Fn. The error bars represent the standard deviations over three replicates with separately cultured cells.
∗ denotes significance at differences at $p < 0.05$ from the control (bare glass).

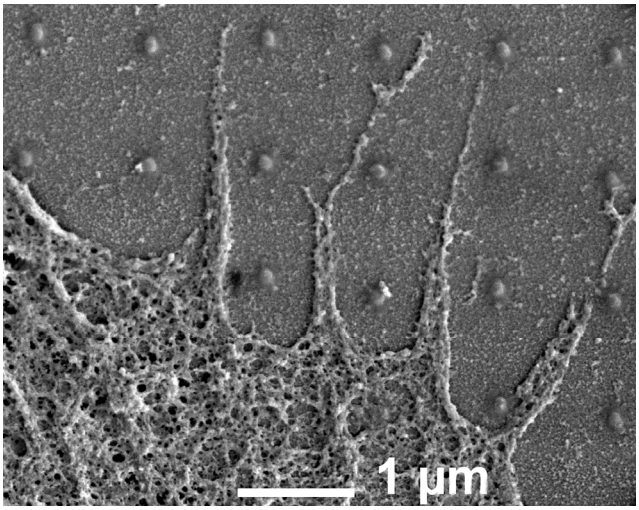

Figure 6 SEM micrograph showing that after 48 h of culture U2OS cells grow over, and filopodia extend between, non-adhesive PEG microgels on surfaces patterned at 1 µm spacings and exposed to Fn prior to cell culture.

DISCUSSION

PEG-based coatings are well known for their excellent resistance to protein adsorption and to cell adhesion. This property makes PEG-based coatings good candidates to render biomaterials surfaces resistant to bacterial colonization and, hence, reduce the threat of BAI. However, when used on implantable biomaterials, continuous PEG coatings exert insufficient attraction to mammalian cells to enable tissue integration. We have previously shown that laterally discontinuous coatings of submicron-sized PEG microgels modulate surface cell adhesiveness, and the spacing between the microgels can be controlled such that bacteria are preferentially repelled while mammalian cells can still adhere. This so-called differential adhesion effect occurs when the spacing between microgels is about the same size as that of individual bacteria [10]. Mammalian cells have fluid cell membranes that can conform to surfaces and, despite the fact that mammalian cells are typically tens of microns in size, they bind to surfaces via submicron-sized focal contacts and focal adhesions [19, 20]. Thus, mammalian cells can bind to exposed adhesive surface regions

present between the non-adhesive PEG microgels, similar to our previous observations of neurite interactions with microgel-patterned surfaces [21].

Here we demonstrate that the mechanism of length-scale-mediated differential adhesion remains operative even when the adhesive interactions between a solid surface and approaching bacteria and mammalian cells is substantially strengthened by pre-adsorbing Fn onto the substrate surfaces. Fibronectin is a well-known and important protein present both in serum and in extracellular matrix. The adsorption of proteins, Fn among them, is a key factor controlling both bacterial and mammalian cell adhesion to biomaterials surfaces [22, 23]. In clinical applications proteins will reach an implant surface first and form an adsorbed conditioning film, which mediates subsequent interactions between the surface and approaching bacteria and mammalian cells. The present studies have addressed the issue of how the relative balance of non-adhesive microgels and exposed surface couple to mediate bacterial adhesion and mammalian cell adhesion when the adhesive interaction is modulated by both pre-adsorbing Fn onto the exposed substratum surface and by using a strain of *S. aureus* known to have specific Fn binding sites [24].

Similar to our previous findings [12, 25, 26] and consistent with the extensive literature on the antifouling properties of PEG-based materials, we find here that electron-beam surface-patterned PEG microgels resist Fn adsorption. This is manifested by the immunofluorescence images presented in Figure 1. The dark contrast corresponds to the positions of the PEG microgels. The case of a 0.5 μm inter-gel spacing presents an almost continuous pad of non-adhesive surface. As the inter-gel spacing increases, discrete points of dark contrast appear, which correspond to the positions of the individual PEG microgels. The green fluorescence in between these points indicates that surface not covered by PEG microgels has been coated with a conditioning film of adsorbed Fn.

Our measurements of adhesive forces between the various surfaces and a Fn-binding *S. aureus* bacterium show that Fn substantially increases the strength of the bacterium-

surface interaction. This can be seen most clearly in Figure 2 for patterns with a 3 μm inter-gel spacing where the microgels are spaced sufficiently far apart that an approaching micron-sized bacterium can interact with the exposed surface exposed between the microgels. These measurements show that Fn increases the strength of the bacterium-surface interaction by a factor of 5 relative to an otherwise identical surface without Fn. However, the strength of the adhesive force drops dramatically as the inter-gel spacing is decreased. When the inter-gel spacing falls to 1.5 μm, the increase in adhesive strength provided by the Fn is only twice that of the Fn-free surface, and we can conclude that the bacterium is interacting with both the Fn-coated surface between the microgels as well as with the microgels themselves. The attractive force of the Fn-coated surface is mitigated substantially by the PEG microgels. Finally, since the magnitude of the adhesive force is small and there is no significant effect of Fn, the measurements of adhesive force with and without Fn exposure for the 0.5 μm inter-gel spacing (Figure 2) support the conclusion that the there is an insignificant amount of Fn on this surface.

The results presented in Figure 3 and Table 1 indicate that both the inter-gel spacing and the presence of Fn have a significant effect on the initial rate of microbial adhesion. The Weibull function (Fig. 3B) is often used to model random events, and it provides two parameters, α and β, which give further insight into the microbial adhesion process. Importantly, the scale parameter, α, characterizing the surfaces with pre-adsorbed Fn, is 1.9 μm, while that for surfaces without adsorbed Fn it is 2.9 μm. This indicates that a much smaller amount of exposed substratum surface is necessary to bind an individual *S. aureus* 8325-4 bacterium when that surface presents Fn relative to one presenting bare glass. Furthermore, the fact that the shape factor β is larger for the Fn-free surface again indicates that increasing the area of exposed surface has a greater impact on the probability of adhesion onto a Fn-free surface than onto a surface with pre-adsorbed Fn. These differences are consistent with the fact that the adhesive force between an individual *S. aureus* 8325-4 bacterium and a Fn-coated surface is significantly higher than that between an individual bacterium and a Fn-free glass surface. There are either more

bonding sites per unit area in the case involving Fn or the strength of each bacterium-Fn bond is sufficiently strong so fewer such bonds are needed to enable adhesion.

In addition to the enhanced bacterial adhesion we observe due to the presence of Fn, we also find that Fn simultaneously enhances the adhesion and spreading of osteoblast-like U2OS cells. The effect of Fn on U2OS binding to microgel-modified surfaces is illustrated by Figure 5B, which compares the change in fractional surface coverage, ΔX, between times points of 1.5 and 48 h of culture. The data from Fn-treated surfaces were collected during the present experiments, and the data on Fn-free surfaces, collected under otherwise identical conditions, were reported previously [10]. The fractional change in surface coverage was calculated as

$$\Delta X = \frac{X_{48} - X_{1.5}}{X_{1.5}} \tag{3}$$

Figure 5B shows that U2OS cells avoid surfaces patterned at an inter-gel spacing of 0.5 μm, since ΔX is negative for such surfaces. It furthermore shows that the cells spread on patterned surfaces with inter-gel spacings of 1 μm or more, since ΔX is positive for these surfaces. For inter-gel spacings of 1.5 μm or more, Figure 5B shows that the surface coverage roughly doubles ($\Delta X \approx 1$) over the two-day culture period irrespective of the presence or absence of Fn. There is, however, a very significant effect of Fn on U2OS spreading on surfaces patterned at 1 μm inter-gel spacing. Here ΔX is 2.5, whereas ΔX is less than 1 on an otherwise identical surface with no Fn. This finding suggests that the ability of Fn to localize integrin assembly and create focal contacts is particularly important within the confined area between the 400 nm diameter microgels spaced at 1 μm intervals. This result is particularly significant, because it shows that the enhanced bacterial adhesion due to the presence of adsorbed Fn is compensated by enhanced U2OS adhesion and spreading. The differential cell-interactive property of the surface is thus preserved, and Fn shifts the window of lateral modulations in cell adhesiveness for reduced bacterial adhesion and enhanced cell adhesion/spreading to slightly smaller inter-gel spacing.

CONCLUSIONS

We have experimentally explored the emerging concept of length-scale-mediated differential mammalian/bacterial cell adhesion using non-adhesive PEG microgels patterned on an otherwise cell-adhesive substratum. In addition to inter-gel spacing as an important independent variable, we also tuned the strength of the adhesive component of the surface by the adsorption of Fn. This protein not only promotes the adhesion of a number of mammalian cells but also enables specific binding of quite a number of pathogens that possess FnBPs, including the *S. aureus* strain we used in our experiments. The spacing between microgels has a significant effect on the rate of bacterial adhesion with the rate falling dramatically when the inter-gel spacing is comparable to the bacterial dimensions. The enhanced adhesive strength provided by the Fn specific binding requires a smaller inter-gel spacing to achieve a level of bacterial resistance similar to that of surfaces without pre-adsorbed Fn, as shown in previous experiments. However, because of the important role Fn plays on mammalian-cell adhesion via the development of submicron sized focal adhesions, adsorbed Fn substantially enhances the ability of a U2OS cells to adhere and grow to patterned surfaces, especially when patterned at a 1 μm inter-gel spacing, while such patterns still resist the adhesion of a *S. aureus* strain possessing FnBPs. Thus, laterally modulating cell adhesiveness using patterned PEG microgels provides a means with which to develop biomaterials surfaces that resist staphylococcal adhesion while simultaneously stimulating adhesion and spreading of mammalian tissue cells even under conditions where the adhesive strength is increased by Fn specific binding.

ACKNOWLEDGEMENTS

Y. Wang and M. Libera thank the U.S. Army Research Office (grant W911NF-07-0543) and the National Science Foundation (grant #CBET-0708379) for financial support. This project also used microscope resources partially funded by the National Science Foundation (grant #DMR-0922522).

REFERENCES

1. Schmidt AH, Swiontkowski MF. Pathophysiology of infections after internal fixation of fractures. J Am Acad Orthop Surg 2000;8:285-91.
2. Azeredo J, Sutherland IW. The use of phages for the removal of infectious biofilms. Curr Pharm Biotechnol 2008;9:261-6.
3. Gristina AG, Naylor P, Myrvik Q. Infections from biomaterials and implants: a race for the surface. Med Prog Technol 1988;14:205-24.
4. Groll J, Fiedler J, Bruellhoff K, Moeller M, Brenner RE. Novel surface coatings modulating eukaryotic cell adhesion and preventing implant infection. Int J Artif Organs 2009;32:655-62.
5. Norowski PA, Jr., Bumgardner JD. Biomaterial and antibiotic strategies for peri-implantitis: a review. J Biomed Mater Res B Appl Biomater 2009;88:530-43.
6. Katsikogianni M, Missirlis YF. Concise review of mechanisms of bacterial adhesion to biomaterials and of techniques used in estimating bacteria-material interactions. Eur Cell Mater 2004;8:37-57.
7. Gristina AG, Giridhar G, Gabriel BL, Naylor PT, Myrvik QN. Cell biology and molecular mechanisms in artificial device infections. Int J Artif Organs 1993;16:755-63.
8. Sukenik CN, Balachander N, Culp LA, Lewandowska K, Merritt K. Modulation of cell adhesion by modification of titanium surfaces with covalently attached self-assembled monolayers. J Biomed Mater Res 1990;24:1307-23.
9. Tosatti S, De Paul SM, Askendal A, VandeVondele S, Hubbell JA, Tengvall P, *et al*. Peptide functionalized poly(L-lysine)-g-poly(ethylene glycol) on titanium: resistance to protein adsorption in full heparinized human blood plasma. Biomaterials 2003;24:4949-58.
10. Wang Y, Subbiahdoss G, Swartjes J, Van der Mei HC, Busscher HJ, Libera M. Length-scale mediated differential adhesion of mammalian cells and microbes. Adv Funct Mat 2011; 21:3916–23.
11. Krsko P, Mansfield M, Sukhishvili S, Clancy R, Libera M. Electron-beam patterned poly(ethylene glycol) microhydrogels. Langmuir 2003;19:5618-25.

12. Krsko P, Saaem I, Clancy R, Geller H, Soteropoulos P, Libera M. E-beam patterned hydrogels to control nanoscale surface bioactivity In: Lai WY, Ocola LE, Pau S, editors. Nanofabrication: Technologies, Devices, and Applications II. Bellingham: SPIE 2005. p. 600201.
13. Christman KL, Enrique-Rios VD, Maynard HD. Nanopatterning proteins and peptides. Soft Matter 2006;2:928-39.
14. Saravia-Otten P, Muller HP, Arvidson S. Transcription of *Staphylococcus aureus* fibronectin binding protein genes is negatively regulated by agr and an agr-independent mechanism. J Bacteriol 1997;179:5259-63.
15. Camesano TA, Natan MJ, Logan BE. Observation of changes in bacterial cell morphology using tapping mode atomic force microscopy. Langmuir 2000;16:4563-72.
16. Subbiahdoss G, Kuijer R, Grijpma DW, Van der Mei HC, Busscher HJ. Microbial biofilm growth vs. tissue integration: "the race for the surface" experimentally studied. Acta Biomater 2009;5:1399-404.
17. De Ruijter JE, Ter Brugge PJ, Dieudonne SC, Van Vliet SJ, Torensma R, Jansen JA. Analysis of integrin expression in U2OS cells cultured on various calcium phosphate ceramic substrates Tissue Eng 2001;7:279-89.
18. Pautke C, Schieker M, Tischer T, Kolk A, Neth P, Mutschler W, *et al*. Characterization of osteosarcoma cell lines MG-63, Saos-2 and U-2 OS in comparison to human osteoblasts. Anticancer Res 2004;24:3743-8.
19. Zhao T, Li Y, Dinner AR. How focal adhesion size depends on integrin affinity. Langmuir 2009;25:1540-6.
20. Sastry SK, Burridge K. Focal adhesions: a nexus for intracellular signaling and cytoskeletal dynamics. Exp Cell Res 2000;25;261:25-36.
21. Krsko P, McCann TE, Thach TT, Laabs TL, Geller HM, Libera M. Length-scale mediated adhesion and directed growth of neural cells by surface-patterned poly(ethylene glycol) hydrogels. Biomaterials 2009; 30: 721-9

22. Cole MA, Voelcker NH, Thissen H, Griesser HJ. Stimuli-responsive interfaces and systems for the control of protein-surface and cell-surface interactions. Biomaterials 2009;30:1827-50.
23. Bazaka K, Jacob MV, Crawford RJ, Ivanova EP. Plasma-assisted surface modification of organic biopolymers to prevent bacterial attachment. Acta Biomater 2011;7:2015-28.
24. Agerer F, Lux S, Michel A, Rohde M, Ohlsen K, Hauck CR. Cellular invasion by *Staphylococcus aureus* reveals a functional link between focal adhesion kinase and cortactin in integrin-mediated internalisation. J Cell Sci 2005;118:2189-200.
25. Hong Y, Krsko P, Libera M. Protein surface patterning using nanoscale PEG hydrogels. Langmuir 2004;20:11123-6.
26. Saaem I, Papasotiropoulos V, Wang T, Soteropoulos P, Libera M. Hydrogel-based protein nanoarrays. J Nanosci Nanotechnol 2007;7:2623-32.

Chapter 5

Conditions of Bacterial Confinement on a Surface that Favor Tissue Integration over Biofilm Growth

Will be submitted to Biomatarials

Yi Wang, Guruprakash Subbiahdoss, Henny C. van der Mei, Henk J. Busscher, Matthew Libera

ABSTRACT

Biomaterials-associated infections are difficult to eradicate, because once adhering bacteria start growing and form a biofilm, they embed themselves in a matrix of extracellular polymeric substances, yielding protection against antibiotic treatment and the host immune system. PEGylated surfaces are known to show reduced bacterial adhesion and delayed growth of weakly adhering biofilm, but at the same time do not support tissue integration which protects an implant surface against infection. The aim of the current paper is to determine whether spatial confinement of adhering bacteria on adhesive patches in PEG microgels yields reduced biofilm formation while favoring adhesion, spreading and growth of mammalian cells. To this end, PEGylated films were microstructured to create circular, exposed glass areas (patches) with a diameter ranging from 1 to 5 μm and different inter-patch distances, resulting in adhesive area fractions of 0.1, 0.2 and 0.35. To enhance the adhesiveness of the glass, fibronectin was adsorbed onto the patches, and adhesion and biofilm formation of a *Staphylococcus aureus* strain possessing Fn-binding proteins was compared to adhesion, spreading and growth of osteoblast-like cells. An adhesive area fraction of 0.1 proved to be too low to support tissue integration while bacterial growth was still possible, especially on the adhesive patches with larger diameters. Increasing the adhesive area fraction supported cell adhesion, spreading and growth while still limiting bacterial growth by confining adhering bacteria to the adhesive areas. Therewith this paper describes a new approach to design bi-functional coatings for permanent, totally internal implants or devices requiring tissue integration, with a reduced risk of infection.

INTRODUCTION

Infection is a primary risk factor associated with biomaterials implant surgery. It is difficult to eradicate because the biofilm mode of growth offers protection to colonizing bacteria against the host immune system and antibiotic therapy [1, 2]. Biomaterials-associated infection (BAI) generates high costs for the healthcare system along with great discomfort to patients, since the treatment of BAI involves extensive antibiotic administration and is usually accompanied by surgical removal and replacement of the infected implant or device. Unlike contact lenses and catheters, which temporarily contact with tissue, totally internal, permanent biomaterials implants like prosthetic joints and vascular grafts require tissue integration, and there is thus a need to simultaneously preserve viable tissue-implant interactions while minimizing the probability of bacterial adhesion. However, biomaterial surfaces that favor tissue integration over bacterial adhesion and biofilm growth are difficult to design, since most surfaces that demonstrate bacterial repellence are also unfavorable for mammalian cell adhesion, spreading and growth. Hydrophilic poly(ethylene glycol) (PEG) coatings [3-5] present one of the most repellent surfaces towards proteins and bacteria, but they are equally effective at hindering mammalian cell adhesion.

There is an increasing awareness that mono-functional surfaces – ones that are entirely cell repulsive or entirely cell adhesive - are inadequate for differentially controlling bacterial and mammalian cell adhesion. Instead, surfaces need to be equipped with at least dual functionality to repel bacteria and promote mammalian cell adhesion. Coatings consisting, for instance, of poly(L-lysine)-graft-poly(ethylene glycol) (PLL-g-PEG) copolymer equipped with an arginine-glycine-aspartic acid (RGD) peptide sequence [6], which is one of the major recognition sites of integrin receptors through which mammalian cells bind to extracellular matrix [7], supported mammalian cell growth while at the same time showed reduced bacterial adhesion [8, 9].

Another way to achieve differential cell-surface interactions is to exploit the different dimensions of mammalian cells and bacteria by patterning. PEG coatings, for example, can be used to pattern surfaces into adhesive and repulsive regions to enable mammalian cell adhesion, spreading and growth, while maintaining a sufficient fraction and spatial distribution of PEGylated surface to discourage bacterial adhesion. PEG can be patterned by a variety of techniques including micro-contact printing [10, 11] and photolithography [12-14]. PEG micro- [15] and nano- [16] structured surfaces demonstrated preferred protein adsorption and cellular adhesion as compared with continuous PEGylated films, although significantly lower than glass controls [17]. Not much work has been done on bacterial adhesion to patterned PEG surfaces. Most of it lacks quantitative analysis because of the limitation of precise control of patterning techniques. For example, PEG patterns composed of microwells as large as 30 × 30 μm squares showed reduced *Escherichia coli* adhesion compared to an unpatterned surface, but that inhibition only came from less-exposed adhesive area [18]. With the development of e-beam lithography, initial work with precise patterns of repulsive hydrogels combined with circular, exposed glass substratum areas of 1, 5, 10 and 20 μm diameter, trapped bacteria in the glass area yielding spatially controlled growth of a *Staphylococcus epidermidis* strain over a 60 min time scale [19]. Based on those observations, we hypothesize that PEG patterns with adhesive patches whose size is on the order of bacterial length scales will confine bacteria within surrounding PEG film boundaries and that this confinement can further limit biofilm formation above and beyond the effect due to reduced adhesive fractions while patterns with micro-sized adhesive patches still favor mammalian cell adhesion and spreading.

The aim of this study is firstly to determine whether spatial confinement of adhering bacteria also yields reduced biofilm formation after 24 h of growth and secondly to optimize the conditions of spatial confinement of adhering bacteria and biofilm formation as compared with adhesion, spreading and growth of mammalian cells. To this end, PEGylated films were patterned to create circular cell-adhesive patches consisting of exposed glass with diameters ranging from 1 to 5 μm and different inter-patch distances,

resulting in adhesive area fractions of 0.1, 0.2 and 0.35. Adsorbed fibronectin was used to enhance the adhesiveness of glass, and adhesion and biofilm formation of a *Staphylococcus aureus* strain possessing Fn-binding proteins was compared to adhesion, spreading and growth of osteoblast-like cells. Since fibronectin not only functions as a key adhesive protein for mammalian cells, while being recognized as well by adhesins on different bacterial strains, including the *S. aureus* strain used here, this study may be considered as a stringent evaluation of the possibilities of bacterial confinement in the design of bi-functional biomaterials coatings.

MATERIALS AND METHODS

PEG-microgel patterning

PEG-microgel patterned glass slides were prepared using established procedures [20, 21]. Briefly, glass slides were sonicated in (96%) ethanol, deep cleaned in a Piranha solution, water rinsed and exposed to an O_2 plasma prior to silanization with 2% [v/v] vinyl-methoxy siloxane (Gelest). A solution of 2 wt% PEG (6 kDa; Fluka) in tetrahydrofuran was used to make thin films by spin casting on the glass slides. The film thickness was measured to be around 120 nm by ellipsometry.

PEG was locally crosslinked during e-beam lithography [21, 22]. Briefly, spincoated PEG thin film was irradiated in a Zeiss Auriga FIB-SEM microscope (point dose of 10 fC, and incident beam energy of 2 keV). The e-beam position and dwell time were controlled using an external control system (NPGS, Nabity NanoPattern Generation System). After e-beam exposure, the slides were washed in Milli-Q water for 30 min to remove unexposed PEG. The resulting surface consisted of silanized glass between surface-bound patterned PEG thin-film gel. Patterned areas were made as 200 μm × 200 μm squares of PEG thin-film gel containing circular patches (diameters α of 1, 2, 3 or 5 μm) of exposed glass with inter-patch distances β of 1/2 α, α and 2α. This yielded patterns with a different adhesive area fractions χ of 0.1, 0.2 and 0.35. Multiple substrata were prepared, each having twelve arrays patterned on one glass slide such that each array was separated from an adjacent

array by a 100 µm wide strip of silanized glass. After patterning, substrata were stored under vacuum (50 mTorr). Light microscopic images of the arrays were taken with a Nikon Eclipse E1000. The final cross-linked PEG film thickness was determined by atomic force microscopy (AFM) and estimated to be around 60 nm in the dry state and around 120 nm when measured under wet conditions.

Fibronectin adsorption on PEG-microgel patterns

A 0.05 mL droplet of Fn (25 µg/mL human Fn; Sigma-Aldrich BV, Zwijndrecht, The Netherlands) was placed on the patterned region of a glass slide for 30 min at room temperature. To demonstrate Fn adsorption, the entire slide was immersed in phosphate buffered saline (PBS; 10 mM potassium phosphate and 0.15 M NaCl, pH 7.0) containing 1% BSA for 1 min to block non-specific adsorption of proteins, and the slide was rinsed 3 $\times$ 5 min with the same PBS solution. Primary antibody (rabbit-anti-human fibronectin Ab, polyclonal, dilution 1:400 in PBS) was then adsorbed for 30 min, and slides were rinsed again for 3 $\times$ 5 min. Finally, a fluorescent secondary antibody (FITC conjugated Donkey-anti-rabbit IgG, dilution 1:100 in PBS) was adsorbed and rinsed as described above, the patterned glass slide was put in a petri dish filled with PBS and examined with confocal laser scanning microscopy (CLSM, Leica DMRXE with confocal TCS SP2 unit).

Bacterial strain, growth and harvesting

S. aureus 8325-4, possessing FnBPs (provided by T.J. Foster, Moyne Institute of Preventive Medicine, Dublin, Ireland), was used in this study. The staphylococci were maintained at -80°C in tryptone soy broth (TSB; Oxoid, Basingstoke, United Kingdom) containing 7% dimethyl sulfoxide (Merck, Germany). For culturing, *S. aureus* were incubated on TSB agar plates overnight at 37°C. Subsequently, one bacterial colony was grown in 10 mL TSB batch cultures overnight with constant rotation (120 rpm). Each preculture was used to inoculate a main culture of 190 mL TSB which was grown under the same conditions. After approximately 2 h, representing early stationary phase bacteria with peak expression of FnBPs in *S. aureus* 8325-4 [23], staphylococci were harvested by centrifugation at 6500g

for 5 min at 10°C and washed twice in sterile PBS. Bacterial aggregates were broken by mild, intermittent sonication on ice for 3 × 10 s at 30 W (Wibra Cell model 375, Sonics and Materials Inc., Danbury, Connecticut, USA) and resuspended to a concentration of 3×10^6 bacteria/mL in PBS.

Staphylococcal adhesion and growth

Bacterial adhesion was studied in a parallel plate flow chamber [24] on PEG-microgel patterned glass slides, after 30 min of Fn pre-adsorption. Initial staphylococcal adhesion was monitored by digital phase-contrast microscopy (Olympus BH-2; 40× objective). After removing air bubbles in the tubing by flowing PBS, the *S. aureus* suspension in PBS was perfused through the chamber (11 s^{-1} shear rate) for 3 h at room temperature. Images were taken from each PEG-microgel patterned square and from surrounding unpatterned, silanized glass at 1 min time intervals. From these, the number of adhering bacteria on each array was determined at different time points.

After 3 h of initial deposition, sterile PBS was flowed through the chamber, also at a shear rate of 11 s^{-1} for 30 min to remove the bacterial suspension from the chamber and from the tubing. TSB was then flowed through the chamber at a low shear rate of 0.14 s^{-1} for 24 h. A heating element was used to keep the chamber temperature at 37 °C. After 24 h, another 30 min of PBS washing (shear rate = 11 s^{-1}) was carried out before fixing the biofilm with 2% glutaraldehyde in 0.1 M cacodylate buffer. For scanning electron microscopic (SEM) observation, slides were further fixed with OsO_4 (1% in 0.1 M cacodylate buffer) for 1 h, and then dehydrated using an ethanol series. Slides were incubated in tetramethylsilane for 15 min, air dried and sputter coated with Au/Pd. Imaging was done using a Zeiss Auriga Dual-Beam SEM at 2 kV.

Mammalian cell culturing, harvesting and adhesion

U2OS osteosarcoma cells were cultured in low-glucose Dulbecco's Modified Eagles Medium (DMEM) supplemented with 10% fetal bovine calf serum (FBS) and 0.2 mM of

ascorbic acid-2-phosphate. U2OS cells were maintained in T75 culture flasks at 37 °C in humidified 5% CO_2 and harvested at 90% confluency using trypsine/ethylenediamine–tetra-acetic acid. The harvested cells were diluted to 6 x 10^5 cells/mL. U2OS is an immortalized human cell line derived from osteosarcoma cells and was chosen from a broad selection of human osteoblastic cell lines used previously [25]. It has been demonstrated that osteosarcoma cell lines exhibit meaningful osteoblastic phenotypes [26].

U2OS adhesion and spreading on PEG-microgel patterned surfaces with pre-adsorbed Fn were studied by *in situ* phase-contrast imaging in the parallel plate flow chamber and by *ex situ* immunofluorescence imaging. The flow chamber was maintained at 37 °C throughout the experiments. Once fully filled and free of air-bubbles, a U2OS cell suspension in cell culture medium (DMEM + 10% FBS) was introduced. After filling the chamber, flow was stopped for 1.5 h to allow U2OS cells to adhere and spread. Phase-contrast images were taken at this time point from each patterned array and also from the silanized-glass area as a control to determine the initial surface coverage of spread U2OS cells. Modified culture medium supplemented with 2% HEPES buffer was then perfused through the flow chamber at 0.14 s^{-1} shear rate for 48 h. After 48 h the substrata were removed, fixed twice in 30 mL of 3.7% formaldehyde in cytoskeleton stabilization buffer (CS; 0.1 M Pipes, 1 mM EGTA, 4% (w/v) PEG 8000, pH 6.9), incubated in 0.5% Triton X-100 (3 min), rinsed with PBS, and stained for 30 min in 5 mL PBS containing 49 µL DAPI and 2 µg/mL of TRITC–Phalloidin. After four washes in PBS, the slides were examined by fluorescence microscopy (Leica DM 4000B). The total surface coverage of adhering cells on the patterned surfaces was determined by Scion image software.

RESULTS

Fn adsorption on PEG-microgel patterns

Figure 1 demonstrates the surface morphology of the PEG-microgel patterns obtained using light microscopy, AFM and CLSM after Fn adsorption. Adsorbed Fn (green

fluorescence) is only visual within the circular, silanized glass areas constituting the pattern, but not on the surrounding PEG-film.

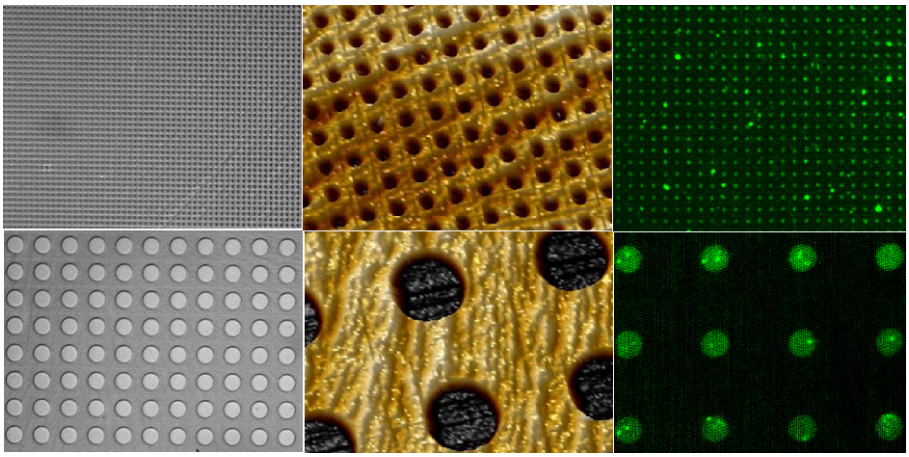

Figure 1 The morphology of patterned surfaces with adhesive patches of 1 µm (top row) and 5 µm (bottom row) diameters at different adhesive area fractions.
Left panel: Light microscopic images show dry patterns with an adhesive area fraction of 0.35. Middle panel: AFM topographic mapping of dry patterns with an adhesive area fraction of 0.2. Right panel: CLSM images showing the preferential adsorption of Fn (green fluorescence) onto the exposed glass patches on patterns with an adhesive area fraction of 0.1.

Staphylococcal adhesion and biofilm formation on PEG-microgel patterns

After 3 h, averaged over three separate experiments, 2.9×10^5 staphylococci adhered per cm^2 to the silanized glass surface outside the PEG patterns. Figure 2 shows the numbers of adhering staphylococci on the patterned area, regardless of whether adhesion occurred within the adhesive patch or on the surrounding PEG. At the highest adhesive area fraction, the numbers of adhering staphylococci clearly increase with increasing diameter of the adhesive patch, while at lower adhesive area fractions (0.1 and 0.2) a clear trend with the patch diameter is more difficult to discern. Interestingly, overall the reduction of staphylococcal adhesion on patterned surfaces didn't show a significant difference with different α and β. However, there is around a 50% drop compared to bare glass even in the presence of adsorbed Fn for which the staphylococcal strain used has a much higher affinity than for the surrounding PEG-microgel.

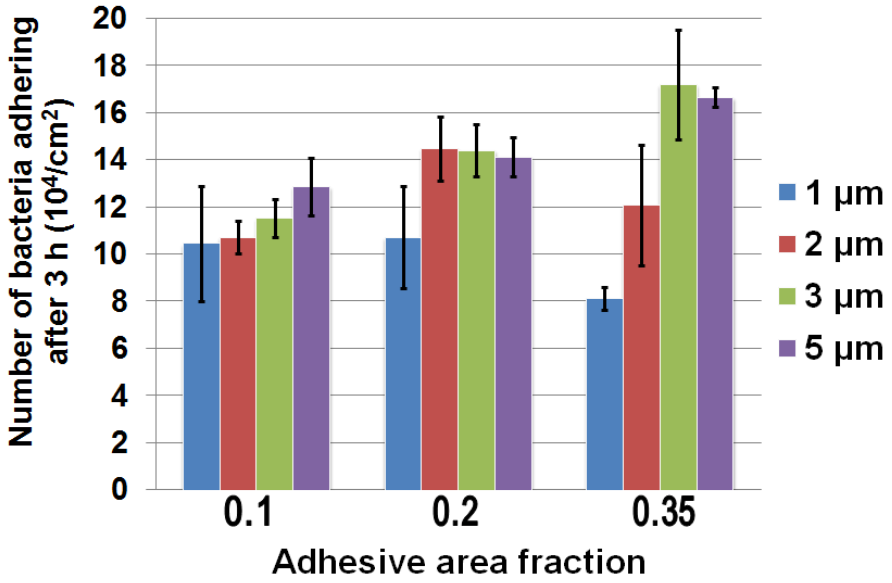

Figure 2 The number of adhering *S. aureus* 8325-4 after 3 h on fibronectin coated PEG-microgel patterns consisting of adhesive patches with different diameters of the adhesive areas and inter-patch distances, yielding the adhesive area fractions indicated.
All data are averages over 3 experiments with separately cultured staphylococci with bars representing the SD.

SEM images after 24 h of staphylococcal growth on the PEG-microgel patterns are shown in Figure 3 for two different patterns (χ = 0.35, α = 3 µm and 5 µm). Thick biofilms are visible on the silanized glass outside the patterns, while growth is largely confined to the adhesive areas in the patterned region. The effect of confinement for different patterns on bacterial growth is described in Table 1, which summarizes the ratio of the number of bacteria growing inside the patches to the total number of bacteria on a pattern. It can be seen that adhesive patches of 1 µm gave the highest inhibition of bacterial growth and staphylococcal growth is more confined. When the diameter of the adhesive area increases, confinement is stronger with increasing adhesive area fraction.

Table 1 Confined, 20 h growth of adhering staphylococci on microstructured PEG-patterns, expressed as the ratio between the numbers of bacteria on the adhesive areas and surrounding PEG-films, for patterns with different adhesive area diameters α and surface adhesive fractions χ. For calculation of the confinement ratios, the numbers of staphylococci on the adhesive patches was divided by the total number of bacteria on a pattern. Data pertain to triplicate experiments with separately grown staphylococcal cultures, with ± representing the SD.

χ	**0.1**			**0.2**			**0.35**		
α	1 µm	2 µm	5 µm	1 µm	2 µm	5 µm	1 µm	2 µm	5 µm
Confinement ratio	0.43 ± 0.08	0.31 ± 0.11	0.14 ± 0.03	0.71 ± 0.09	0.57 ± 0.05	0.27 ± 0.09	0.93 ± 0.07	0.55 ± 0.08	0.33 ± 0.08

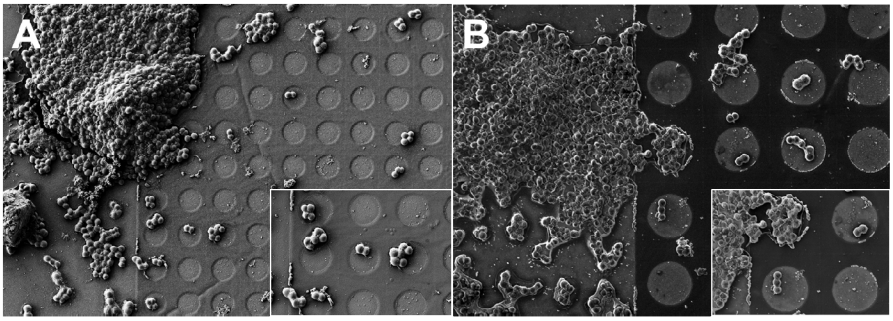

Figure 3 SEM images showing *S. aureus* 8325-4 biofilm formation after 24 h of growth in TSB under low shear (0.14 s^{-1}) on fibronectin adsorbed PEG-microgel patterns consisting of adhesive patches with an adhesive area fraction of 0.35 and their border zone with glass. A: diameter of the adhesive patch equals 3 µm B: diameter of the adhesive patch equals 5 µm.

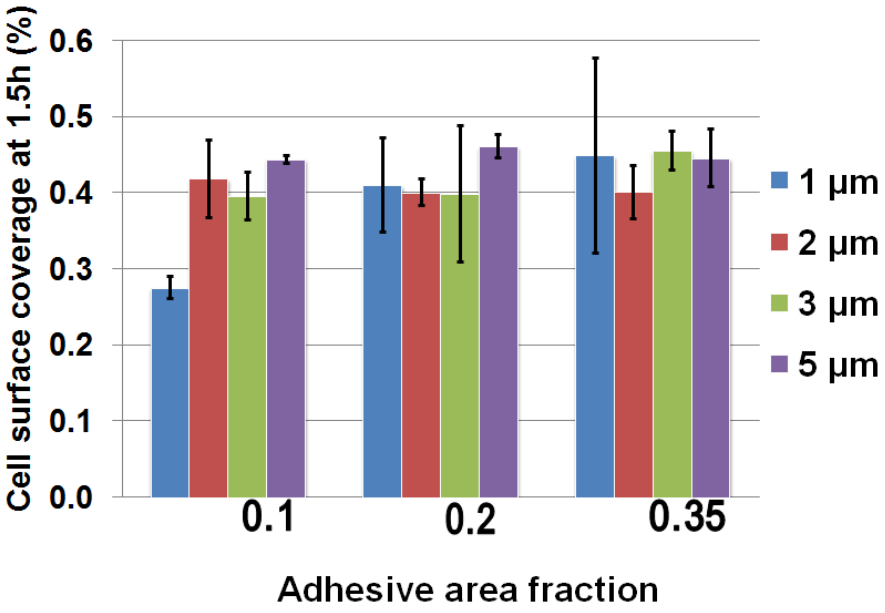

Figure 4 U2OS cell surface coverage after 1.5 h on fibronectin adsorbed PEG-microgel patterns consisting of adhesive patches with different adhesive patch diameters and adhesive area fractions. All data are represented as averages over three experiments with separately cultured cells with bars representing the SD.

Mammalian cells adhesion, spreading and growth on PEG-microgel patterns

The initial adhesion and spreading of U2OS cells after 1.5 h of seeding is similar on all of the patterned surfaces, yielding a surface coverage on the patterns of approximately 40% ± 5% (Figure 4). After 48 h of growth, however (see Figure 5), we observed cell migration on the pattern with the smallest patch diameter, as we can also see in Figure 6. Patch patterns with smaller diameters and the lowest adhesive area fraction (0.1) show negative change in cell surface coverage, demonstrating that this pattern provides an insufficient number of strongholds for the cells to adhere and spread.

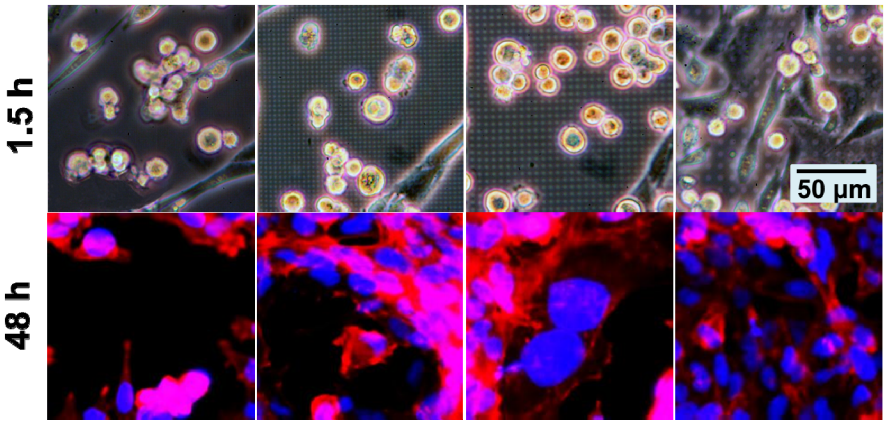

Figure 5 U2OS cell adhesion after 1.5 h (upper panel, images taken from phase contrast microscope) and after 48 h (lower panel, images taken from CLSM) of growth on fibronectin adsorbed PEG-microgel patterns consisting of adhesive patches with different patch diameters (left to right: 1, 2, 3 and 5 µm) and an adhesive area fraction of 0.2.

Conditions for bacterial confinement *versus* tissue integration

In order to evaluate the merits of the different patterns with respect to confining staphylococcal growth and mediating tissue integration, the percentage change in surface coverage by U2OS cells after 48 h of growth has been plotted as a function of the increase in number of adhering staphylococci after growth on the patterns over their respective experimental periods (Figure 6). Evidently, since the ultimate goal would be elimination of all initially adhering bacteria combined with maximal growth of adhering cells, the top-left corner of the graph constitutes optimal conditions for bacterial confinement *versus* tissue integration. The trend-lines show that strong bacterial growth and reduced cell growth rotate the trend line in an undesired clockwise direction for patterns with the smallest adhesive area fraction, while the trend-lines rotate in the desired counter-clockwise direction when the adhesive area fraction increases.

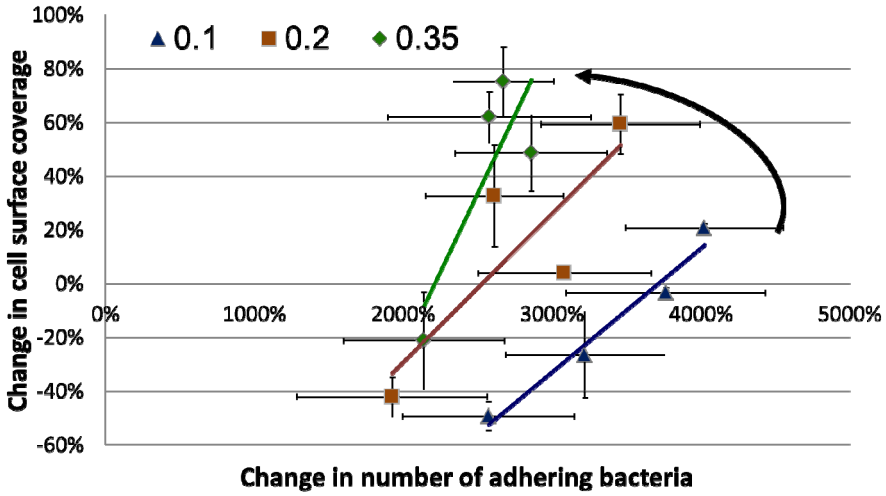

Figure 6 The percentage increase in surface coverage by U2OS cells as a function of the increase in the number of staphylococci during growth on the different patterns over the indicated experimental periods (U2OS: grow from 1.5 h to 48 h, *S. aureus* 8325-4: grow from 3 h to 24 h) for the three different adhesive area fractions applied in this study. Data points for a given adhesive area fraction relate to the different diameters of the adhesive areas. The arrow indicates the desired direction of rotation of these bi-functional surfaces toward increased cell surface coverage and reduced bacterial adhesion.

DISCUSSION

In this paper we analyzed conditions under which surfaces patterned by PEG thin-film gels facilitate tissue integration and reduce bacterial growth. The surfaces consisted of adhesive patches with adsorbed Fn surrounded by continuous PEG film with different patch diameters and spacings yielding adhesive area fractions ranging from 0.1 to 0.35. An adhesive area fraction of 0.1 proved to be too low to support tissue integration while bacterial growth was inhibited due to both the effect of the non-adhesive PEG film and also bacterial confinement to the adhesive patches. Increasing the adhesive area fraction supported cell adhesion, spreading and growth, while still confining bacterial growth to the adhesive areas. Therewith this study describes a new approach to design bi-functional

coatings for permanent, totally internal implants or devices requiring tissue integration, with a reduced risk of infection.

In general, PEGylated surfaces typically do not support protein adsorption resulting in the inhibition of mammalian cell and bacterial adhesion [27-29]. Such behavior is mainly due to the steric repulsion between the hydrated PEG chains and proteins. Consistent with this behavior, we find that adsorbed Fn is visualized (green fluorescence in Figure 1) within the circular, silanized glass areas constituting the pattern. In contrast, little fluorescent intensity is observed on the surrounding PEG film confirming the non-adhesive behavior of the patterned PEG films in these experiments.

Bacteria adhere and grow to virtually all surfaces. Biofilms have even been grown on PEGylated surfaces although, in general, the continuous, highly hydrated and extended polymer chains of PEGylated surfaces exert an extremely low attraction to proteins, cells and bacteria [30, 31]. Indeed, bacterial growth on monofunctional PEGylated surfaces was strongly delayed with respect to growth on uncoated silicone rubber surfaces [30]. Consistent with this previous observation, also in the present study massive biofilm growth can be observed next to the PEG-microgel patterns that tend to overgrow the PEGylated film (Figure 3). Biofilms do not only show a delayed growth on PEGylated surfaces but also adhere weakly, and minor increases in shear rate have been demonstrated to be sufficient to remove biofilms adhering to PEGylated surfaces and prevent bacterial adhesion [32]. This may explain why on PEG-microgel patterns we see bacterial growth confined to the adhesive patches. Confined growth will have been enhanced by adsorption of Fn to the patches and the use of a staphylococcal strain that has a high affinity for Fn. Owing to their larger dimensions and depending on the size of the adhesive areas and the adhesive area fraction, mammalian cells were able to find strongholds for their growth on PEGylated patterns.

Clinically it is very difficult to insert a biomaterials implant or device in an absolutely sterile fashion, and additional antibiotic treatment is usual. Antibiotic treatment after surgery is only effective however, when applied before per-operatively introduced bacteria have had the opportunity to develop into their protective biofilm mode of growth. Alternatively, tissue integration provides protection against BAI, but this is especially so for bacteria that spread through a haematogenous route toward an implant or device surface [33]. The conditions of confinement of growth of per-operatively introduced bacteria *versus* tissue integration by PEG-microgel patterns is elegantly summarized in Figure 6. Whereas the top-left corner is the desired position for an optimal bi-functional coating, it is clear from the current data that a vertical line (no bacterial growth) pointing to maximal coverage of the surface by mammalian cells is the best we can establish by PEG-microgels patterns in absence of bacterial killing or removal. A combination with antibiotics, however, will yield killing of the bacteria while their growth is simultaneously confined to the adhesive areas and this will bring us toward the desired top-left corner. Also in the human body, macrophages will assist in removing adhering bacteria which thrives the end-result of our coating towards the top-left corner again. In this respect it is important to emphasize, that macrophages have been demonstrated to be more mobile and therewith more effective in removing adhering bacteria from PEGylated surfaces due to their low adhesion forces with the substratum [34]. Therefore confined growth of bacteria on PEG-microgel patterns could be advantageous to macrophages in the clearance of bacteria from an implant surface.

CONCLUSION

By introducing PEG-microgel patterns with different diameters of the adhesive patches and different adhesive area fractions, we have demonstrated that bacterial growth is confined to the adhesive areas while at the same time the adhesive areas provide sufficient strongholds for mammalian cells to adhere, spread and grow, when the adhesive area diameter and fraction are sufficiently high. The conditions of bacterial confinement were enhanced in the present study, by adsorbing Fn to the patterns and

using a staphylococcus strain possessing FnBps. On the other hand however, the use of a staphylococcal strain that utilizes the same peptide sequence for their adhesion as mammalian cells constitutes a clinically most stringent evaluation of the possibilities of confined bacterial growth *versus* tissue integration on PEG-microgel patterns.

REFERENCES

1. Gotz F. Staphylococcus and biofilms. Mol Microbiol 2002;43:1367-78.
2. Donlan RM, Costerton JW. Biofilms: survival mechanisms of clinically relevant microorganisms. Clin Microbiol Rev 2002;15:167-93.
3. Saravia V, Kupcu S, Nolte M, Huber C, Pum D, Fery A, *et al*. Bacterial protein patterning by micro-contact printing of PLL-g-PEG. J Biotechnol 2007;130:247-52.
4. Sankar S, Rajalakshmi T. Application of poly ethylene glycol hydrogel to overcome latex urinary catheter related problems. Biofactor 2007;30:217-25.
5. Banerjee I, Pangule RC, Kane RS. Antifouling coatings: recent developments in the design of surfaces that prevent fouling by proteins, bacteria, and marine organisms. Adv Mater 2011;23:690-718.
6. VandeVondele S, Voros J, Hubbell JA. RGD-grafted poly-L-lysine-graft-(polyethylene glycol) copolymers block non-specific protein adsorption while promoting cell adhesion. Biotechnol Bioeng 2003;82:784-90.
7. LeBaron RG, Athanasiou KA. Extracellular matrix cell adhesion peptides: functional applications in orthopedic materials. Tissue Eng 2000;6:85-103.
8. Maddikeri RR, Tosatti S, Schuler M, Chessari S, Textor M, Richards RG, *et al*. Reduced medical infection related bacterial strains adhesion on bioactive RGD modified titanium surfaces: a first step toward cell selective surfaces. J Biomed Mater Res A 2008;84:425-35.
9. Shi Z, Neoh KG, Kang ET, Poh C, Wang W. Bacterial adhesion and osteoblast function on titanium with surface-grafted chitosan and immobilized RGD peptide. J Biomed Mater Res A 2008;86:865-72.
10. Csucs G, Michel R, Lussi JW, Textor M, Danuser G. Microcontact printing of novel co-polymers in combination with proteins for cell-biological applications. Biomaterials 2003;24:1713-20.
11. Mrksich M, Chen CS, Xia Y, Dike LE, Ingber DE, Whitesides GM. Controlling cell attachment on contoured surfaces with self-assembled monolayers of alkanethiolates on gold. Proc Natl Acad Sci U S A 1996;93:10775-8.

12. Revzin A, Russell RJ, Yadavalli VK, Koh WG, Deister C, Hile DD, *et al.* Fabrication of poly(ethylene glycol) hydrogel microstructures using photolithography. Langmuir 2001;17:5440-7.
13. Hui EE, Bhatia SN. Microscale control of cell contact and spacing via three-component surface patterning. Langmuir 2007;23:4103-7.
14. Papavasiliou G, Songprawat P, Perez-Luna V, Hammes E, Morris M, Chiu YC, *et al.* Three-dimensional pattering of poly (ethylene glycol) hydrogels through surface-initiated photopolymerization. Tissue Eng Part C Methods 2008;14:129-40.
15. Suh KY, Seong J, Khademhosseini A, Laibinis PE, Langer R. A simple soft lithographic route to fabrication of poly(ethylene glycol) microstructures for protein and cell patterning. Biomaterials 2004;25:557-63.
16. Kim P, Kim DH, Kim B, Choi SK, Lee SH, Khademhosseini A, *et al*. Fabrication of nanostructures of polyethylene glycol for applications to protein adsorption and cell adhesion. Nanotechnology 2005;16:2420-6.
17. Moorman AV, Richards SM, Robinson HM, Strefford JC, Gibson BE, Kinsey SE, *et al.* Prognosis of children with acute lymphoblastic leukemia (ALL) and intrachromosomal amplification of chromosome 21 (iAMP21). Blood 2007;109:2327-30.
18. Koh W-G, Revzin A, Simonian A, Reeves T, Pishko M. Control of mammalian cell and bacteria adhesion on substrates micropatterned with poly(ethylene glycol) hydrogels. Biomed Microdevices 2003;5:11-9.
19. Krsko P, Kaplan JB, Libera M. Spatially controlled bacterial adhesion using surface-patterned poly(ethylene glycol) hydrogels. Acta Biomater 2009;5:589-96.
20. Krsko P, Mansfield M, Sukhishvili S, Clancy R, Libera M. Electron-beam patterned poly(ethylene glycol) microhydrogels. Langmuir 2003;19:5618-25.
21. Krsko P, Saaem I, Clancy R, Geller H, Soteropoulos P, Libera M. E-beam patterned hydrogels to control nanoscale surface bioactivity In: Lai WY, Ocola LE, Pau S, editors. Nanofabrication: Technologies, Devices, and Applications II. Bellingham: SPIE; 2005. 600201.

22. Christman KL, Enrique-Rios VD, Maynard HD. Nanopatterning proteins and peptides. Soft Matter 2006;2:928-39.
23. Saravia-Otten P, Muller HP, Arvidson S. Transcription of *Staphylococcus aureus* fibronectin binding protein genes is negatively regulated by agr and an agr-independent mechanism. J Bacteriol 1997;179:5259-63.
24. Subbiahdoss G, Kuijer R, Grijpma DW, Van der Mei HC, Busscher HJ. Microbial biofilm growth vs. tissue integration: "the race for the surface" experimentally studied. Acta Biomater 2009;5:1399-404.
25. De Ruijter JE, Ter Brugge PJ, Dieudonne SC, Van Vliet SJ, Torensma R, Jansen JA. Analysis of integrin expression in U2OS cells cultured on various calcium phosphate ceramic substrates. Tissue Eng 2001;7:279-89.
26. Pautke C, Schieker M, Tischer T, Kolk A, Neth P, Mutschler W, *et al.* Characterization of osteosarcoma cell lines MG-63, Saos-2 and U-2 OS in comparison to human osteoblasts. Anticancer Res 2004;24:3743-8.
27. Park KD, Kim YS, Han DK, Kim YH, Lee EH, Suh H, *et al*. Bacterial adhesion on PEG modified polyurethane surfaces. Biomaterials 1998;19:851-9.
28. Roosjen A, Kaper HJ, Van der Mei HC, Norde W, Busscher HJ. Inhibition of adhesion of yeasts and bacteria by poly(ethylene oxide)-brushes on glass in a parallel plate flow chamber. Microbiology 2003;149:3239-46.
29. Ostuni E, Chapman RG, Liang MN, Meluleni G, Pier G, Ingber DE, *et al*. Self-assembled monolayers that resist the adsorption of proteins and the adhesion of bacterial and mammalian cells. Langmuir 2001;17:6336-43.
30. Nejadnik MR, Van der Mei HC, Norde W, Busscher HJ. Bacterial adhesion and growth on a polymer brush-coating. Biomaterials 2008;29:4117-21.
31. Roosjen A, De Vries J, Van der Mei HC, Norde W, Busscher HJ. Stability and effectiveness against bacterial adhesion of poly(ethylene oxide) coatings in biological fluids. J Biomed Mater Res B Appl Biomater 2005;73:347-54.
32. Nejadnik MR, Van der Mei HC, Busscher HJ, Norde W. Determination of the shear force at the balance between bacterial attachment and detachment in weak-

adherence systems, using a flow displacement chamber. Appl Environ Microbiol 2008;74:916-9.

33. Gottenbos B, Busscher HJ, Van Der Mei HC, Nieuwenhuis P. Pathogenesis and prevention of biomaterial centered infections. J Mater Sci Mater Med 2002;13:717-22.
34. Saldarriaga Fernandez IC, Da Silva Domingues JF, Van Kooten TG, Metzger S, Grainger DW, Busscher HJ, *et al*. Macrophage response to staphylococcal biofilms on crosslinked poly(ethylene) glycol polymer coatings and common biomaterials *in vitro*. Eur Cell Mater 2011;21:73-9.

Chapter 6

In Vitro Interactions between Bacteria and Macrophages on PEG-microgel Patterned Adhesive Patches in the Pathogenesis of Biomaterial-Associated Infections

INTRODUCTION

Biomaterials play an important role in human life to support and restore function in order to create a better quality of life. Surfaces of modern biomaterials are highly engineered to regulate their interactions with physiological systems. Yet, biomaterial-associated infection (BAI) remains a serious problem in modern medicine. BAI is often difficult to treat, as the biofilm mode of growth protects pathogenic microorganisms against both the host defense system and antibiotics [1]. In most cases, the final outcome is removal of the implant in order to cure the infection. Biomaterial implants can become contaminated by microorganisms through different routes as e.g. direct contamination of the implant surface during surgery (peri-operative contamination) or contamination during hospitalization (post-operative contamination). Whether or not microbial contamination eventually results in BAI, depends on the outcome of the so-called 'race for the surface' between successful tissue integration of the implant surface and biofilm formation [2]. If tissue cells win this race, the implant surface will be covered by a cellular layer and is then less vulnerable to biofilm formation. Alternatively, in the inverse case, bacteria will colonize the implant surface and thus tissue cell functions are hampered by bacterial virulence factors and excreted toxins [2-4].

Staphylococcus epidermidis and *Staphylococcus aureus* are the most frequently isolated pathogens from infected biomaterials implant surfaces [2, 5], whereas *S. aureus* is detected in approximately 23% of infections associated with prosthetic joints [6]. The pathogenesis of BAI is complex and depends on factors such as bacterial virulence, physico-chemical properties of the biomaterial surface and alterations in the host defense [7]. Following biomaterials implantation, tissue trauma and injury trigger a cascade of events that activate the immune system [8]. Macrophages are one of the most predominant immune cells that arrive within minutes to hours at an implant site and can remain at a biomaterials surface for several weeks to orchestrate the inflammatory process and foreign body reactions [8]. During infection, macrophages detect bacteria via cell surface receptors that bind to bacterial ligands and opsonins [9-11]. Subsequently,

macrophages ingest pathogens and activate cellular functions such as proliferation, secretion of proteins and cytokines, and respiratory burst to destroy phagocytized microorganisms and recruit other cells from the adaptive immune system [9]. Therefore, bacteria-biomaterial-macrophage interactions are important factors contributing to the pathogenesis of BAI.

Several surface modifications have been developed to mitigate bacterial colonization [12-14]. However, while they inhibit bacterial colonization, they simultaneously prevent tissue integration. A surface that differentially promotes interactions with desirable mammalian cells while simultaneously reducing microbial colonization is required. In our previous study (Chapter 5), we observed that adhesive patches of varying diameters showed confined bacterial adhesion and growth at patterned surfaces with minimally adhesive fractions (≤ 0.35). Interestingly, mammalian cell adhesion, spreading and growth were still favored on those patterns. Based on those results, we hypothesize that confined bacterial growth in the adhesive patches can be advantageous for macrophages in clearance of bacteria from the biomaterials surface. We chose an adhesive patch size of 5 μm (α) to observe the interactions of bacterial and macrophages on these surfaces. Inter-patch distances of 2.5 μm and 10 μm (β) were used to generate different adhesive fractions (0.1 and 0.35).

MATERIALS AND METHODS

PEG-patterned adhesive patches

PEG-microgel patterned glass slides were prepared using established procedures [15, 16]. Briefly, glass slides were sonicated in 96% ethanol, deep cleaned in a Piranha solution, water rinsed and exposed to an O_2 plasma prior to silanization with 2% (v/v) vinyl-methoxy siloxane (Gelest, Morrisville, PA, USA). A solution of 2 wt% PEG (6 kDa; Fluka, Sigma-Aldrich, USA) in tetrahydrofuran was used to make thin films by spin casting on the glass slides. The film thickness was measured to be around 120 nm by ellipsometry.

PEG was locally crosslinked during e-beam lithography [16, 17]. After e-beam exposure, the slides were washed in Milli-Q water for 30 min to remove unexposed PEG. The resulting surface consisted of silanized glass between surface-bound patterned PEG thin-film gel. Patterned areas were made as 200 µm × 200 µm squares of PEG thin-film gel containing circular patches (diameters α of 5 µm) of exposed glass with inter-patch distances β of 1/2 α and 2α. This yielded patterns with a different adhesive area fractions χ of 0.1 and 0.35. Multiple substrates were prepared, each having adhesive-patch patterns. Different inter-patch distances were patterned on one glass slide such that each patterned area was separated from an adjacent array by a 100 µm wide strip of silanized glass. After patterning, substrata were stored under vacuum (50 mTorr). Light microscopic images of the arrays were taken with a Nikon Eclipse E1000. The film thickness after e-beam irradiation and cleaning with deionized water was determined by atomic force microscopy (AFM) and estimated to be around 60 nm in the dry state and around 120 nm when measured under wet conditions.

Bacterial strain, growth and harvesting

S. aureus 8325-4, possessing FnBPs (provided by T.J. Foster, Moyne Institute of Preventive Medicine, Dublin, Ireland) was used in this study. The *S. aureus* 8325-4 was maintained at -80 °C in tryptone soy broth (TSB; Oxoid, Basingstoke, United Kingdom) containing 7% dimethyl sulfoxide (Merck, Germany). For culturing, *S. aureus* was incubated on a TSB agar plate overnight at 37 °C. Subsequently, one bacterial colony was precultured in 10 mL TSB batch culture overnight with constant rotation. Each preculture was used to inoculate a main culture of 190 mL TSB. After approximately 2 h, representing early stationary phase bacteria with peak expression of FnBPs in *S. aureus* 8325-4 [18], staphylococci were harvested by centrifugation at 6500g for 5 min at 10 °C and washed twice in sterile phosphate-buffered saline (PBS; 10 mM potassium phosphate and 0.15 M NaCl, pH 7). Bacterial aggregates were broken by mild, intermittent sonication on ice for 3 × 10 s at 30 W (Wibra Cell model 375, Sonics and Materials Inc., Danbury, Connecticut, USA) and resuspended to a concentration of 3×10^8 bacteria/mL in sterile PBS.

Macrophages culturing and harvesting

J774A.1 murine macrophages (ATCC number: TIB-67; obtained from LGC standards, Wesel, Germany) were routinely cultured in DMEM-high glucose supplemented with 10% FBS. Macrophages were maintained at 37 °C in a humidified atmosphere with 5% CO_2, and passaged at 70–80% confluency by scraping. The harvested cells were counted using a Bürker-Türk hemocytometer and subsequently diluted to a concentration of 6×10^6 cells/mL.

Staphylococcal adhesion and biofilm growth on PEG-patterned adhesive patches

Bacterial adhesion and biofilm formation on PEG-patterned patch surfaces were studied in a parallel-plate flow chamber, equipped with heating elements and kept at 37ºC throughout the experiments. Prior to each experiment, all tubes and the flow chamber were filled with sterile PBS, taking care to remove all air bubbles from the system. Once the system was filled, and before the addition of the bacterial suspension, PBS was allowed to flow through the system at a shear rate of 11 s^{-1}. Then, a bacterial suspension in PBS was perfused through the chamber at the same shear rate and phase-contrast images were obtained for 30 min of adhesion. Flow of the bacterial suspension was then switched to sterile PBS in order to remove the non-adhering bacteria from the tubes and chamber. After 10 min of PBS, flow was replaced with TSB, which was perfused for 1 h to grow a biofilm. Phase-contrast images were taken from each pattern and from unpatterned, silanized glass at 1 min time intervals, from which the number of adhering bacteria was determined.

Macrophages interaction with staphylococcal biofilm on PEG-patterns with adhesive patches

J774A.1 interactions with *S. aureus* 8325-4 on PEG-patterned Fn-adhesive patch surfaces were studied by *in situ* imaging in the parallel-plate flow chamber. After biofilm growth for 1 h, the entire volume of TSB inside the chamber was replaced by cell culture medium (DMEM-HG + 10% FBS), to remove the non-adhering bacteria from the tubes and chamber.

Subsequently, a J774A.1 suspension (6×10^6 cells/mL) in culture medium was allowed to enter the flow chamber. Once the entire volume of culture medium inside the chamber was replaced by the J774A.1 suspension, flow was stopped for 2 h in order to allow macrophages to adhere to the substratum surface. Subsequently, macrophage-bacteria interactions were followed real-time with a CCD camera (Basler AG, Germany) mounted on a phase-contrast microscope Olympus BH-2 (Olympus, Germany). We use the change in number of adhering bacteria per unit area before and after macrophage insertion to evaluate macrophage engulfment for both the patterned surface and bare glass. The number of bacteria engulfed per macrophage was normalized with respect to the number of bacteria adhering to glass or the patterned surface prior to the insertion of macrophages.

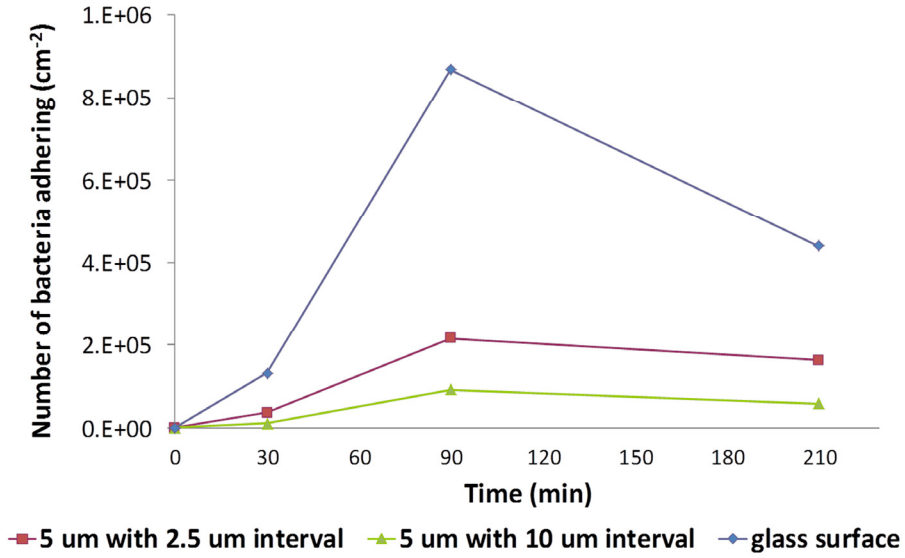

Figure 1 Number of adhering *S. aureus* 8325-4 on glass and different PEG-gel patterned surfaces at 30 min (after initial bacterial adhesion), 90 min (after bacterial biofilm growth for 60 min) and 210 min (after macrophage-bacteria interactions for 120 min) in a parallel-plate flow chamber.

RESULTS AND DISCUSSION

In order to study the interactions between bacteria and macrophages *in vitro* on PEG-patterned surfaces, bacteria were firstly introduced to PEG-patterned surfaces for a period of 30 min under flow prior to adding macrophages, mimicking the situation of peri-operative bacterial contamination of implant surfaces [19]. As shown in Figure 1, bare glass showed the highest number of bacteria per unit area compared to the patterned surfaces. The reduction in bacterial deposition on patterned surfaces was mainly due to reduced adhesive surface exposed for the bacterial interaction and the PEGylated surface effectively prevented bacterial adhesion. Similar observations were reported in a previous study clearly indicating reduced bacterial adhesion on PEG-microgel patterned surfaces compared to bare glass [20]. After 1 h of biofilm growth, an increase in number of bacteria was observed on all surfaces. Since bare glass had the highest number of bacteria after 30 min of deposition, also the increase after 1 h (around 9×10^5 cm^{-2}, see Table 1) of growth was much higher than on the patterned surfaces. After the macrophages were introduced at 90 min, a decrease in number of adhering *S. aureus* was observed due to the clearance by macrophages (see Figure 1 and Table 1) on all surfaces.

Table 1 Adhesion and growth of *S. aureus* 8325-4 on different surfaces before (N) and after exposure to J774A.1 macrophages (N_{2h}) for 2 h, together with the number of macrophages per unit surface area, the number of bacteria taken per macrophage for the different patterns and the bacteria taken per macrophage normalized with respect to the initial number of bacteria adhering on the surface.

Surface	Glass	α = 5 µm β = 2.5 µm	α = 5 µm β = 10 µm
N ($10^5/cm^2$)	8.69	2.18	0.92
N_{2h} ($10^5/cm^2$)	4.40	1.63	0.60
Macrophages ($10^4/cm^2$)	5.19	3.50	4.75
Bacteria/Macrophage	8.3	1.6	0.7
(Bacteria/Macrophage)/N (cm^2)	$1x10^{-5}$	$7x10^{-6}$	$7x10^{-6}$

The migration of macrophages towards *S. aureus* and subsequent engulfment of *S. aureus* by macrophages on the patterned surface of 5 μm patch diameter and 2.5 μm inter-patch distance was shown in Figure 2. Macrophages showed better migration on patterned surfaces compared to bare glass, similar to what Saldarriaga Fernandez *et al.* [21] observed. They found that macrophage migration towards bacteria and phagocytosis was enhanced on highly hydrated, cross-linked poly(ethylene)-glycol (PEG) based polymer coatings compared to uncoated substrata. The percentage reduction of bacteria after 2 h of macrophage-*S. aureus* interactions was 50% on bare glass surface, while being 25% and 35% for patterns with 2.5 μm and 10 μm inter-patch distance, respectively. However, even after 50% of bacterial clearance on bare glass, the number of *S. aureus* that remain on the bare glass after 2 h of macrophage-*S. aureus* interactions was 2.7 times higher than for the pattern with 2.5 μm inter-patch distance and 7 times higher for the 10 μm inter-patch distance (see Figure 1).

The number of *S. aureus* engulfed by a single macrophage was calculated by dividing the number of bacteria removed in the presence of macrophages by the total number of macrophages on each patterned surface or bare glass surface. These results were further normalized taking into account the number of bacteria adhering on the surface before insertion of macrophages (see also Table 1). This then shows that the removal of bacteria from the surface by macrophages is happening with the same probability for both patterns (7×10^{-6} cm^2), while on bare glass, bacteria are being eliminated from the surface a bit faster (1×10^{-5} cm^2) compared to the patterns. An obvious explanation could be that on bare glass *S. aureus* were abundantly present, while on patterned surfaces, macrophages need to travel considerable distances from patch to patch, to find the confined *S. aureus*.

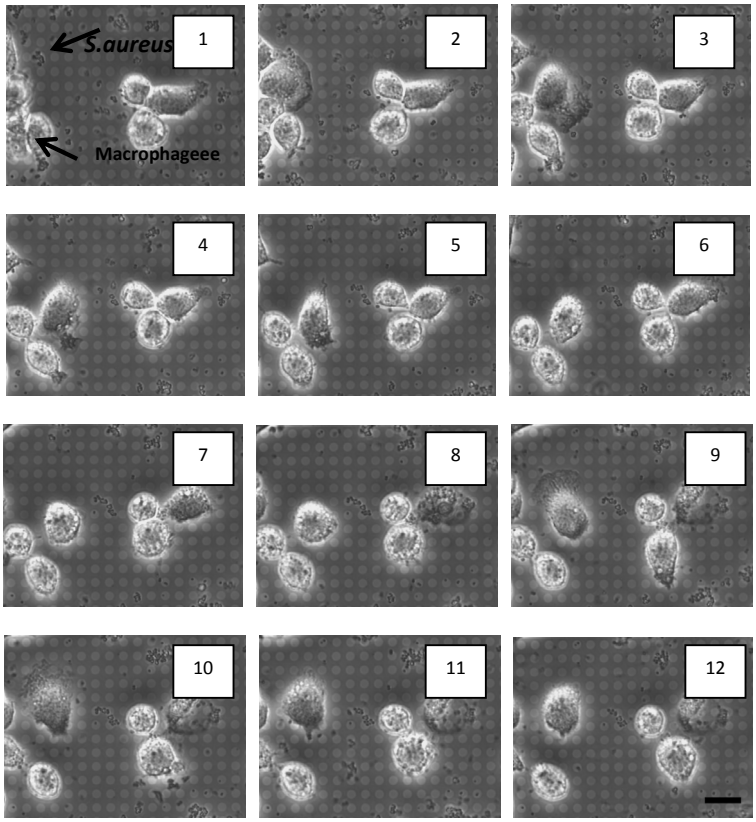

Figure 2 Macrophage migration towards *S. aureus* and phagocytosis. Phase-contrast images of macrophage activity toward *S. aureus* 8325-4 on a PEG-patterned surface with adhesive patches of 5 μm diameter and 2.5 μm inter-patch distance. The interval between the images is 5 min, increasing from 1 to 12 and starting directly after the insertion of the macrophages. The bar denotes 20 μm.

REFERENCES

1. Trampuz A, Zimmerli W. New strategies for the treatment of infections associated with prosthetic joints. Curr Opin Investig Drugs 2005;6:185-90.
2. Gristina AG. Biomaterial-centered infection: microbial adhesion versus tissue integration. Science 1987;237:1588-95.
3. Gristina AG, Naylor P, Myrvik Q. Infections from biomaterials and implants: a race for the surface. Med Prog Technol 1988;14:205-24.
4. Gristina AG. Implant failure and the immuno-incompetent fibro-inflammatory zone. Clin Orthop Relat Res 1994;298:106-18.
5. Gristina AG, Costerton JW. Bacterial adherence to biomaterials and tissue. The significance of its role in clinical sepsis. J Bone Joint Surg Am 1985;67:264-73.
6. Khalil H, Williams RJ, Stenbeck G, Henderson B, Meghji S, Nair SP. Invasion of bone cells by *Staphylococcus epidermidis*. Microbes Infect 2007;9:460-5.
7. Boelens JJ, Dankert J, Murk JL, Weening JJ, van der Poll T, Dingemans KP, *et al*. Biomaterial-associated persistence of *Staphylococcus epidermidis* in pericatheter macrophages. J Infect Dis 2000;181:1337-49.
8. Anderson JM. Inflammation, wound healing, and the foreign-body response. In: Ratner BD, Hoffman AS, Schoen FJ, JE L, editors. Biomaterials Science An Introduction ot the Materials in Medicine: Elsevier 2004. p. 296-304.
9. Aderem A, Underhill DM. Mechanisms of phagocytosis in macrophages. Annu Rev Immunol 1999;17:593-623.
10. Underhill DM, Ozinsky A. Phagocytosis of microbes: complexity in action. Annu Rev Immunol 2002;20:825-52.
11. Stuart LM, Ezekowitz RA. Phagocytosis: elegant complexity. Immunity 2005;22:539-50.
12. Hucknall A, Simnick AJ, Hill RT, Chilkoti A, Garcia A, Johannes MS, *et al*. Versatile synthesis and micropatterning of nonfouling polymer brushes on the wafer scale. Biointerphases 2009;4:FA50-7.
13. Lichter JA, Rubner MF. Polyelectrolyte multilayers with intrinsic antimicrobial functionality: the importance of mobile polycations. Langmuir 2009;25:7686-94.

14. Magin CM, Long CJ, Cooper SP, Ista LK, Lopez GP, Brennan AB. Engineered antifouling microtopographies: the role of Reynolds number in a model that predicts attachment of zoospores of Ulva and cells of *Cobetia marina*. Biofouling 2010;26:719-27.
15. Krsko P, Mansfield M, Sukhishvili S, Clancy R, Libera M. Electron-beam patterned poly(ethylene glycol) microhydrogels. Langmuir 2003;19:5618-25.
16. Krsko P, Saaem I, Clancy R, Geller H, Soteropoulos P, Libera M. E-beam patterned hydrogels to control nanoscale surface bioactivity In: Lai WY, Ocola LE, Pau S, editors. Nanofabrication: Technologies, Devices, and Applications II. Bellingham: SPIE; 2005. p. 600201.
17. Christman KL, Enrique-Rios VD, Maynard HD. Nanopatterning proteins and peptides. Soft Matter 2006;2:928-39.
18. Saravia-Otten P, Muller HP, Arvidson S. Transcription of *Staphylococcus aureus* fibronectin binding protein genes is negatively regulated by agr and an agr-independent mechanism. J Bacteriol 1997;179:5259-63.
19. Subbiahdoss G, Kuijer R, Grijpma DW, Van der Mei HC, Busscher HJ. Microbial biofilm growth *vs.* tissue integration: "the race for the surface" experimentally studied. Acta Biomater 2009;5:1399-404.
20. Krsko P, Kaplan JB, Libera M. Spatially controlled bacterial adhesion using surface-patterned poly(ethylene glycol) hydrogels. Acta Biomater 2009;5:589-96.
21. Saldarriaga Fernandez IC, Da Silva Domingues JF, Van Kooten TG, Metzger S, Grainger DW, Busscher HJ, *et al*. Macrophage response to *staphylococcal* biofilms on crosslinked poly(ethylene) glycol polymer coatings and common biomaterials *in vitro*. Eur Cell Mater 2011;21:73-9.

Chapter 7

General Discussion

GENERAL DISCUSSION

Infection is the leading cause of failure in permanent biomaterial implants, and its incidence will increase as bacterial resistance to antibiotics continues to increase. Prevention of biofilm formation on biomaterials implant surfaces is the most advocated way of reducing the risk of implant infection. Microbial adhesion is the first step in biofilm formation on and pathogenesis around a biomaterials implant. Nowadays biomaterials coatings are mainly developed to inhibit microbial adhesion, but often only allow very little or no tissue integration [1, 4]. In this thesis, a change in paradigm is proposed, suggesting the development of coatings with multiple functionalities, i.e. inhibition of microbial adhesion while stimulating cellular adhesion, spreading and growth at the same time [5, 6].

We have prepared bi-functional, differentially adhesive surfaces based on patterning surfaces with controlled combinations of protein/cell adhesive and non-adhesive features. In the concept of the race for the surface, as forwarded by A.G. Gristina in the late 1980's, the competition between microorganisms and tissue integration is determinant for the ultimate fate of a biomaterials implant in the human body [1]. Here, we investigated the specific length scales that effectively inhibit microbial adhesion and biofilm formation as well as stimulate cell adhesion, spreading, and growth at the same time.

PEG-microgel patterns were prepared on glass slides using electron beam lithography, and Figure 1 shows the size and swelling properties of a PEG-microgel generated by a focused-beam exposure under optimized conditions (Chapter 2). Swelling is considered as one of the strategies that reconstructs a PEG-microgel at the solid-water interface and thus confers anti-fouling properties onto surfaces [7, 8].

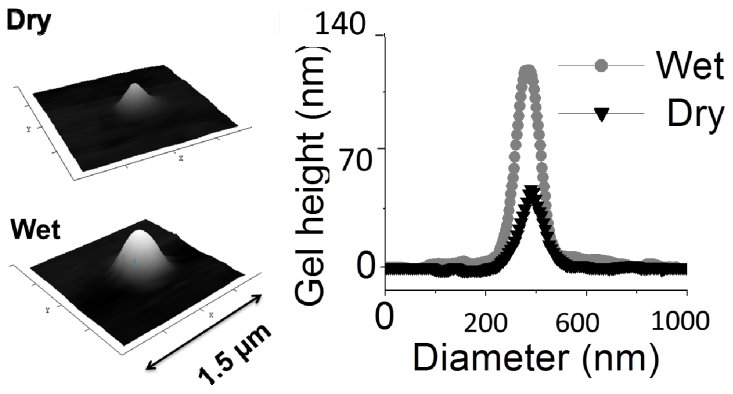

Figure 1 PEG-microgel formed by focused-beam exposure with an electron dose of 10 fC and beam energy of 2 keV. AFM images (left) show the morphology of a single PEG-microgel under dry and wet conditions, and the lateral and vertical data generated from the cross section of the gel (right) showing a swelling ratio of around 2.

Though it is possible to fabricate PEG-microgel patterns over extended surface areas, we prepared patterns with multiple spatial arrangements on one glass slide. This allowed us to evaluate multiple patterns in a single experiment but turned out to make simultaneous evaluation of bacterial and mammalian cell responses to the patterns in co-culture experiments, mimicking the race for the surface, difficult. We have shown that bacterial and mammalian cell monoculture results identified a robust differential adhesive window of 1 µm inter-gel spacing in the presence of Fn pre-adsorption (Chapter 4). PEG-microgel patterned surfaces showed significant inhibition (> 75%) of bacterial deposition, while better mammalian cell adhesion was maintained as compared to a bare glass surface. These monoculture results were used to find the optimal inter-gel spacings for co-cultures. Following the *in situ* monoculture results, we studied the race for PEG-microgel patterned surfaces in co-culture experiments between bacteria and mammalian cells based on a peri-operative contamination model. In this pilot study, staphylococci were allowed to adhere prior to U2OS cell adhesion and spreading, which mimics the situation of peri-operative bacterial contamination of implant surfaces. As shown in Figure 2, in the presence of about 10^3 *Staphylococcus aureus* 8325-4 cm^{-2}, U2OS cells remained spread up

to 330 min on patterns with a 0.5 μm inter-gel spacing with pre-adsorbed Fn (patterns as described in Chapter 4), but after prolonged times cells rounded up, died and detached. On patterns with a 1.5 μm inter-gel spacing, cells remained spread for at least 450 min, similar as on glass. However, on all surfaces we observed cell death after 900 min, in line with previous results that *S. aureus* is too virulent to allow mammalian cells to win the competition with these strains in co-culture experiments [9].

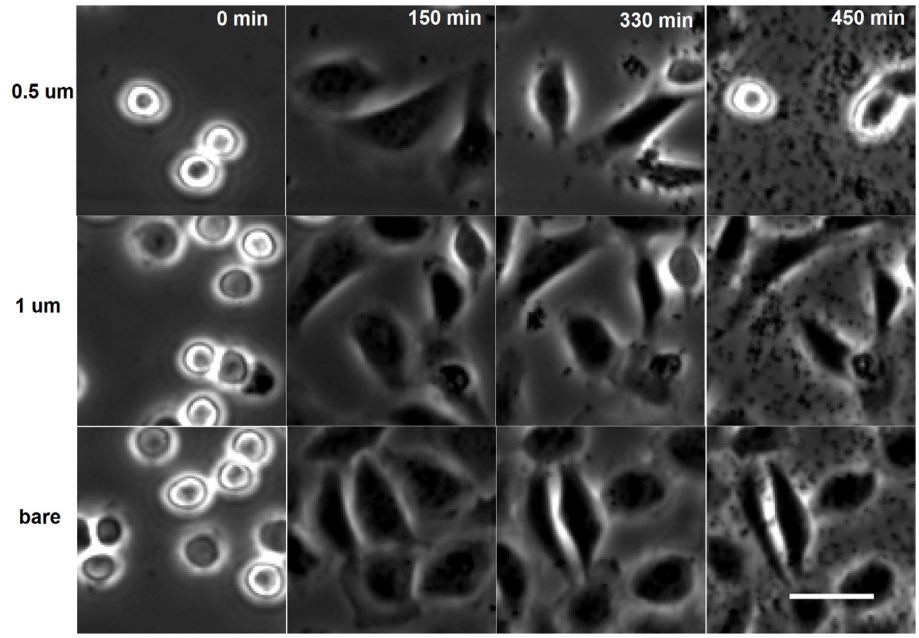

Figure 2 Phase contrast images of U2OS cell adhesion, spreading and growth at different time points in the presence of *S. aureus* 8325-4 on different PEG-microgel patterns in the presence of pre-adsorbed Fn. The bar denotes to 20 μm.

Co-culture experiments with a less virulent *Staphylococcus epidermidis* ATCC 35983 showed survival of U2OS cells at least for 48 h (Figure 3). It is of interest to notice from Figure 3, that cells spread equally well on 1.0 to 1.5 μm patterns as on glass, but we observed far less bacteria on the patterns than on glass. However, the co-culture experiments were less decisive with respect to the benefits of the bi-functional PEG-microgel patterns than we had hoped, which we attribute to the use of multiple patterns on one glass slide in one and the same experiment. Subbiahdoss *et al*. [10], when

developing the co-culture method, noticed that removal of bacterial toxins by flow was necessary in order to give mammalian cells a chance in co-culture protocols. Under static conditions, mammalian cells did not survive in the presence of adhering bacteria, even not in the presence of *S. epidermidis* with its relatively low virulence. Likely the use of multiple patterns and a large surrounding glass surface in a single experiment impeded us from obtaining co-culture data pertinent to one pattern only. There is influence of toxins from bacteria on adjacent, less favorable patterns and the surrounding glass. Future research should therefore include improving the throughput of our lithography system for a larger, precisely controlled surface.

Despite the above problems in obtaining reliable co-culture results, the differences in the outcome of the race between both staphylococcal strains and U2OS cells for PEG-microgel patterned surfaces are consistent with the higher virulence of *S. aureus* as compared with *S. epidermidis*. These observations are also consistent with clinical findings that biomaterials-associated-infection due to *S. aureus* and *Pseudomonas aeruginosa* usually progresses much more aggressively than those caused by *S. epidermidis* [11, 12]. In a similar study involving highly virulent *S. aureus* and *P. aeruginosa*, death of all adherent U2OS cells on PMMA was observed within 24 h despite the suspected removal of the majority of the bacterial toxins by flow [9].

A main theme of this thesis centered on the role of lateral modulations in surface cell adhesiveness in differently controlling the interactions between synthetic surfaces and different cell types. We have demonstrated that U2OS cells could bridge non-adhesive PEG-microgels with inter-gel spacing equals to the length scale of a single bacterium while the same kind of patterns inhibit bacteria adhesion (Chapter 3 and 4). We attribute this effect to fundamental differences in the physiology, size, and structure of staphylococci and mammalian cells (Chapter 3). Staphylococci are spherically shaped, are about 1 µm in diameter, and have relatively strong cell walls with little plasticity. They are thus unable to conform to a substratum if there are non-adhesive surface features that prevent an individual bacterium from sufficiently contacting the adhesive portions of a surface to bind.

In contrast, mammalian cell membranes have substantial plasticity and are able to readily conform to surfaces modulated at sub-cellular microscopic length scales. Furthermore, mammalian cells such as osteoblasts and fibroblasts bind to external surfaces – both natural ECM and synthetic biomaterials surfaces - by means of submicron size focal adhesions involving transmembrane integrins that cluster at adhesion sites [13, 14].

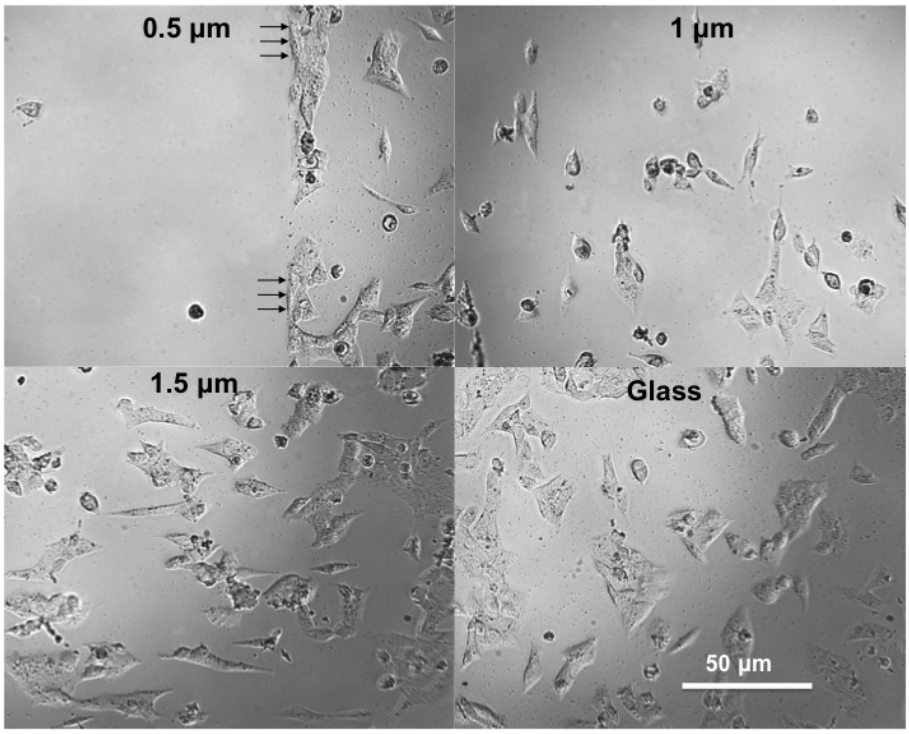

Figure 3 Phase contrast images of U2OS cell adhesion, spreading and growth after 48 h in the presence of *S. epidermidis* ATCC 35983 on PEG-microgel patterns with inter-gel spacings from 0.5 to 1.5 µm.

The differential effect from length scale mediation is not only significant between very different cell types such as microbial and mammalian cells. As shown in Figure 4A, patterned sub-micron-sized cell-repulsive features have also been used to differentiate adhesion and growth of two different mammalian cells: neurite growth was allowed on

the patterned surface while astrocyte adhesion and growth was inhibited (not shown) when inter-gel spacing equals to 2 μm. In our research, patterns with a 2 μm inter-gel spacing show differential adhesion of *S. epidermidis* and U2OS cells (Figure 4B). The mammalian U2OS cell is able to grow right over the non-adhesive microgels and exhibits extended filipodia that preferentially bind to adhesive sites on the surface in between non-adhesive microgels. Despite a larger size of single PEG-microgels (slightly smaller than 1 μm), compared to our microgel (around 400 nm), the mechanisms behind this length scale mediated adhesion and growth was also due to the characteristic size distribution of these two different type of cells: astrocytes were about an order of magnitude larger than the lateral dimension of neurites [15]. Although the mechanisms behind cellular adhesion, spreading and growth are complicated and do not only depend on different characteristic sizes, there is a size effect that regulates differential adhesion of microbial *versus* mammalian cells and between different types of mammalian cells. A precise spatial controlled patterned surface could serve as a potential model to solve the general and fundamental problem of how to create surfaces that differentially interact with different cell types in biomaterials science. Moreover, when optimal dimensions of such patterns have been established with respect to the different biological processes occurring at a biomaterials interface in the human body, results may become directly applicable.

Another biological process of importance with respect to biomaterials-associated infection is the response of macrophages. With the previous exploring of bacterial and mammalian cell responses to PEG-patterned adhesive patches (chapter 5), we were interested in finding out the interactions between bacteria and immune cells on PEG-patterned adhesive patches which had constrained effect for bacteria growth. Macrophages have been demonstrated to be more mobile on PEGylated surfaces due to their low adhesion forces with the substratum [16] and were therewith more effective in removing adhering bacteria. We were not able in the present study to demonstrate an advantage of increased mobility of macrophages on PEG-microgels with adhesive patches as compared with glass, presumably because bacteria on glass were abundantly present while

macrophages have to travel over considerable distances from patch to patch, to find the bacteria adhering on the patch (chapter 6). Considering the net effect of non-adhesiveness of patterned surfaces and influence of macrophages, PEG-microgels with adhesive patches were more effective in reducing bacterial adhesion than bare surfaces. Future research will have to reveal optimal distances between patches to increase phagocytosis, while maintaining cell adhesiveness and bacterial repulsion.

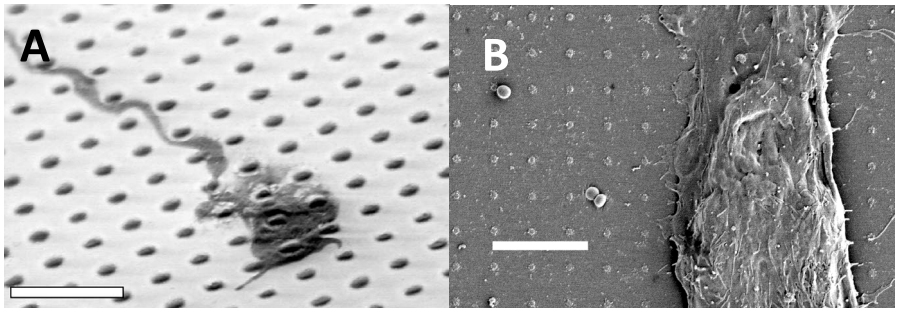

Figure 4 A. SEM image of a DRG neurite grow on an e-beam patterned PEG gel arrays with inter-gel spacing of 2 μm [15]. B. SEM image of a U2OS cell and *S. epidermidis* ATCC 35983 in a co-culture on a PEG-microgel pattern with inter-gel spacing of 2 μm. Bar denotes 5 μm.

REFERENCES

1. Gristina AG. Biomaterial-centered infection: microbial adhesion versus tissue integration. Science 1987;237:1588-95.
2. Rodrigues LR. Inhibition of bacterial adhesion on medical devices. Adv Exp Med Biol 2011;715:351-67.
3. Wu Y, Zitelli JP, TenHuisen KS, Yu X, Libera MR. Differential response of *Staphylococci* and osteoblasts to varying titanium surface roughness. Biomaterials 2011;32:951-60.
4. Subbiahdoss G, Pidhatika B, Coullerez G, Charnley M, Kuijer R, Van der Mei HC, *et al*. Bacterial biofilm formation *versus* mammalian cell growth on titanium-based mono- and bi-functional coating. Eur Cells Mater 2010;19:205-13.
5. Katsikogianni M, Missirlis YF. Concise review of mechanisms of bacterial adhesion to biomaterials and of techniques used in estimating bacteria-material interactions. Eur Cells Mater 2004;8:37-57.
6. Montanaro L, Speziale P, Campoccia D, Ravaioli S, Cangini I, Pietrocola G, *et al*. Scenery of *Staphylococcus* implant infections in orthopedics. Future Microbiol 2011;6:1329-49.
7. Banerjee I, Pangule RC, Kane RS. Antifouling coatings: recent developments in the design of surfaces that prevent fouling by proteins, bacteria, and marine organisms. Adv Mater 2011;23:690-718.
8. Gudipati CS, Greenlief CM, Johnson JA, Prayongpan P, Wooley KL. Hyperbranched fluoropolymer and linear poly(ethylene glycol) based amphiphilic crosslinked networks as efficient antifouling coatings: An insight into the surface compositions, topographies, and morphologies. J Pol Sci Part A: Pol Chem 2004;42:6193-208.
9. Subbiahdoss G, Saldarriaga Fernández IC, Da Silva Domingues JF, Kuijer R, Van der Mei HC, Busscher HJ. Interactions between bacteria, osteoblast-like cells and macrophages in the pathogenesis of biomaterial-associated infections. PLoS ONE 2011;6:e24827.

10. Subbiahdoss G, Kuijer R, Grijpma DW, Van der Mei HC, Busscher HJ. Microbial biofilm growth *vs*. tissue integration: "the race for the surface" experimentally studied. Acta Biomater 2009;5:1399-404.
11. Buchholz HW, Elson RA, Engelbrecht E, Lodenkamper H, Rottger J, Siegel A. Management of deep infection of total hip replacement. J Bone Joint Surg Br 1981;63:342-53.
12. Robinson DA, Enright MC. Multilocus sequence typing and the evolution of methicillin-resistant *Staphylococcus aureus*. Clin Microbiol Infect 2004;10:92-7.
13. Biggs MJ, Richards RG, Dalby MJ. Nanotopographical modification: a regulator of cellular function through focal adhesions. Nanomed: Nanotechnol, Biol Med 2010;6:619-33.
14. Guillame-Gentil O, Semenov O, Roca AS, Groth T, Zahn R, Voros J, *et al*. Engineering the extracellular environment: Strategies for building 2D and 3D cellular structures. Adv Mater 2010;22:5443-62.
15. Krsko P, McCann TE, Thach TT, Laabs TL, Geller HM, Libera MR. Length-scale mediated adhesion and directed growth of neural cells by surface-patterned poly(ethylene glycol) hydrogels. Biomaterials 2009;30:721-9.
16. Saldarriaga Fernandez IC, Da Silva Domingues JF, Van Kooten TG, Metzger S, Grainger DW, Busscher HJ, *et al*. Macrophage response to *staphylococcal* biofilms on crosslinked poly(ethylene) glycol polymer coatings and common biomaterials *in vitro*. Eur Cell Mater 2011;21:73-9.

Summary

SUMMARY

Infection is the number one cause of failure of biomaterials implants and devices, despite decades of research into the development of anti-adhesive coatings. The main aim of this thesis was to investigate up to what extent spatially modified, non-adhesive PEG-microgel patterns could favorably influence microbial adhesion, mammalian cell adhesion and spreading, and, ultimately, the outcome of the race for the surface to reduce the chance of occurrence of biomaterials-associated-infection.

In **chapter 1**, we postulated that anti-adhesive coatings may be of value for particular applications such as urinary or intravenous catheters, contact lens cases, and voice prostheses. The paradigm underlying the ideal biomaterial for biofilm control on totally internal, permanent implants, however, needs to change if we want to effectively reduce the occurrence of biomaterials-associated infections. Multi-functional coatings need to be developed that include anti-adhesive and anti-microbial functionalities, promote a proper immune response, and stimulate tissue integration, which could ultimately reduce the threat of bacterial colonization of an implant surface.

To develop multi-functional surfaces, we used electron-beam lithography to develop precise PEG-microgel patterns to control the interfacial behavior with multiple biological components **(chapter 2)**. Importantly, we needed to identify the most appropriate electron-irradiation conditions to create PEG-microgels with high-swelling behavior in order to repel proteins and, consequently, cells. We thus studied electron-irradiation conditions using different electron energies (2-30 keV) and different electron doses (0.005-500 fC/dot). We characterized the resulting patterned surfaces using a variety of different microscopic techniques. Most significant, was the use of immuno-fluorescence imaging to determine the extent of fibronectin adsorption onto patterned surfaces. There are different ranges of exposure conditions to create microgels of varying sizes with non-adhesive character. Immunofluorescence imaging proved that electron-beam scattering could generate a thin layer of lightly crosslinked PEG which largely extend the interactive

volume excluded from normal measurement for surface architecture. High incident beam energy of 30 keV significantly minimized forward scattering on our thin PEG film (120 nm), and consequently provided PEG gel with small interactive volumes at lower electron doses. Although low electron energy (< 5 keV) is not a good option for industrialized lithography to provide high resolutions, it can decrease the proximity effect dramatically and maximally preserve the anti-adhesive property of PEG.

Subsequently, with the optimized PEG-microgel fabricating parameters, we created surfaces with submicron-sized, non-adhesive microgel patterns on an otherwise cell-adhesive surface in order to determine up to what extent such surfaces can simultaneously promote tissue integration while reducing the probability of infection **(chapter 3)**. Quantitative force measurements between a staphylococcus and a patterned surface showed that the adhesion strength decreased significantly at inter-gel spacings comparable to bacterial dimensions. Time-resolved flow-chamber measurements showed that the microbial deposition rate dramatically decreased with respect to a decrease in inter-gel spacing. Importantly, the adhesion and spreading of osteoblast-like cells was preserved despite the sub-cellular non-adhesive surface features. Since such length-scale-mediated differential interactions do not rely on antibiotics, this mechanism could be particularly significant in mitigating biomaterials-associated infection by antibiotic-resistant bacteria such as methicillin-resistant *Staphylococcus aureus*.

While the above work was able to successfully demonstrate differential mammalian cell- and microbial-surface interactions, it did not address how these interactions would be affected by modulations in the cell adhesiveness of the underlying glass substratum. Therefore, we advanced this mechanism of length-scale-mediated differential adhesion under the more rigorous condition where modulated surfaces were pre-exposed to fibronectin (Fn) and probed by a Fn-binding *S. aureus* in **chapter 4**. Non-adhesive PEG-microgels were patterned at inter-gel spacings between 0.5 to 3.0 μm on glass, and the surfaces were exposed to Fn. Quantitative measurements using an atomic force

microscope with a single-bacterium probe showed that the adhesion force between *S. aureus* 8325-4, which is known to possess FnBPs, and a modulated surface increased substantially when the surface was coated with Fn but still decreased with decreasing inter-gel spacing. Time-resolved flow-chamber measurements also showed a decrease in staphylococcal adhesion rate with decreasing inter-gel spacing on the Fn-coated glass. Nevertheless, osteoblast-like cells could bind to modulated surfaces despite the non-adhesive microgels. Pre-exposure to Fn substantially amplified this effect. After 48 h of growth, Fn enabled osteoblast-like cells to adhere to and spread on surfaces with microgels patterned as closely as 1 μm. Thus, even when the adhesiveness of a modulated biomaterial surface was increased, a window of modulation length scale of 1 μm remained to promote implant healing while simultaneously reducing the risk of infection.

In **chapter 5**, we used a different pattern design composed of bio-adhesive Fn-coated patches on a continuous, non-adhesive PEG film. This was the inverse case of the previous chapters 3 and 4. The surfaces created were explored with respect to the behavior of both bacterial and mammalian cells. PEGylated films were micro-structured to create circular, exposed glass areas (patches) with diameters ranging from 1 to 5 μm and different inter-patch distances, resulting in adhesive area fractions of 0.1, 0.2 and 0.35. To enhance the adhesive features of the glass, Fn was adsorbed onto the adhesive patches. The adhesion and biofilm formation of *S. aureus* 8325-4 possessing Fn-binding proteins was compared with adhesion, spreading and growth of osteoblast-like cells. An adhesive area fraction of 0.1 proved to be too low to support tissue integration while bacterial growth was sizeable, especially on the adhesive patches with larger diameters. Increasing the adhesive area fraction supported cell adhesion, spreading and growth, while limiting bacterial growth by confining adhering bacteria to the adhesive areas. Therewith this chapter described a new approach to design bi-functional coatings for permanent, total internal implants or devices requiring tissue integration, with a reduced risk of infection.

Based on the results in **chapter 5**, showing that PEG gel patterned surfaces reduces biofilm formation while mammalian cells can still anchor on those adhesive Fn patches, we further postulated that confinement of bacteria by the adhesive patches could be advantageous for macrophages in the clearance of bacteria from the biomaterial surface. We tested this hypothesis in **chapter 6**, but the pilot study carried out was too limited to gain sufficient evidence to fully evaluate this hypothesis. Results revealed that bacterial growth was confined to patches and macrophage migration towards bacteria and subsequent engulfment was observed. A slightly higher removal of *S. aureus* was observed on surfaces with 5 μm patch size and 2.5 μm inter-patch distance compared to the patterned surfaces with 10 μm inter-patch distance. However, the average number of bacteria engulfed by a macrophage was higher on bare glass surface compared to the patterned surfaces. After 2 h of macrophage-bacterial interactions, the number of bacteria present on the patterned surfaces was less compared to bare glass.

In the general discussion **(chapter 7)**, we explain why co-culture experiments on the simultaneous interaction of bacteria and mammalian cells with the patterned surfaces were difficult to carry out. Pilot experiments failed to demonstrate benefits of the patterned surfaces in the race for the surface, probably because we were unable to pattern the entire substratum area with one and the same pattern. Hence, cross talk of bacterial toxins occurred between patterned areas and the uncoated glass surrounding the patterns. This cross talk impeded reliable measurements of simultaneous interactions. However, we observed that osteoblast-like cell killing was dependent on the virulence factor of pathogens. Osteoblast-like cells were able to survive longer in the presence of adhering *S. epidermidis* than in the presence of more virulent *S. aureus*. It is suggested that co-culture experiments require fully coated samples, for which a high throughput manufacturing device needs to be developed.

Samenvatting

SAMENVATTING

Infecties zijn de belangrijkste oorzaak voor het falen van een implantaat of apparaat gemaakt van een biomateriaal, ondanks decennia van onderzoek naar het ontwikkelen van anti-hechting coatings. Het doel van dit proefschrift was het onderzoeken van het mogelijk gunstige effect van ruimtelijk gemodificeerde, anti-hechting polyethyleen glycol (PEG)-microgel patronen op de hechting van micro-organismen, de hechting en spreiding van weefselcellen en, uiteindelijk, de uitkomst van 'the race for the surface', om op die manier de kans op een biomateriaal-geassocieerde infectie te verlagen.

In **hoofdstuk 1** stellen we dat anti-hechting coatings van grote waarde kunnen zijn voor bepaalde toepassingen, zoals intraveneuze katheters, contactlensdoosjes en stem protheses. Echter, het paradigma onderliggend aan het ideale biomateriaal om biofilm formatie op geheel interne, permanente implantaten te voorkomen, moet veranderen als we de incidentie van biomateriaal-geassocieerde infecties effectief willen verlagen. Er zullen multifunctionele coatings ontwikkeld moeten worden die anti-hechting en antimicrobiële eigenschappen bevatten, de juiste immuunrespons opwekken en weefselintegratie stimuleren, wat uiteindelijk de dreiging van bacteriële kolonisatie van het implantaat oppervlak zou kunnen verminderen.

Om multifunctionele oppervlakken te ontwikkelen hebben we elektronenbundel lithografie gebruikt om nauwgezette PEG-microgel patronen te creëren om het gedrag van meerdere biologische componenten met het interface te beheersen (**Hoofdstuk 2**). Belangrijk was dat we in staat waren de meest geschikte elektronenbundel condities te identificeren, om PEG-microgels te maken die een hoge mate van zwelling vertonen zodat ze de hechting van eiwitten, en daarmee ook van cellen, zouden verhinderen. Vandaar dat we de elektronenbundel condities hebben onderzocht met behulp van verschillende elektron energieën (2-30 keV) en verschillende doses elektronen (0.005-500 fC/dot). We hebben de hieruit resulterende oppervlakte patronen gekarakteriseerd met behulp van verschillende microscopische technieken. Het meest waardevol was het gebruik van

immunofluorescentie waarmee de hoeveelheid fibronectine die op het oppervlak hechtte werd bepaald. Er zijn meerdere stralings condities die gebruikt kunnen worden om microgels met anti-hechting eigenschappen te produceren van verschillende groottes. Immunofluorescentie toonde aan dat verstrooiing van de elektronenbundel een dunne laag licht gecrosslinkt PEG kon generen die het interactieve volume, dat bij normale metingen naar de oppervlakte structuur niet wordt waargenomen, vergrootte. Een hoog energetische elektronenbundel van 30 keV minimaliseerde de voorwaartse verstrooiing op onze dunne PEG film (120 nm) en leidde vervolgens tot PEG gels met kleine interactieve volumes bij een lagere elektron doses. Hoewel een lage elektron energie (< 5 keV) geen goede optie is voor hoge resolutie lithografie op industriële schaal, kan daarmee het omgevingseffect drastisch verlaagd worden en kunnen de maximale anti-hechting eigenschappen van PEG behouden blijven.

Vervolgens hebben we, met de geoptimaliseerde parameters voor het fabriceren van PEG-microgels, een oppervlak gecreëerd met anti-hechting microgel patronen op een oppervlak welke normaliter de hechting van cellen toelaat, om op die manier te bepalen tot op welke hoogte een dergelijk oppervlak weefselintegratie kan bevorderen terwijl tegelijkertijd de kans op infectie verlaagd wordt (**Hoofdstuk 3**). Kwantitatieve krachtmetingen tussen een stafylokok en een microgel oppervlak laten zien dat de hechtingskracht significant daalde wanneer de afstand tussen opeenvolgende gels vergelijkbaar was met de grootte van een bacterie. Metingen in een parallelle plaat stroom kamer toonden aan dat de initiële hechting van bacteriën drastisch afnam met het kleiner worden van de afstand tussen opeenvolgende gels. Belangrijk is dat hierbij de hechting en spreiding van osteoblast-achtige cellen nog steeds mogelijk was ondanks de anti-hechting eigenschappen van het oppervlak. Aangezien zulke lengteschaal gemedieerde differentiële interacties niet gebaseerd zijn op het gebruik van antibiotica, zou dit mechanisme vooral van belang kunnen zijn in het verminderen van biomateriaal-geassocieerde infecties door antibiotica resistente bacteriën, waaronder methicilline-resistente *Staphylococcus aureus*.

Terwijl het bovenstaande werk succesvol was in het aantonen van differentiële weefselcel- en microbiële-oppervlakte interacties, is geen aandacht besteed aan hoe deze interacties beïnvloed worden door aanpassingen in de cel hechting eigenschappen van het onderliggende glas. Daarom hebben we dit mechanisme van lengteschaal gemedieerde differentiële hechting gebruikt onder meer ingrijpende omstandigheden, waarbij de gemoduleerde oppervlakken eerst werden blootgesteld aan fibronectine (Fn) en vervolgens werden onderzocht met een aan Fn hechtende *S. aureus* stam (**hoofdstuk 4**). Anti-hechting PEG-microgels werden aangebracht op glas met een afstand tussen opeenvolgende gels variërend van 0.5 tot 3 µm en de oppervlakken werden vervolgens gecoat met Fn. Kwantitatieve metingen met behulp van atomische kracht microscopie, met een tip met daaraan een enkele bacterie, hebben aangetoond dat de hechtingskrachten tussen *S. aureus* 8325-4, waarvan het bekend is dat deze FnBP's bezit, en een gemoduleerd oppervlak substantieel groter werden wanneer het oppervlak gecoat was met Fn, maar nog steeds kleiner werden met kleiner wordende afstand tussen de gels. Metingen met de parallelle plaat stroom kamer lieten eveneens een verlaging zien in de hechting van de stafylokok met afnemende afstand tussen opeenvolgende gels op Fn gecoat glas. Desalniettemin waren osteoblast-achtige cellen nog steeds in staat te hechten aan het gemoduleerde oppervlak, ondanks de anti-hechting microgels. Het vooraf blootstellen aan Fn versterkte dit effect substantieel. Na 48 h groei was het, dankzij Fn, voor osteoblast-achtige cellen mogelijk om te hechten aan en te spreiden op oppervlakken met microgels waarbij de afstand tussen opeenvolgende gels slechts 1 µm bedroeg. Dit toont aan dat zelfs wanneer de aandrang om te hechten aan een gemoduleerd biomateriaal oppervlak verhoogd werd door het blootstellen aan Fn, een moduleringsruimte van 1 µm overbleef om integratie van het implantaat te bevorderen terwijl tegelijkertijd de kans op infectie verkleind werd.

In **hoofdstuk 5** hebben we een ander patroon gebruikt bestaande uit Fn gecoate gedeelten die geschikt waren voor bio-adhesie, op een aaneengesloten anti-hechting PEG film. Dit was het omgekeerde van de oppervlakken gebruikt in hoofdstuk 3 en 4. De zo

gecreëerde oppervlakken zijn onderzocht betreffende het effect op zowel bacteriën als weefselcellen. PEG films werden bewerkt om een ronde microstructuur te verkrijgen van blootgelegde glas patronen (patches) met diameters van 1 tot 5 µm en verschillende afstanden tussen deze glas patronen, wat uiteindelijk resulteerde in een hechtingsoppervlakte fractie van 0.1, 0.2, en 0.35. Om de hechting aan het glas te stimuleren werden deze gedeelten eerst gecoat met Fn. De hechting en biofilm formatie van *S .aureus* 8325-4, welke Fn bindende eiwitten bezit, werd vergeleken met de hechting, spreiding en groei van osteoblast-achtige cellen. Een hechtingsoppervlakte fractie van 0.1 bleek te laag voor het bevorderen van weefselintegratie terwijl bacteriële groei, met name op de hechting ondersteunende glas patronen met grote diameter, aanzienlijk was. Een grotere hechtingsoppervlakte fractie bevorderde cel hechting, spreiding en groei, terwijl bacteriële groei geremd werd doordat bacteriële hechting beperkt bleef tot de hechting op de glas patronen. Dit hoofdstuk beschrijft een nieuwe aanpak voor het ontwerpen van bi-functionele coatings voor permanente, totaal interne implantaten of apparaten waarbij weefselintegratie van cruciaal belang is, met een verlaagde kans op infectie.

Op basis van de resultaten in hoofdstuk 5, die tonen dat PEG-microgel patronen biofilm formatie remmen terwijl weefselcellen goed in staat waren te hechten op de met Fn gecoate gebieden, stelden we dat het feit dat de hechting van bacteriën beperkt bleef tot hechting op de glas patronen voordelig kan zijn voor macrofagen bij het opruimen van bacteriën van het biomateriaal oppervlak. In **hoofdstuk 6** hebben we deze hypothese getest. Echter, de eerste experimenten die we hebben uitgevoerd waren te gelimiteerd om voldoende bewijs te verzamelen om de hypothese goed te kunnen evalueren. De resultaten toonden dat de groei van bacteriën beperkt bleef tot de hechting op de glas patronen en dat macrofagen richting de bacteriën migreerden waarna fagocytose werd waargenomen. Er werd meer fagocytose van *S. aureus* waargenomen op oppervlakken met 5 µm grote glas patronen en 2.5 µm afstand tussen opeenvolgende glas patronen, dan op de oppervlakken waarbij de glas patronen 10 µm uiteen lagen. Het gemiddeld aantal bacteriën dat door een macrofaag opgenomen werd was echter hoger op kaal glas

dan op patroon oppervlakken. Na 2 uur macrofaag-bacterie interacties was het aantal bacteriën op het oppervlak met patronen lager dan op kaal glas.

In de algemene discussie (**hoofdstuk 7**) leggen we uit waarom experimenten, waarbij bacteriële en cellulaire co-culturen werden gebruikt om de interactie tussen bacteriën en weefselcellen gelijktijdig te bestuderen, zo moeilijk waren om uit te voeren. Eerste experimenten slaagden er niet in de meerwaarde van de patroon oppervlakken in 'the race for the surface' te laten zien. Dit komt waarschijnlijk omdat we er niet toe in staat waren om het gehele oppervlak met één en hetzelfde patroon te coaten, waardoor er crosstalk van bacteriële toxines plaatsvond tussen de oppervlakken met patronen en de delen van het glas zonder coating die de patronen omringden. De aanwezigheid van deze crosstalk belemmerde betrouwbare metingen met betrekking tot directe interactie tussen cellen en bacteriën. Wel bleek hieruit dat het overleven van osteoblast-achtige cellen in sterke mate afhankelijk was van de virulentie van de gebruikte bacteriën. Osteoblast-achtige cellen waren in staat langer te overleven in de aanwezigheid van *S. epidermidis* dan in de aanwezigheid van de meer virulente *S. aureus*. Wij stellen dat co-cultuur experimenten volledig gecoate samples vereisen, waarvoor een fabricage methode ontwikkeld moet worden die het mogelijk maakt om op grote schaal dit soort samples te produceren.

Acknowledgements

ACKNOWLEDGMENTS

Throughout life, we rely on small groups of people for love, admiration, respect, moral support and help. - Ralph Waldo Emerson

For the past five years, my life adventure was greatly pushed forward by all kinds of love, support and help. Simple gestures, maybe, but I know I have been changed for the better.

My dissertation would not have been possible without all my supervisors. Ever since I got involved in the dual-PhD program at UMCG, I owe my gratitude greatly to my Groningen supervisors Prof. dr. Henk J. Busscher and Prof. dr. H.C. Van der Mei. It was Henk who guided me to think “less is more” and “better is the enemy of good” during the intense experimental discussion and writing processes. Henk also affected me with his passion both for research and for a fulfilling life. And I will always be grateful to Henny for her professional support, for her reinforcement in all aspects of my dissertation and, also for kindly taking care of the arrangements for during each of my 3-month stay. Together with Guruprakash, I always feel myself lucky and also I truly enjoyed working with such a professional team.

I’d like to thank my Stevens supervisor, Prof. Matthew Libera for not only being as my supervisor, but also encouraged and challenged me throughout my academic program. I would like to thank him for patiently guiding me through the small investments and training from the beginning of my program, helping to shape up the main theme of my thesis “length scale mediated differential adhesion” gradually, and introducing me to Groningen, which gave the wonderful opportunity to pursue this dual PhD program. I finally got a platform to test the entire hypothesis of this thesis.

Special thanks are due to Dr. Guruprakash Subbiahdoss, who served as a great friend, valuable colleague and also my co-advisor during my dual program. His enthusiasm and supportive attitude during every meeting and discussion gave me great strength to turn the original ideas into solid evidence. From the beginning of this co-operation to the final

thesis writing, he was always right there and trying to offer help. Now he is heading to the path of developing an academic career. I wish him great success, and I will look forward to further opportunities for collaboration.

As the first one who engaged in the dual PhD program between Stevens and UMCG, I have been fortunate that I got so much technical support both during my stay and after I left Groningen. I would like to thank Joop de Vries for his patient help with AFM force measurements. Minie Rustema-Abbing, Betsy van de Belt-Gritter, and Hans Kaper, thank you all for the bacteria preparation and flow chamber experiments. I am grateful to Prof. Theo van Kooten and Dr. Bastiaan Krom, who provided me with the more standard way of performing operations during experiments and also with constructive criticism.

Travel between two countries requires a lot of work involving arranging the necessary documents, getting settled down and all the trivial but time-consuming issues. I owe a lot of gratitude to Wya, Ina and Willy for all kinds of help time after time. Most of all, I would like to thank Willy for helping me correct the format of my dissertation. That was really a big helping hand for me when I was struggling with writing.

And I cannot express my gratitude enough for all the great moments of sharing fun and frustrations together with all my friends, both from Hoboken and Groningen. Thank you, Aaron, as the only classmate with me through the entire course work; thank you for all the encouragement and hope there will be a chance to play badminton with you again. Chris, Crystal, and Helen, thank you for always being there for me when I feel stressed. I enjoyed working with Xiaoguang, Emre and Yong; actually they came to our lab of multiscale imaging one year after I did, but I learnt a lot from them, both from their scientific way of thinking and also from the smart way of playing board games. Alex Chou, thank you for maintaining all the equipment in the best way and also for being there patiently to guide me out through. Jan, Joana and Chongxia, thank you all for taking care of my lab work occasionally when I had my hands full. And Jesse, thank you for teaching me to draw schematic graphs in a much more elegant way. It would not have been possible to write this doctoral thesis without the help and support of the kind people around me, to only

some of whom it is possible to give particular mention here. Thank you Doctor Bu, Dr. Li Mei, Lei Song, Katya, Wenwen, for being my friends!

Finally, and above all, I would like to thank my parents for giving me their unequivocal support, even merely by asking the date of my return. My small expression of thanks, as usual, does not suffice when facing this unconditional love. But I do know that the place where they are is my real and only home.